UNIVERSITY OF CALIFORNIA
RIVERSIDE

Form, Function, and Evolution of Shark Pectoral Fins

A Dissertation submitted in partial satisfaction
of the requirements for the degree of

Doctor of Philosophy

in

Evolution, Ecology and Organismal Biology

by

Phillip C. Sternes

June 2024

Dissertation Committee:
Dr. Timothy E. Higham, Chairperson
Dr. Kimberly Hammond
Dr. David Reznick

The Dissertation of Phillip C. Sternes is approved:

_____

_____

_____

Committee Chairperson

University of California, Riverside

ACKNOWLEDGEMENTS

In my mind, it is impossible to thank and express my sincere gratitude to all those who helped me complete this journey. However, I will do the best I can. First, I would like to thank the University of California, Riverside and the Department of Evolution, Ecology, and Organismal Biology for allowing me the opportunity to continue my shark passion. I also thank my various fellow graduate students who have been incredibly supportive over the years.

I would like to thank my advisor, Tim Higham, for giving me a chance to conduct some shark studies, making me a better scientist, and just for listening to my ravings about sharks. I would like to thank all the past and current members of the Higham Lab, Emily, Anthony, Amanda, Marina, Connor, Seth, Erik, and Joseph for also being incredibly supportive and dealing with my shark nonsense. I also thank the various undergrads for helping me collect critical shark data for this dissertation including Sophia and Ryan.

I cannot thank the full amount of others from museums and other academics outside the university that have helped but names include, Kenshu, Patrick, Scott, Joel, Bill, Todd, and Ben. Thank you all for your incredible assistance over the years. For chapter 2, a very special thanks to Lars for his incredible help with analyses. I learned so much and my brain still hurts. For chapter 3, deepest thanks to Sam for introducing me to CFD and teaching me its incredible capabilities.

I am grateful to my amazing friends from the Midwest, Kerri, Abbey, Erin, and Alex, who have continued to support me for all these years, I could not have done it

without them. I am also grateful to all the new friends I have made here in California: Camil, Fernando, Tej, Oscar, Jaime, Joanna, and Carlos. I thank you all for also supporting and helping in my shark endeavors.

I am grateful to my family, Mom, Dad, Alex, Grace, Jack and yes George too, for seeing my journey all the way through and also enabling my shark obsession.

Chapter Acknowledgements

Chapter 1 is a reprint of material as it appears in Biological Journal of the Linnean Society.

ABSTRACT OF THE DISSERTATION

Form, Function, and Evolution of Shark Pectoral Fins

by

Phillip C. Sternes

Doctor of Philosophy, Graduate Program in Evolution, Ecology and Organismal Biology
University of California, Riverside, June 2024
Dr. Timothy E. Higham, Chairperson

The origin and evolution of pectoral fins remains one of the most important components of vertebrate history. Sharks represent one of the oldest representatives to exhibit paired fins. Yet, there is a paucity of data on the functional and evolutionary aspects of shark pectoral fins. This dissertation aims to bridge those gaps. In Chapter 1, we measured the external pectoral fin morphology of a shark species, the scalloped hammerhead (*Sphyrna lewini*), that undergoes ecological shifts through ontogeny. We found the pectoral fins changed in shape that are most likely in response the difference in ecological demands that this shark experiences. In Chapter 2, we measured the pectoral fin aspect ratio (AR) of nearly every known (89%) extant shark species and various extinct species. In addition, we coded each species based on their ecology and performed sophisticated evolutionary model fitting analyses. We determined sharks were most likely benthic (i.e., bottom-dwelling) or benthopelagic (i.e., near bottom) in origin and that

when sharks shifted to the pelagic (open water) zone of the marine ecosystem, their pectoral fin morphology also changed, clearly demonstrating adaptive evolution. We also realized temperature was a critical driver in shark evolution. In Chapter 3, we used the computational fluid dynamics (CFD) approach to understand the functional aspects of pelagic shark pectoral fins. Our results showed that pelagic shark pectoral fins have different functions compared to benthic sharks. In Chapter 4, we followed up our work in Chapter 1, and compared the scaling trends of shark pectoral fins with various ecologies to determine if any noticeable patterns were present. We realized the scaling of shark pectoral fins is highly complex and that further broader research is warranted.

TABLE OF CONTENTS

TABLES

FIGURES

Chapter 1

Chapter 2

Chapter 3

Chapter 4

APPENDICES

Chapter 1

Chapter 2

INTRODUCTION

The origin of pectoral fins represents a key moment in vertebrate history (Shubin, 1995; Coates, 2003). Pectoral fins along with jaws led to a major diversification event during the Devonian, also known as the 'Age of Fishes' (Friedman and Sallan, 2012; Benton, 2014). These critical control structures were important for fish locomotion which most likely led to the vast ecological diversity present in fishes today. There has been high interest in both the form and function of fish pectoral fins dating all the way back to the days of Aristotle. Indeed, considerable work has been done on morphological and functional diversity of fish pectoral fins but this has mainly centered on bony fishes (Osteichthyes) (Webb, 1982; 1984; 1994; Blake, 2004).

The cartilaginous fishes (Chondrichthyes) are sister taxa to the bony fishes, appearing over 400 million years ago and represent one of the oldest vertebrate clades to have pectoral fins (Heinicke et al., 2009; Whitenack et al., 2022). Chondrichthyan fishes have undergone major evolutionary events throughout their long history and have experienced major moments of diversity and decline (Friedman and Sallan, 2012; Guinot and Cavin, 2016; Whitenack et al., 2022). Modern chondrichthyan fishes are represented with two major groups, the Holocephali and Elasmobranchii, which total over 1400 living species (White et al., 2022; Whitenack et al., 2022). Within Elasmobranchii are the modern sharks, or selachians, which total over 540 living species (Ebert et al., 2021; White et al., 2022). Modern sharks are living representatives of one of the oldest vertebrate linages to have pectoral fins, yet there is a paucity of information on them.

Although studies are limited, a few general observations have been made regarding the form, function, and evolution of shark pectoral fins. For example, in terms of external morphology, shark qualitatively show a broad diversity of pectoral fin shapes (Thomson and Simanek, 1977; Compagno, 1990) but a recent study on 20 species suggested there are no significant differences in shark pectoral fin shapes even when species differ ecologically (Hoffmann et al., 2020). In terms of function, only two studies have recorded quantitative data on shark pectoral fins, which has led to some hypotheses (Wilga and Lauder, 2000; 2001) but these limited studies greatly underappreciate the diversity of species present today, implying that further study is required. In terms of evolution, there are gaps in understanding the evolution of even overall shark body form due to their poor preservation as cartilaginous skeletons (Sternes and Shimada, 2020). Although sharks are primarily represented by teeth in the fossil record, some preserved full body forms do exist and along with sophisticated evolutionary analyses, this presents a significant opportunity to fully tease out if and how shark pectoral fins have changed for the past 200 million years.

Shark pectoral fins represent a rather exciting and major gap in our understanding of vertebrate evolution. It is clear that evolution of pectoral fins in bony fishes were an important factor for their vast diversity seen today as bony fishes number over 32,000 total species (Webb, 1982; Nelson et al., 2016). Whereas modern sharks are much lower in species number compared to bony fishes, a majority of sharks are key predators in their respective marine habitats (Compagno, 1990; Cortes, 1999). This dissertation aims to address the major gaps in understanding the form, function, and evolution of shark

pectoral fins and aims to present new hypotheses and data to improve our understanding of not only shark evolution but vertebrate evolution as a whole.

Benton MJ. 2014. *Vertebrate paleontology, fourth edition.* Hoboken (NJ): Wiley-Blackwell.

Blake RW. 2004. Fish functional design and swimming performance. *Journal of Fish Biology* 65: 1193–1222.

Coates MI. 2003. The evolution of paired fins. *Theory of Biosciences* 122: 266–287.

Compagno LJV. 1990. Alternative life-history strategies of cartilaginous fishes in time and space. *Environmental Biology of Fishes* 28: 33–75.

Cortés E. 1999. Standardized diet compositions and trophic levels of sharks. *ICES Journal of Marine Science* 56: 707–717.

Ebert DA, Dando M, Fowler S. 2021. *Sharks of the world: a complete guide*. Princeton (NJ): Princeton University Press.

Friedman M, Sallan LC. 2012. Five hundred million years of extinction and recovery: a Phanerozoic survey of the large scale diversity patterns in fishes. *Palaeontology* 55: 707–742.

Guinot G, Cavin L. 2016. 'Fish' (Actinopterygii and Elasmobranchii) diversification patterns through deep time. *Biological Reviews* 91: 950–981.

Heinicke MP, Naylor GJP, Hedges SB. 2009. Cartilaginous fishes (Chondrichthyes). In Hedges SB, Kumar S, eds. *The timetree of life.* Oxford, UK: Oxford University Press, pp. 320–327.

Hoffmann SL, Buser TJ, Porter ME. 2020. Comparative morphology of shark pectoral fins. *Journal of Morphology* 281: 1501–1516.

Nelson JS, Grande TC, Wilson MVH. 2016. *Fishes of the world, fifth edition*. Hoboken, New Jersey: Wiley.

Shubin N. 1995. The evolution of paired fins and the origin of tetrapod limbs: phylogenetic and transformational approaches. In Hecht MK, MacIntyre RJ, Clegg MT, eds. *Evolutionary Biology, Volume 28.* New York New York: Plenum Press, 39–86.

Sternes PC, Shimada K. 2020. Body form in sharks (Chondrichthyes: Elasmobranchii) and their functional, ecological, and evolutionary implications. *Zoology* 140: 125799.

Thomson KS, Simanek DE. 1977. Body form and locomotion in sharks. *American Zoologist* 17: 343–354.

Webb PW. 1982. Locomotor patterns in the evolution of Actinopterygian fishes. *American Zoologist* 22: 329–342.

Webb PW. 1984. Body form, locomotion and foraging in aquatic vertebrates. *American Zoologist* 24: 107–120.

Webb PW. 1994. The biology of fish swimming. In Bone ML, Rayner JMV, eds. *Mechanics and physiology of animal swimming.* Cambridge, Massachusetts: Cambridge University Press, 45–62.

White WT, O'Neill HL, Naylor GJP. 2022. Taxonomy and diversity of extant elasmobranchs. In Carrier JC, Simpfendorfer CA, Heithaus MR, Yopak KE, eds. *Biology of sharks and their relatives, third edition*. Bocar Raton, FL: CRC Press, pp. 31–57.

Whitenack LB, Kim SL, Sibert EC. 2022. Bridging the gap between paleobiology and biology. In Carrier JC, Simpfendorfer CA, Heithaus MR, Yopak KE, eds. *Biology of sharks and their relatives, third edition*. Bocar Raton, FL: CRC Press, pp. 1–29.

Wilga CD, Lauder GV. 2000. Three-dimensional kinematics and wake structure of the pectoral fins during locomotion in leopard sharks *Triakis semifasciata*. *Journal of Experimental Biology* 203: 2261–2278.

Wilga CD, Lauder GV. 2001. Functional morphology of the pectoral fins in bamboo sharks, *Chiloscyllium plagosium*: Benthic vs. pelagic station-holding. *Journal of Morphology* 249: 195–209.

CHAPTER 1

Hammer it out: Shifts in Habitat are Associated with Changes in fin and body Shape in the Scalloped Hammerhead (*Sphyrna lewini*)

Abstract

Major shifts in habitat often occur during life history and can have significant impacts on the morphology and function of an animal. However, little is known about how such ecological changes influences the locomotor system of large aquatic vertebrates. Scalloped hammerheads (*Sphyrna lewini*) are large sharks found in warm temperate and tropical waters. Smaller scalloped hammerheads are generally found in near shore habitats but, as they grow larger, individuals spend time in deep-water, pelagic habitats. We measured a number of morphological traits of scalloped hammerheads, ranging from 32 to 130 cm, to determine if there are allometric changes in locomotor morphology in association with this shift in habitat. We found that head morphology, caudal fin area, and lateral span scaled with negative allometry, whereas the lengths of their pectoral, dorsal, and caudal fins, in addition to pectoral and caudal fin aspect ratios, scaled with positive allometry. Furthermore, the largest shark in our dataset exhibited an optimal body fineness ratio for locomotor efficiency. This suggests the changes in ecology have profound influences on the functional morphology of scalloped hammerheads. We discuss how these drastic morphological changes relate to potential changes in scalloped hammerhead swimming function and performance.

Introduction

As organisms grow larger in body size, they may experience changes in ecology and their life history (Calder, 1984; Schmidt-Nielsen, 1984; LaBarbera, 1989). Such shifts in habitat may strongly impact animal function (Koehl, 1996; Higham et al., 2021) by imparting new functional demands. This, in turn, may cause changes in morphology in order to effectively execute these functions (Wainwright and Reilly, 1994; Wainwright et al., 2002). For fishes, changes in habitat and diet cause not only changes in body, head, and jaw morphology, but also impact growth patterns through ontogeny (Svanbäck and Eklöv, 2002; Ward-Campbell and Beamish, 2005; Fu et al., 2016). Among larger fishes, such as sharks, these kinds of changes may not only lead to a shift in trophic level from a mesopredator to an apex predator but may also lead to shifts in marine habitats (Tricas, 1984; Grubbs 2010; Fu et al., 2016).

Changes in habitat in aquatic organisms are well documented, although most of the focus has been on freshwater fishes. For example, juvenile bluegill sunfish (*Lepomis macrochirus*) are often restricted to highly vegetated littoral habitats whereas adults tend to be in open water (Mittelbach and Osenberg, 1993). This, in turn, influences both predation and feeding biology. Bluegill shift to feeding on zooplankton in open water as they increase in size, which has a cascade of changes in selective pressures. In largemouth bass (*Micropterus salmoides*), a closely related species, a diet shift from littoral invertebrates to fish typically occurs in the fish's first year (Olson, 1996). Similarly, marine Eurasian perch (*Perca fluviatilis*), which occupy two different habitats, exhibit differences in head, body, and fin shapes which affected the diet between the two

groups (Svanbäck and Eklöv, 2002). Specifically, perch in the littoral habitat have deeper bodies, larger heads, and longer fins compared to those in the pelagic habitat. Another classic is example is for threespine stickleback (*Gasterosteus aculeatus*), which exhibit drastic morphological changes when shifting habitats as pelvic spines emerged when moving from a vegetative habitat to an open water habitat (Sillet and Foster, 2000; Spoljaric and Reimchen, 2011). Nevertheless, given the magnitude of marine habitats, tracking and understanding how changes in ecology and performance are linked is challenging.

Scalloped hammerheads (*Sphyrna lewini*) (Griffith and Smith, 1834) are large apex predators with a worldwide distribution, but they are generally found in warm temperate and tropical seas (Ebert et al., 2021; Roff et al., 2016; Wells et al., 2018). Scalloped hammerheads are seasonally migratory and are often observed in large schools (Klimley et al., 1988; Ebert et al., 2021). Interestingly, smaller scalloped hammerheads (30–90 cm total length) are generally found in near shore, shallow water habitats whereas larger individuals (>90 cm total length) are generally found in deep-water, pelagic habitats (Clarke, 1971; Klimley, 1987; Duncan and Hollland, 2006; Hoyos-Padilla et al., 2014; Ebert et al., 2021; Estupiñán-Montaño et al., 2021). Additionally, these different habitats present different prey types as smaller scalloped hammerheads tend to feed on benthic prey such as isopods, octopods, and scorpion fish compared to the larger pelagic individuals that consume larger and more evasive prey such as deep-water squid and pelagic crabs (Gallagher and Klimley, 2018). Furthermore, the ability to forage on deep

water squid requires frequent vertical migrations which has been well documented in scalloped hammerheads (Klimley, 1993; Bessudo et al., 2012; Ketchum et al., 2014).

Given the shift in both habitat and feeding requirements, changes in the locomotor system are likely important. The caudal fin is specifically responsible for generating thrust in sharks (Ferry and Lauder, 1996), and it has been proposed that caudal fin shape is critical for being able to capture certain types of prey. For example, lamnid sharks (e.g., mako sharks, porbeagle, salmon, and white sharks) have a stiff, symmetrical, lunate caudal fin (Thomson and Simanek, 1977; Lingham-Soliar, 2005b) which is thought be essential for catching evasive prey such as seals, swordfish, and tuna (Stillwell and Kohler, 1982; Tricas, 1984; Ebert et al., 2021). On the other hand, a majority of sharks have a highly asymmetrical caudal fin which is likely utilized for swimming slowly and also rapid maneuvers for prey capture (Thomson and Simanek, 1977; Webb, 1984; Maia et al., 2012).

Sharks exhibit a wide range in pectoral fin shapes, and this can likely be attributed to differences in ecology (Maia et al., 2012). However, a recent analysis of limited number of species suggests this may not be the case as external morphology was not significantly different among sharks with different ecology (Hoffmann et al., 2020). Despite the lack of difference in external morphology, there were considerable differences based on internal morphology such as the amount of skeletal support between benthic and pelagic sharks (Hoffmann et al., 2020). Nevertheless, benthic sharks have shorter and more rounded pectoral fins (Wilga and Lauder, 2000; 2001; Maia et al., 2012) whereas the pectoral fins of truly pelagic sharks are long and narrow most likely for

improved lift to drag ratio (Vogel, 1994; Alexander, 2003; Maia et al., 2012). Functionally, pectoral fins are responsible for vertical movements in the water column (Maia et al., 2012). In contrast, benthic sharks routinely use their pectoral fins for station-holding (Wilga and Lauder, 2001). This division highlights the importance of considering pectoral fin morphology and function when considering ecological differences among sharks and other fishes.

Considering the drastic differences in the ecology of shallow and deep-water habitats, it is likely that different morphological traits of scalloped hammerheads may be favored in each habitat. Do the pectoral fins of scalloped hammerheads exhibit allometric growth given the reliance on vertical migrations for foraging in deep water habitats? Does this also lead to a more symmetrical caudal fin and/or changes to other parts of the body? To answer these questions, we measured 50 museum specimens of *S. lewini* (over a range of body sizes (32–130 cm total length)) gathering 13 morphometric linear measurements and five area measurements for each specimen. We followed the methods of Irschick and Hammerschlag (2014) and Higham et al. (2018) as these measurements specifically address lengths and areas of the head, pectoral, dorsal, and caudal fins, and overall 'girth' of the shark body. From this data, we aimed to address if there are any morphological differences present in *S. lewini* and discuss the implications of these results in relation with the shark's life history.

Materials and Methods

Samples

We examined specimens of *S. lewini* from the following four institutions: California Academy of Sciences (CAS), San Francisco, California, USA; Field Museum of Natural History (FMNH), Chicago, Illinois, USA; Natural History Museum of Los Angeles County (LACM), Los Angeles, California, USA; Scripps Institution of Oceanography (SIO), University of California, San Diego, California, USA. Table S1 (Supporting information) lists all samples of *S. lewini* examined in this study.

Limitations of samples

Our study utilized preserved museum specimens, unlike other studies using live sharks (Irschick and Hammerschlag, 2014; Fu et al., 2016; Irschick et al., 2017). That said, several studies (Reiss and Bonnan, 2010; Anhelt et al., 2020) have examined ontogenetic change using museum specimens. Thus, despite the potential for shrinkage of specimens, we are confident that we captured true changes in form since all of the specimens were measured under the same conditions. Additionally, we acknowledge scalloped hammerheads are long-lived species and adults may reach total lengths of 400 cm (Ebert et al., 2021). However, because there are significant logistical challenges of housing and maintaining such large specimens, we are constrained to museum specimens of a maximum total length of 130 cm. Furthermore, scalloped hammerheads are listed as critically endangered by the IUCN and they are highly sensitive to non-lethal sampling (Gallagher et al., 2014); thus, any capture and measurement of larger live individuals may

negatively impact the population. Lastly, it is known that scalloped hammerheads become highly migratory and are found in offshore habitats around 100 cm total length (Klimley, 1987; Hoyos-Padilla et al., 2014). Thus, we feel confident about the use of museum specimens in our study.

Morphological measurements

To document morphological differences in *S. lewini*, we followed the approach of Irschick and Hammerschlag (2014) and Irschick et al. (2017) and quantified the following morphological measurements (Figure 1) using a standard metric tape measure (accurate to 1 mm): (1) the cephalofoil or head size (EE): distance between the inner part of the eyes; (2) lateral span (LS): the distance from (i.e. around the curved dorsal side of the shark) from the insertion point of the anterior edge of one pectoral fin to the insertion point of the other pectoral fin; (3) frontal span (FS): the distance (i.e. around the curved dorsal side of the shark) from the insertion point of the anterior edge of the dorsal fin to a line oriented parallel to the horizontal plane of the pectoral fin; (4) proximal span (PS): the distance spanning (i.e. around the curved dorsal side of the shark) from the insertion point of the posterior edge of the dorsal fin to a line oriented parallel to the horizontal plane of the pectoral fin; (5) caudal keel circumference (CKC): total circumference at the base of the tail as measured at the caudal keel; (6) pectoral fin length (PFL): the linear distance from the insertion of the pectoral fin at the distal edge to the tip of the pectoral fin when fully extended; (7) dorsal fin 1 (DF1): distance from the anterior insertion point

of the dorsal fin to the tip of the dorsal fin; (8) dorsal fin 2 (DF2): distance from the tip of the dorsal fin to the posterior insertion point of the dorsal fin; (9) dorsal fin 3 (DF3): distance horizontally across the shark body between the anterior and posterior insertion points of the dorsal fin; (10) caudal fin 1 (CF1): the linear distance from the dorsal insertion of the caudal fin to the dorsal tip of the caudal fin; (11) caudal fin 2 (CF2): the linear distance from the dorsal tip of the caudal fin to the ventral tip of the bottom part of the caudal fin; (12) caudal fin 3 (CF3): the linear distance from the bottom anterior edge of the caudal fin to the bottom posterior edge of the caudal fin; and (13) pre-caudal length (PCL): the linear distance from the tip of the snout to the pre-caudal pit, which is a longitudinal notch on the caudal peduncle directly on the anterior side of the caudal fin.

In addition to linear measurements, we obtained digital images of the head, first dorsal fin, pectoral fin, and the caudal fin. We used ImageJ to calculate the area of the various fins and head (Fig. 1). Subsequently, we calculated aspect ratio (AR) of each fin, defined as L^2/S, where L and S are the length and area of the fin, respectively.

Furthermore, to investigate body shape diversity due to changes in habitat, we measured fineness ratio (Porter et al., 2009; 2011). The fineness ratio is associated with a minimum drag coefficient and can be defined as L/d where L is the body length and d is the profile height. In this case we used PCL as L and FS as d. We calculated the fineness ratio of each individual and regressed these values against PCL to tease out any trends through ontogeny.

Scaling and statistical analysis

We determined the scaling relationships using the power-law function $y=mx^b$, where in this case, x=PCL (body length in cm), y is the variable of interest, and b is the scaling exponent. All data were Log_{10} transformed prior to analyses. Linear and area measurements have expected isometric slopes of 1.0 and 2.0, respectively. To compare the scaling exponents to those expected from isometry, the 95% confidence interval of the slope was first calculated. If the expected value fell within the confidence interval, the relationship was considered isometric, but an exponent below or above the expected value was considered negative or positive allometry, respectively. The significance of each regression was assessed using a cutoff of $P<0.05$.

Results

All morphological variables were significantly correlated with body length. An overwhelming majority of the variables had R^2 values > 0.75 (Table 1). Eye-to-eye, frontal span, proximal span, caudal keel circumference, dorsal fin 1, dorsal fin 3, caudal fin 1, caudal fin 2, and dorsal fin area all scaled with isometry. Lateral span, caudal fin upper area, caudal fin lower area, caudal fin area, and head area all scaled with negative allometry. Pectoral fin length, dorsal fin 2, caudal fin 3, pectoral fin area, pectoral fin aspect ratio, and caudal fin aspect ratio exhibited positive allometry (Figs. 2-4; Table 1). For body fineness ratio, values ranged from 1.9 to 4.8. The slope observed was 0.013 with an R^2 value of 0.2 ($p<0.05$). The largest value of 4.8 belonged to the largest individual in our study. All other individuals ranged from 1.9 to 2.7.

Discussion

Scalloped hammerhead sharks undergo significant morphological changes in shape that are likely associated with major shifts in habitat and ecology. Pectoral fin length and area, pectoral fin and caudal fin aspect ratio, dorsal fin height, and the length of the caudal fin lower lobe exhibited positive allometry. These changes point towards an increase in swimming efficiency through reductions in drag, which are indicative of sustained swimming activity. These results suggest that the drastic ecological changes that scalloped hammerheads experience are accompanied by changes in functional demand, leading to allometric patterns of growth.

Caudal fin shape in different habitats

The use of the caudal fin for propulsion is widespread throughout the evolution of fishes (Webb, 1982). Whereas other fishes can also utilize other fins for propulsion, the caudal fin is exclusively responsible for generating thrust in most sharks (Gray, 1933; Alexander, 1965; Ferry and Lauder, 1996). However, the shape of the caudal fin varies considerably among species (Thomson, 1976; Sternes and Shimada, 2020) and this is most likely related to differences in function (Maia et al., 2012). Sharks with more asymmetric caudal fins tend to swim slower but exhibit high maneuverability (Maia *et al*., 2012). Sharks with a more symmetrical caudal fin are faster and often perform long-distance migrations (Lingham-Soliar, 2005a,b; Maia et al., 2012). The caudal fin of scalloped hammerheads in our study transition from a more asymmetric shape as smaller

individuals to a more symmetrical shape as larger more pelagic individuals (Fig. 3; Table 1). This is likely directly associated with the changes in ecology as smaller scalloped hammerheads live in shallow water habitats with limited home ranges. As individual grow larger nearing 100 cm TL, they move into the pelagic realm to perform long distance migrations (Duncan and Hollland, 2006; Hoyos-Padilla et al., 2014; Ebert et al., 2021; Estupiñán-Montaño *et al*., 2021). For example, one individual scalloped hammerhead (95 cm TL) travelled 3,350 km in a 10.5-month period (Hoyos-Padilla et al., 2014). Thus, a high aspect ratio, more symmetrical caudal fin would greatly improve the cost of transport for such distances.

Pectoral fin shape in different habitats

The AR of the pectoral fin in scalloped hammerheads increases with body size (Fig. 4; Table 1). For benthic sharks, the pectoral fins do not generate lift but are critical in vertical movements in the water column and most likely maneuverability (Wilga and Lauder, 2000; 2001). On the other hand, it has been suggested the higher aspect ratio pectoral fins in pelagic sharks generate lift (Lingham-Soliar, 2005a). However, quantitative data supporting this are lacking. Nevertheless, in general, high aspect ratio fins can achieve greater lift and therefore lower the cost of transport (Vogel, 1994; Alexander, 2003; Biewener and Patek, 2018), which is likely necessary for long-distance migrations.

The pectoral fins of scalloped hammerheads appear to follow the similar pattern of benthic and pelagic fishes (Wainwright et al., 2002; Fish and Lauder, 2017). Smaller

scalloped hammerheads live a more benthic life-style which corresponds with low aspect ratio pectoral fins whereas mid-size and larger scalloped hammerheads are more pelagic and they exhibit high aspect ratio pectoral fins. The low aspect ratio pectoral fins likely aid in turning to capture benthic prey, whereas the high aspect ratio pectoral fins provide more lift for the pelagic habitat and long-distance migrations of adults (Fontanella et al., 2013; Martinez et al., 2016). Furthermore, in the pelagic habitat, scalloped hammerheads perform vertical migrations to feed on deep water prey (Klimley, 1993; Jorgensen et al., 2009; Bessudo et al., 2012; Ketchum et al., 2014). Because pectoral fins are critical in vertical movements (Maia et al., 2012), the high aspect ratio pectoral fins of adult scalloped hammerheads are important for lowering cost of transport.

Dorsal fin shape in different habitats

The dorsal fin height of scalloped hammerheads scales with positive allometry (Fig. 2; Table 1). This is highly intriguing as hammerheads generally possess very tall dorsal fins relative to other sharks (Ebert et al., 2021). Depending on location along the body axis, the dorsal fin of sharks either aids in stability or thrust production (Lingham-Soliar, 2005c; Maia and Wilga, 2013; 2016). Scalloped hammerheads possess more anteriorly located dorsal fins which therefore aid in stability. However, scalloped hammerheads are known to perform a peculiar swimming behavior by swimming on a rolled angle of 90 degrees otherwise known as side swimming (Royer et al., 2020). Hydrodynamic models on similarly shaped great hammerheads (*Sphyrna mokarran*) (Rüppell, 1837), which also swim on their side at times, indicate this swimming behavior

may reduce drag or more importantly the cost of transport compared to normal upright swimming (Payne et al., 2016). The large dorsal fin of the hammerhead is hypothesized to generate thrust during rolled swimming. Therefore, the additional thrust from the dorsal fin reduces the cost of transport from the posterior portion of the body (Payne et al., 2016). Interestingly, all scalloped hammerheads that swim on their side ranged from subadult to adult (Royer et al., 2020). This suggests that the positive allometry of the dorsal fin facilitates this swimming behavior in larger individuals. Thus, the larger dorsal fin may benefit larger pelagic scalloped hammerheads when they perform long distance migrations (Duncan and Hollland, 2006; Hoyos-Padilla et al., 2014; Ebert et al., 2021; Estupiñán-Montaño et al., 2021).

Head and body shape in different habitats

The primary function of the hammerhead cephalofoil remains unclear. Previous hypotheses suggested that the cephalofoil increases sensory capabilities, prey capture performance, maneuverability, and lift (Thomson and Simanek, 1977; Strong et al., 1990; Nakaya, 1995; Kajiura et al., 2003; Mara et al., 2015; Gaylord et al., 2020). However, a recent study indicated that the cephalofoil increases maneuverability, but not lift, when comparing the hammerhead cephalofoil to non-hammerhead sharks (Gaylord et al., 2020). This enhanced maneuverability would also aid in prey capture performance (Gaylord et al., 2020). Previous studies (Kajiura, 2001; Cavalcanti, 2004) and our study (Fig. 3; Table 1) indicate that the scalloped hammerhead undergoes a change in head shape as individuals grow larger. Specifically, the head area is negatively allometric (Fig.

3; Table 1) and the head itself becomes compressed on the anterior-posterior axis and expands laterally (Cavalcanti, 2004). If the cephalofoil already increases maneuverability, does the change in head shape alter its overall performance? Because scalloped hammerheads shift their diets from slower benthic prey to quicker pelagic prey (Gallagher and Klimley, 2018; Estupiñán-Montaño et al., 2021) it is possible this change in head shape may further increase maneuverability to aid in the capture of more evasive prey. On the other hand, changes in head shape may be due to sexual maturity which is a pattern observed in bonnethead sharks (Kajiura et al., 2005). Future studies should investigate sexual dimorphism in scalloped hammerheads.

The scalloped hammerhead undergoes changes in its body shape with increase in body size. Specifically, the lateral span is negatively allometric (Fig 3; Table 1). Whereas the lateral span is negatively allometric through change in body size, the posterior portions of the body (i.e., frontal and proximal spans) remain isometric (Fig. 3; Table 1). Previous work found that large scalloped hammerheads had much narrower trunks compared to the anterior body region (Hoffmann et al., 2017). Combined, these indicate that scalloped hammerheads are becoming more streamlined as a result of shifts in functional demands. For any swimming animal, a streamlined body will reduce drag which will in turn lower the cost of transport (Vogel, 1994; Alexander, 2003; Biewener and Patek, 2018). This is especially important for animals that perform long distance migrations including scalloped hammerheads (Hoyos-Padilla et al., 2014).

The optimum fineness ratio to minimize drag is 4.5 (von Mises, 1945; Schlichting, 1979). Previous studies have investigated how this varies among species of

both fishes and whales (Ahlborn et al., 2009; Porter et al., 2009; 2011; Walker et al., 2013). Our values ranged 1.9 to 4.8, with the largest scalloped hammerhead exhibiting a value of 4.8. Although there was considerable variation in fineness ratio among smaller individuals, it is striking that the highest value was observed in the largest individual and is very close to the optimum of 4.5. This suggests that, at a certain length, the scalloped hammerhead may achieve the optimal fineness ratio to minimize drag for long distance migrations. Additional data may reveal if this pattern is consistent among larger scalloped hammerheads.

Future directions

Future studies should quantify the hydrodynamic changes associated with changes in fin and body shape through ontogeny (Long et al., 2010). This will identify the functional consequences of ecomorphological changes that are evident in scalloped hammerheads. Also, more directly measurements of swimming in both nurseries and in the open ocean are needed. What speeds do they use? How often are maneuvers executed? What are the costs of transport? Additionally, future studies can potentially investigate the full ontogenetic change in scalloped hammerheads. Furthermore, investigations of possible sexual dimorphism would be useful to compare to patterns seen in other hammerheads (Kajiura et al., 2005).

References

Ahlborn BK, Blake RW, Chan KHS. 2009. Optimal fineness ratio for minimum drag in larger whales. *Canadian Journal of Zoology* 87: 124–131.

Alexander RM. 1965. The lift produced by the heterocercal tails of Selachii. *Journal of Experimental Biology* 43: 131–138.

Alexander RM. 2003. *Principles of animal locomotion.* Princeton, NJ: Princeton University Press.

Anhelt H, Sauberer M, Ramle D, Koch, L, Pogoreutz C. 2019. Negative allometric growth during ontogeny in the large pelagic filter-feeding basking shark. *Zoomorphology* 139: 71–83.

Bessudo S, Soler GA, Klimley AP, Ketchum J, Arauz R, Hearn A, Guzmán H, Galmettes B. 2012. Vertical and horizontal movements of the scalloped hammerhead shark (*Sphyrna lewini*) around Malpelo and Cocos Islands (Tropical Eastern Pacific) using satellite telemetry. *Bulletin of Marine and Coastal Research* 40: 91–106.

Biewener A, Patek S. 2018. *Animal locomotion, second edition*. Oxford, UK: Oxford University Press.

Calder WA. 1984. *Size, function and life history*. Cambridge, MA: Harvard University Press.

Cavalcanti MJ. 2004. Geometric morphometric analysis of head shape variation in four species of hammerhead sharks (Carcharhiniformes: Sphyrnidae). In: Elewa AMT,

ed. *Morphometrics–applications in biology and paleontology*. Heidleberg, Germany: Springer-Verlag, 97–113.

Clarke TA. 1971. The ecology of the scalloped hammerhead shark, *Sphyrna lewini*, in Hawaii. *Pacific Scientific* 25: 133–144.

Duncan KM, Holland, KN. 2006. Habitat use, growth rates and dispersal patterns of juvenile scalloped hammerhead sharks *Sphyrna lewini* in a nursery habitat. *Marine Ecology Progress Series* 312: 211–221.

Ebert DA, Dando M, Fowler S. 2021. *Sharks of the world: a complete guide*. Princeton, NJ: Princeton University Press.

Estupiñán-Montaño C, Galván-Magaña F, Elorriaga-Verplancken F, Zetina-Rejón MJ, Sánchez-González A, Polo-Silva CJ. Villalobos-Ramírez DJ, Roajs-Cundumí J, Delgado-Huertas A. 2021. Ontogenetic feeding ecology of the scalloped hammerhead shark *Sphyrna lewini* in the Colombian Eastern Tropical Pacific. *Marine Ecology Progress Series* 663: 127–143.

Ferry LA, Lauder GV. 1996. Heterocercal tail function in leopard sharks: A three-dimensional kinematic analysis of two models. *Journal of Experimental Biology* 199: 2253–2268.

Fish FE, Lauder GV. 2017. Control surfaces of aquatic vertebrates: active and passive design and function. *Journal of Experimental Biology* 220: 4351–4363.

Fontanella JE, Fish FE, Barchi E, Campbell-Malone R, Nichols RH, DiNenno NK, Beneski JT. 2013. Two- and three-dimensional geometries of batiods in relation

to locomotor mode. *Journal of Experimental Marine Biology and Ecology* 446: 273–281.

Fu AL, Hammerschlag N, Lauder GV, Wilga CD, Kuo C, Irschick DJ. 2016. Ontogeny of head and caudal fin shape of an apex marine predator: the tiger shark (*Galeocerdo cuvier*). *Journal of Morphology* 277: 556–564.

Gallagher AJ, Hammerschlag N, Shiffman DS, Giery ST. 2014. Evolved for extinction: The cost of and conservation implications of specialization in hammerhead sharks. *BioScience* 64: 619–624.

Gallagher AJ, Klimley AP. 2018. The biology and conservation status of the large hammerhead shark complex: the great, scalloped, and smooth hammerheads. *Reviews in Fish Biology and Fisheries* 28: 777–794.

Gaylord MK, Blades EL, Parsons GR. 2020. A hydrodynamics assessment of the hammerhead shark cephalofoil. *Scientific Reports* 10: 14495.

Gray J. 1933. The movement of fish with special reference to the eel. *Journal of Experimental Biology* 10: 88–104.

Grubbs RD. 2010. Ontogenetic shifts in movements and habitat use. In: Carrier JC, Musick JA, Heithaus MR, eds. *Sharks and their relatives II: Biodiversity, adaptive physiology, and conservation*. Boca Raton, FL: CRC Press, 319–350.

Higham TE, Seamone SG, Arnold A, Toews D, Janmohamed Z, Smith SJ, Rogers SM. 2018. The ontogenetic scaling of form and function in the spotted ratfish, *Hydrolagus colliei* (Chondrichthyes: Chimaeriformes): Fins, muscles, and locomotion, *Journal of Morphology* 279: 1408–1418.

Higham TE, Ferry LA, Schmitz L, Irschick DJ, Starko S, Anderson PS, Bergmann PJ, Jamniczky HA, Monteiro LR, Navon D, Messier J, Carrington E, Farina SC, Feilich KL, Hernandez LH, Johnson MA, Kawano SM, Law CJ, Longo SJ, Martin CH, Martone PT, Rico-GuevaraA, Santana SE, Niklas KJ. 2021. Linking ecomechanical models and functional traits to understand phenotypic diversity. *Trends in Ecology & Evolution* DOI:https://doi.org/10.1016/j.tree.2021.05.009

Hoffmann SL, Warren SM, Porter ME. 2017. Regional variation in undulatory kinematics of two hammerhead species: the bonnethead (*Sphyrna tiburo*) and the scalloped hammerhead (*Sphyrna lewini*). *Journal of Experimental Biology* 220: 3336–3343.

Hoffmann SL, Buser TJ, Porter ME. 2020. Comparative morphology of shark pectoral fins. *Journal of Morphology* 281: 1501–1516.

Hoyos-Padilla EM, Ketchum JT, Klimley AP, Galván-Magaña F. 2014. Ontogenetic migration of a female scalloped hammerhead shark *Sphyrna lewini* in the Gulf of California. *Animal Biotelemetry* 2: 17.

Irschick DJ, Hammerschlag N. 2014. Morphological scaling of body form in four shark species differing in ecology and life history. *Biological Journal of the Linnean Society* 114: 126–135.

Irschick DJ, Fu A, Lauder G, Wilga C, Kuo C, Hammerschlag N. 2017. A comparative morphological analysis of body and fin shape for eight shark species. *Biological Journal of the Linnean Society* 122: 589–604.

Jorgensen SJ, Klimley AP, Muhlia-Melo AF. 2009. Scalloped hammerhead shark *Sphyrna lewini*, utilizes deep-water, hypoxic zone in Gulf of California. *Journal of Fish Biology* 74: 1682–1687.

Kajiura SM. 2001. Head morphology and electrosensory pore distribution of carcharhinid sharks and sphyrnid sharks. *Environmental Biology of Fishes* 61: 125–133.

Kajiura SM, Forni JB, Summers AP. 2003. Maneuvering in juvenile carcharhinid and sphyrnid sharks: The role of the hammerhead shark cephalofoil. *Zoology* 106: 19–28.

Kajiura SM, Tyminski JP, Forni JB, Summers AP. 2005. The sexually dimorphic cephalofoil of bonnethead sharks, *Sphyrna tiburo*. *Biological Bulletin* 209: 1–5.

Ketchum JT, Hearn A, Klimley AP, Espinoza E, Peñaherrera C, Largier JL. 2014. Seasonal changes in movements and habitat preferences of the scalloped hammerhead shark (*Sphyrna lewini*) while refuging near an oceanic island. *Marine Biology* 161: 755–767.

Klimley AP. 1987. The determinants of sexual segregation in the scalloped hammerhead, *Sphyrna lewini*. *Environmental Biology of Fishes* 18: 27–40.

Klimley AP. 1993. Highly directional swimming by scalloped hammerhead sharks, *Sphyrna lewini*, and subsurface irradiance, temperature, bathymetry, and geomagnetic field. *Marine Biology* 117: 1–22.

Klimley AP, Butler SB, Nelson DR, Stull AT. 1988. Diel movements of scalloped hammerhead sharks, *Sphyrna lewini* Griffith and Smith, to and from a seamount in the Gulf of California. *Journal of Fish Biology* 33: 751–761.

Koehl MAR. 1996. When does morphology matter? *Annual Review of Ecology, Evolution, and Systematics* 27: 501–542.

LaBarbera M. 1989. Analyzing body size as a factor in ecology and evolution. *Annual Review of Ecology and Systematics* 20: 97–117.

Lingham-Soliar T. 2005a. Caudal fin allometry in the white shark *Carcharodon carcharias*: Implications for locomotory performance and ecology. *Naturwissenschaften* 92: 231–236.

Lingham-Soliar T. 2005b. Caudal fin in the white shark, *Carcharodon carcharias* (Lamnidae): A dynamic propeller for fast, efficient swimming. *Journal of Morphology* 264: 233–252.

Lingham-Soliar T. 2005c. Dorsal fin in the white shark, *Carcharodon carcharias*: A dynamic stabilizer for fast swimming. *Journal of Morphology* 263: 1–11.

Long JH, Porter ME, Root RG, Liew CW. Go reconfigure: How fish change shape as they swim and evolve. *Integrative Comparative Biology* 50: 1120–1139.

Maia AMR, Wilga CAD, Lauder GV. 2012. Biomechanics of locomotion in sharks, rays, and chimaeras. In: Carrier JC, Musick JA, Heithaus MR, eds. *Biology of sharks and their relatives: second edition*. Boca Raton, FL: CRC Press, 125–151.

Maia A, Wilga C. 2013. Function of dorsal fins in bamboo sharks during steady swimming. *Zoology* 116: 224–231.

Maia A, Wilga CA. 2016. Dorsal fin function in spiny dogfish during steady swimming. *Journal of Zoology* 298: 139–149.

Mara KR, Motta PJ, Martin AP, Hueter RE. 2015. Constructional morphology within the head of hammerhead sharks (Sphyrnidae). *Journal of Morphology* 276: 526–539.

Martinez CM, Rohlf FJ, Frisk MG. 2016. Re-evaluation of batoid pectoral fin morphology reveals novel patterns of diversity among major lineages. *Journal of Morphology* 277: 482–493.

Mittelbach GG, Osenberg CW. 1993. Stage-structured interactions in bluegill: consequences of adult resource variation. *Ecology* 74: 2381–2394.

Nakaya K. 1995. Hydrodynamic function of the head in hammerhead sharks (Elasmobranchii: Sphyrnidae). *Copeia* 1995: 330–337.

Olson MH. 1996. Ontogenetic niche shifts in largemouth bass: variability and consequences for first-year growth. *Ecology* 77: 179–190.

Payne NL, Iosilevskii G, Barnett A, Fischer C, Graham RT, Gleiss AC, Watanable YY. 2016. Great hammerhead sharks swim on their side to reduce transport costs. *Nature Communications* 7: 12289.

Porter ME, Roque CM, Long Jr. JH. 2009. Turning maneuvers in sharks: Predicting body curvature from axial morphology. *Journal of Morphology* 270: 954–965.

Porter ME, Roque CM, Long Jr. JH. 2011. Swimming fundamentals: Turning maneuvers in leopard sharks (*Triakis semifasciata*) is predicted by body shape and postural reconfiguration. *Zoology* 114: 348–359.

Reiss KL, Bonnan MF. 2010. Ontogenetic scaling of caudal fin shape in *Squalus acanthias* (Chondrichthyes, Elasmobranchii): A geometric morphometric analysis

with implications for caudal fin functional morphology. *The Anatomical Record* 293: 1184–1191.

Roff G, Doropoulos C, Rogers A, Bozec Y, Krueck NC, Aurellado E, Priest M, Birrell C, Mumby PJ. 2016. The ecological role of sharks on coral reefs. *Trends in Ecology and Evolution* 31: 395–407.

Royer M, Maloney K, Meyer C, Cardona E, Payne N, Whittingham K, Silva G, Blandino C, Holland K. 2020. Scalloped hammerhead sharks swim on their side with diel shifts in roll magnitude and periodicity. *Animal Biotelemetry* 8:11.

Schlichting H. 1979. *Boundary layer theory*. New York: McGraw Hill.

Schmidt-Nielsen K. 1984. *Scaling: Why is animal size so important?* Cambridge: Cambridge University Press.

Sillet KB, Foster SA. 2000. Ontogenetic niche shifts in two populations of juvenile threespine stickleback, *Gasterosteus aculeatus*, that differ in pelvic spine morphology. *Oikos* 90: 468–476.

Spoljaric MA, Reimchen TE. 2011. Habitat specific trends in ontogeny of body shape in stickleback from coastal archipelago: Potential for rapid shifts in colonizing populations. *Journal of Morphology* 272: 590–597.

Sternes PC, Shimada K. 2020. Body form in sharks (Chondrichthyes: Elasmobranchii) and their functional, ecological, and evolutionary implications. *Zoology* 140: 125799.

Stillwell CE, Kohler NE. 1982. Food, feeding habits, and estimates of daily ration of the shortfin mako (*Isurus oxyrinchus*) in the northwest Atlantic. *Canadian Journal of Fisheries and Aquatic Sciences* 39: 407–414.

Strong Jr. WR, Snelson Jr. FF, Gruber SH. 1990. Hammerhead shark predation on stingrays: An observation of prey handling by *Sphyrna mokarran*. *Copeia* 1990: 836–840.

Svanbäck R, Eklöv P. 2002. Effects of habitat and food resources on morphology and ontogenetic growth trajectories in perch. *Oecologia* 131: 61–70.

Thomson KS. 1976. On the heterocercal tail in sharks. *Paleobiology* 2: 19–38.

Thomson KS, Simanek DE. 1977. Body form and locomotion in sharks. *American Zoologist* 17: 343–354.

Tricas TC. 1984. Predatory behavior of the white shark (*Carcharodon carcharias*), with notes on its biology. *Proceedings of the California Academy of Sciences* 43: 221–238.

Vogel S. 1994. *Life in moving fluids: The physical biology of flow, second edition*. Princeton: Princeton University Press.

von Mises R. 1945. *Theory of flight*. New York: Dover.

Wainwright PC, Reilly SM. 1994. *Ecological morphology: Integrative organismal biology*. Chicago: University of Chicago Press.

Wainwright PC, Bellwood DR, Westneat MW. 2002. Ecomorphology of locomotion in labrid fishes. *Environmental Biology of Fishes* 65: 47–62.

Walker JA, Alfaro ME, Noble MM, Fulton CJ. 2013. Body fineness ratio as a predictor of maximum prolonged-swimming speed in coral reef fishes. *PLoS One* 8: e75422.

Ward-Campbell BMS, Beamish FWH. 2005. Ontogenetic changes in morphology and diet in the snakehead, *Channa limbata*, a predatory fish in Western Thailand. *Environmental Biology of Fishes* 72: 251–257.

Webb PW. 1982. Locomotor patterns in the evolution of Actinopterygian fishes. *American Zoologist* 22: 329–342.

Webb PW. 1984. Body form, locomotion and foraging in aquatic vertebrates. *American Zoologist* 24: 107–120.

Wells RJD, TinHan, TC, Dance MA, Drymon JM, Falterman B, Ajemian MJ, Stunz GW, Mohan JA, Hoffmayer ER, Driggers III WB, McKinney JA. 2018. Movement, behavior, and habitat use of a marine apex predator, the scalloped hammerhead. *Frontiers in Marine Science* 5: 1–14.

Wilga CD, Lauder GV. 2000. Three-dimensional kinematics and wake structure of the pectoral fins during locomotion in leopard sharks *Triakis semifasciata*. *Journal of Experimental Biology* 203: 2261–2278.

Wilga CD, Lauder GV. 2001. Functional morphology of the pectoral fins in bamboo sharks, *Chiloscyllium plagosium*: Benthic vs. pelagic station-holding. *Journal of Morphology* 249: 195–209.

Table 1.1. Scaling relationships for the variables examined in this study. NA=Not applicable.

Variable	N	R^2	P value	Exp slope	Obs slope	SE slope	lower CI	Upper CI	Scaling
Eye to Eye	49	0.96	<0.001	1.00	0.929	0.024	0.857	1.001	Isometric
Head Area	28	0.93	<0.001	2.00	1.746	0.09	1.533	1.901	Negative
Lateral Span	50	0.81	<0.001	1.00	0.794	0.059	0.676	0.913	Negative
Frontal Span	50	0.79	<0.001	1.00	0.875	0.068	0.739	1.012	Isometric
Proximal Span	50	0.76	<0.001	1.00	0.874	0.076	0.721	1.026	Isometric
Caudal Keel Circ	50	0.92	<0.001	1.00	0.888	0.039	0.769	1.006	Isometric
Pectoral Fin Length	50	0.93	<0.001	1.00	1.172	0.064	1.078	1.267	Positive
Pectoral Fin Area	28	0.94	<0.001	2.00	2.171	0.01	1.987	2.355	Positive
Pectoral Fin *AR*	28	0.24	<0.01	0	0.328	0.11	0.144	0.488	NA
Dorsal Fin 1	48	0.94	<0.001	1.00	0.968	0.035	0.866	1.07	Isometric
Dorsal Fin 2	48	0.90	<0.001	1.00	1.287	0.058	1.127	1.453	Positive
Dorsal Fin 3	50	0.92	<0.001	1.00	1.015	0.038	0.922	1.108	Isometric
Dorsal Fin Area	27	0.91	<0.001	2.00	2.039	0.013	1.769	2.258	Isometric
Dorsal Fin *AR*	27	0.009	0.645	0	-0.052	0.112	-0.28	0.208	NA
Caudal Fin 1	50	0.98	<0.001	1.00	1.01	0.018	0.946	1.055	Isometric
Caudal Fin 2	50	0.96	<0.001	1.00	1.09	0.033	0.989	1.192	Isometric
Caudal Fin 3	50	0.91	<0.001	1.00	1.203	0.033	1.034	1.373	Positive
Caudal Fin Up Area	29	0.92	<0.001	2.00	1.725	0.012	1.549	1.892	Negative
Caudal Fin L. Area	29	0.86	<0.001	2.00	1.87	0.015	1.655	2.176	Negative
Caudal Fin T. Area	29	0.91	<0.001	2.00	1.752	0.019	1.594	1.936	Negative
Caudal Fin *AR*	29	0.29	<0.001	0	0.45	0.114	0.200	0.623	NA

Figure Legends

Figure 1.1 Diagram of scalloped hammerhead with morphological variables measured in this study (See Materials and Methods for more detailed descriptions of each measurement). The upper panel is a lateral view and the lower panel is a ventral view. PCL, pre-caudal length; DFA, dorsal fin area; DF1, dorsal fin 1, distance from the anterior insertion point of the dorsal fin to the tip of the dorsal fin; DF2, dorsal fin 2, distance from the tip of the dorsal fin to the posterior insertion point of the dorsal fin; DF3, dorsal fin 3, distance horizontally across the shark body between the anterior and posterior insertion points of the dorsal fin; EE, distance between the inner part of the eyes; LS, lateral span, the distance from (i.e. around the curved dorsal side of the shark) from the insertion point of the anterior edge of one pectoral fin to the insertion point of the other pectoral fin; FS, frontal span, the distance (i.e. around the curved dorsal side of the shark) from the insertion point of the anterior edge of the dorsal fin to a line oriented parallel to the horizontal plane of the pectoral fin; PS, proximal span, the distance spanning (i.e. around the curved dorsal side of the shark) from the insertion point of the posterior edge of the dorsal fin to a line oriented parallel to the horizontal plane of the pectoral fin; CKC, caudal keel circumference, total circumference at the base of the tail as measured at the caudal keel; PFA, pectoral fin area; PFL, pectoral fin length, the linear distance from the insertion of the pectoral fin at the distal edge to the tip of the pectoral fin when fully extended; CFA, caudal fin area; CF1, caudal fin 1, the linear distance from the dorsal insertion of the caudal fin to the dorsal tip of the caudal fin; CF2, caudal fin 2, the linear distance from the dorsal tip of the caudal fin to the ventral tip of the bottom part

of the caudal fin; CF3, caudal fin 3, the linear distance from the bottom anterior edge of the caudal fin to the bottom posterior edge of the caudal fin.

Figure 1.2 Scaling relationships between log-transformed values of pre-caudal length (PCL) and (A) pectoral fin length (PFL) (B) pectoral fin area (PFA) (C) dorsal fin 2 (DF2, i.e., overall height in length of dorsal fin (D) caudal fin 3 (CF3, i.e., length of lower lobe). All relationships show positive allometry. Each point on the graphs represents an individual. See Fig. 1 for how each variable was measured. Dashed line represents the expected slope under isometry, and the solid line represents the regression using our data.

Figure 1.3 Scaling relationships between long transformed values of pre-caudal length (PCL) and (A) head area (HA) (B) lateral span (LS) (C) caudal fin upper area (CFUA) (D) caudal fin lower area (CFLA). All relationships show negative allometry. Each point on the graphs represents an individual. See Fig. 1 for how each variable was measured. Dashed line represents the expected slope under isometry, and the solid line represents the regression using our data.

Figure 1.4 Scaling relationships between log-transformed values of pre-caudal length (PCL) and (A) dorsal fin aspect ratio (DFAR) (B) pectoral fin aspect ratio (PFAR) (C)

caudal fin aspect ratio (CFAR). PFAR and CFAR were positively related to body size whereas DFAR was negatively associated with body size. Each point on the graphs represents an individual. Solid line represents regression using our data.

Figure 1.1. Diagram of scalloped hammerhead with morphological variables measured in this study

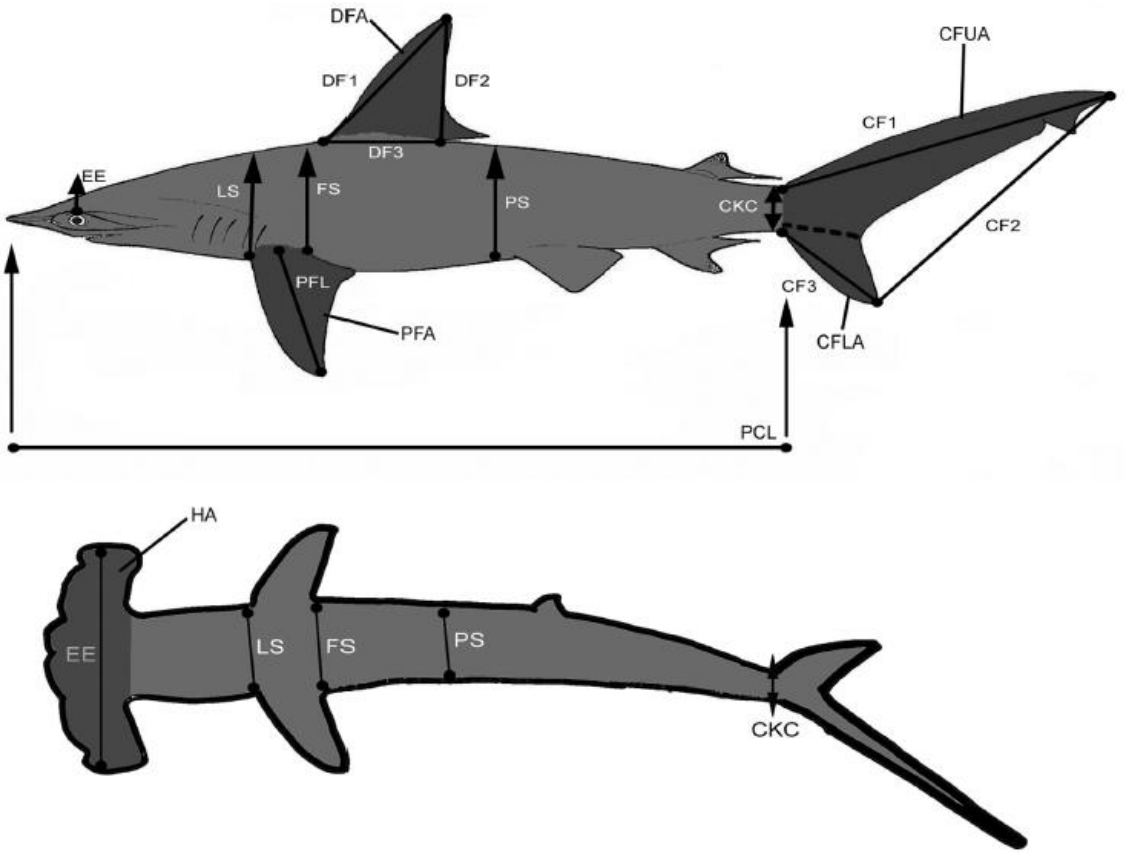

Figure 1.2. Scaling relationships between log10-transformed values of precaudal length (PCL) and: A, pectoral fin length (PFL); B, pectoral fin area (PFA); C, dorsal fin 2 (DF2, i.e. overall height in length of dorsal fin; and D, caudal fin 3 (CF3, i.e. length of lower lobe).

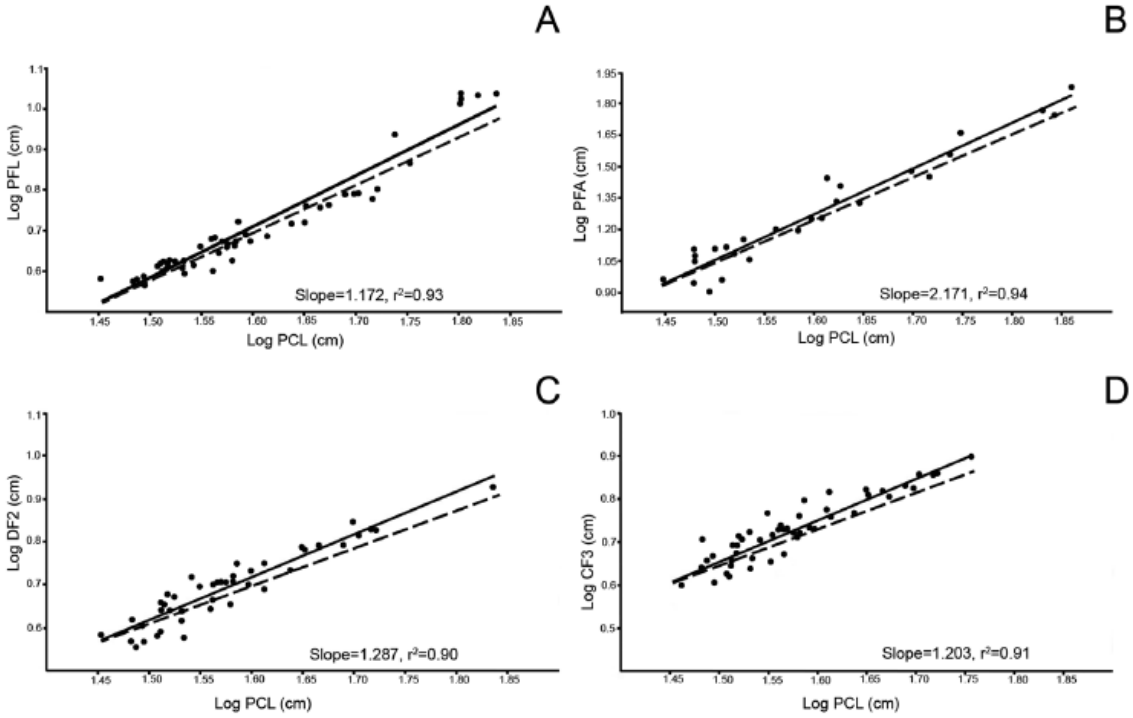

Figure 1.3. Scaling relationships between log10-transformed values of precaudal length (PCL) and: A, head area; B, lateral span (LS); C, caudal fin upper area (CFUA); and D, caudal fin lower area (CFLA).

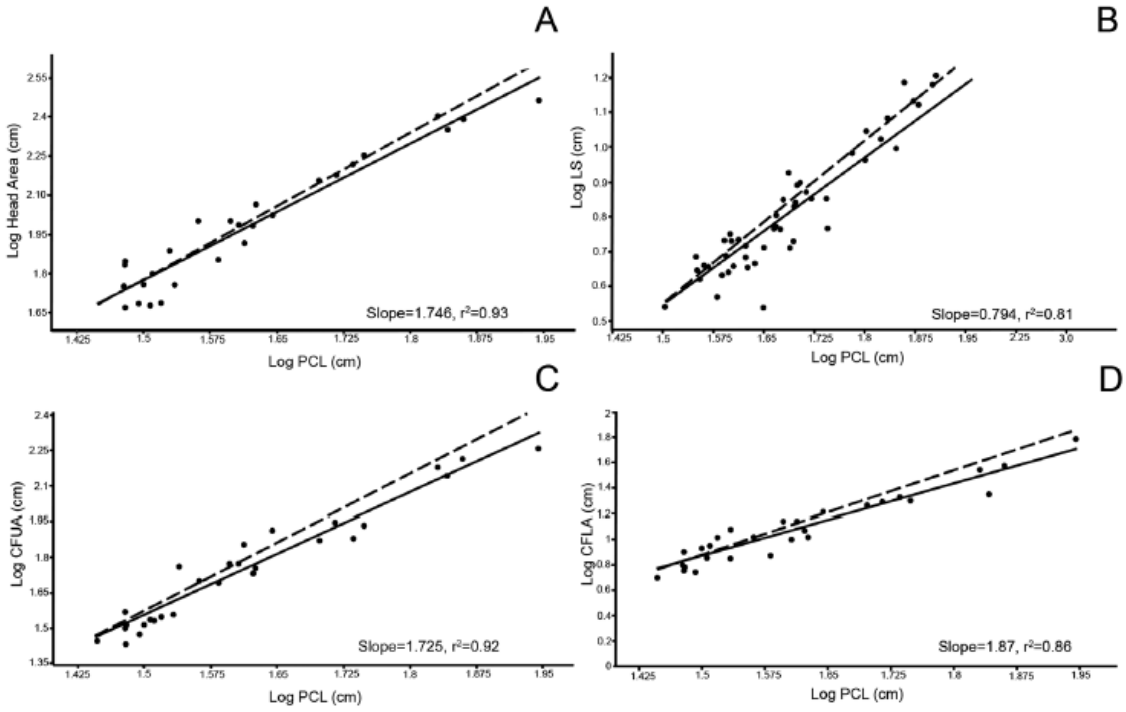

Figure 1.4. Scaling relationships between log10-transformed values of precaudal length (PCL) and: A, dorsal fin aspect ratio (DFAR); B, pectoral fin aspect ratio (PFAR); and C, caudal fin aspect ratio (CFAR).

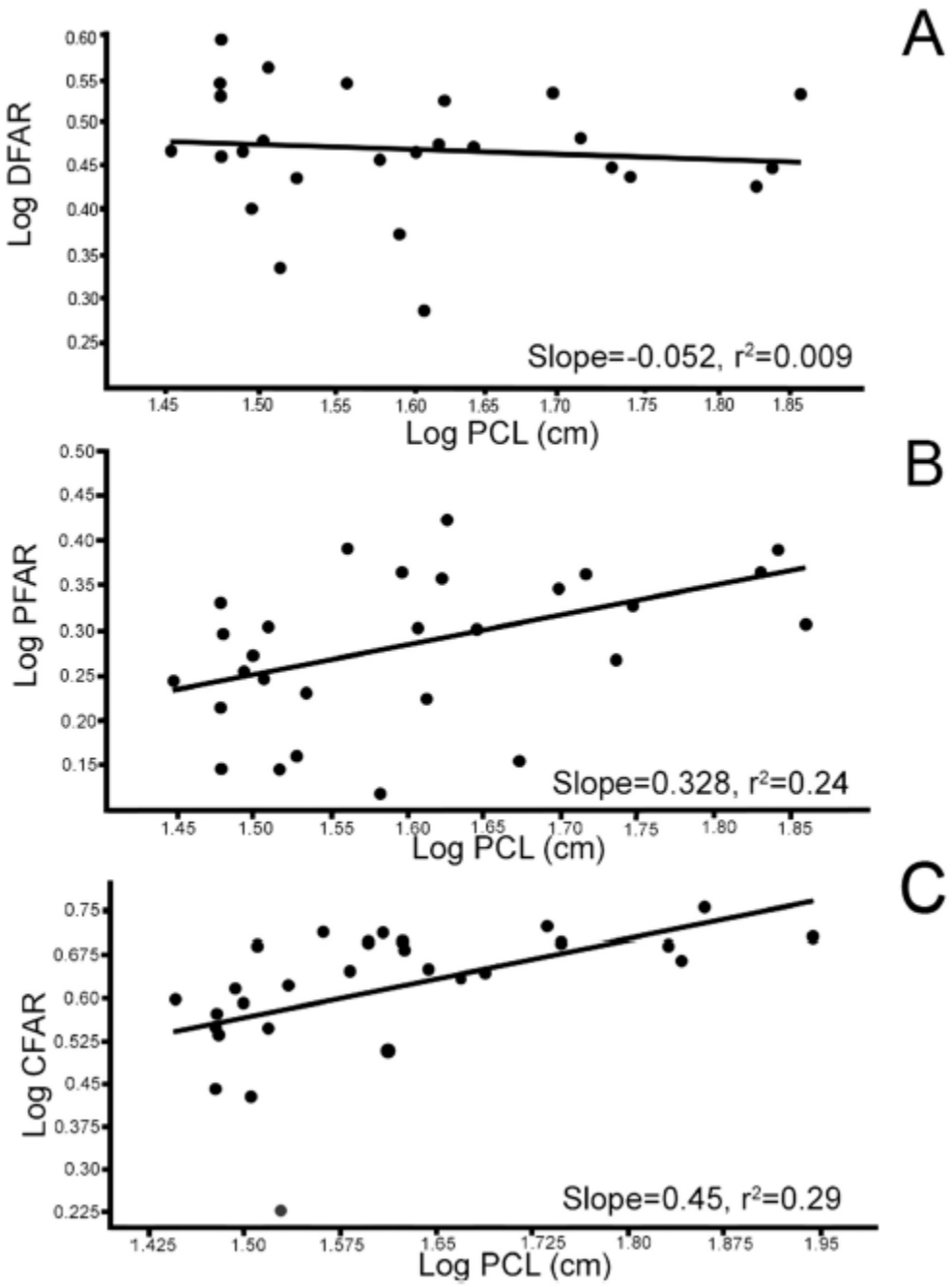

CHAPTER 2

The rise of Pelagic Sharks and Adaptive Evolution of Pectoral fin Morphology During the Cretaceous

Abstract

One of the greatest innovations in the history of vertebrates is the evolution of paired appendages. Fins and limbs are critical for locomotion and have thus played central roles during major habitat transitions throughout the long evolutionary history of vertebrates. The causes of these transitions, along with the associated changes to the locomotor systems of the animals, remain of great interest to biologists. Whereas some of these changes have been heavily investigated, there are major habitat expansions within the marine realm that remain poorly understood. Sharks (Chondrichthyes: Selachii) are among the oldest and most successful clades to invade nearly every part of the marine ecosystem. However, how and when selachians became established in open-water habitats is not well known. Here we present an integrative macroevolutionary, ecomechanical, and ecophysiological perspective on the expansion of selachian sharks into the pelagic zone. Stochastic character mapping revealed selachians were benthic or benthopelagic in origin and expanded to the pelagic zone no later than the Early Cretaceous. This initial shift coincided with an increase in pectoral fin aspect ratio (AR). Subclade disparity of AR increased during the Cretaceous Thermal Maximum (CTM), when sea surface temperatures (SST) of up to 28.2˚C (global average) likely caused elevated swimming performance in sharks. We show that climate change likely impacted the change in habitat occupancy and accompanying pectoral fin evolution.

Introduction

The emergence of paired appendages remains one of the greatest evolutionary innovations in the history of vertebrates (Romer, 1967; Coates, 2003; Shubin et al., 2009; Lauder, 2015). Paired fins were one of several innovations that likely led to a drastic rise in fish diversity during the Devonian, which is known as the 'Age of Fishes' (Alfaro et al., 2009; Friedman and Sallan, 2012). Subsequently, pectoral fins, which are critical control surfaces for fish swimming, would continue to evolve during the major habitat expansions that vertebrates have experienced throughout their history (Romer, 1967; Rayner, 1988; Coates, 2003; Long and Gordon, 2004; Uhen, 2007; Shubin et al., 2009; Lauder, 2015). For example, the expansion from water to land involved substantial changes to the pectoral region in the axial skeleton as a result of the increase in gravitational forces (Romer, 1967; Coates, 2003; Long and Gordon, 2004; Shubin et al., 2009). The aquatic habitat itself includes different ecological zones (i.e., benthic to pelagic) and vertebrates display a strong relationship between appendage form and ecology. For instance, pectoral fin aspect ratio (AR) is routinely used to estimate the swimming behavior and capabilities of ray-finned fishes, as higher AR pectoral fins are found in fast open water cruisers compared to the lower AR pectoral fins that are often observed in slower but more maneuverable species (Vogel, 1994; Wainwright et al., 2002; Weihs, 2002; Blake, 2004; Kane and Higham, 2012; Fish and Lauder, 2017). Ecomorphological analyses of ray finned fishes have provided insights into fish ecology and evolution (Vogel, 1994; Wainwright et al., 2002; Weihs, 2002; Blake, 2004; Kane and Higham, 2012; Fish and Lauder, 2017). However, there remains a paucity of data on

the evolution of pectoral fins among several groups of fishes including lineages with long evolutionary histories such as the cartilaginous fishes (Compagno, 1990; Heinicke et al., 2009; Grogan et al., 2012).

Cartilaginous fishes (Chondrichthyes) are one of the oldest clades of vertebrates with paired fins that have persisted throughout global changes and all four mass extinctions (Compagno, 1990; Heinicke et al., 2009; Grogan et al., 2012). Their earliest ancestors appeared over 400 million years ago (mya) with the selachian shark lineage originating about 200 mya (Compagno; 1977; Compagno, 1990; Heinicke et al., 2009; Grogan et al., 2012; Maisey, 2012). Over their evolutionary history, selachians have invaded nearly every area of the marine realm, including bottom dwelling ambush predators, obligate reef specialists, and migratory oceanic nomads (Compagno, 1990). In many marine communities, selachians occupy a high trophic position (Compagno, 1990; Cortés, 1999), perhaps best represented by iconic megapredators such as the extinct 'Megalodon' (†*Otodus megalodon*) and the extant white shark (*Carcharodon carcharias*) (McCormack et al., 2022). Alongside the orca (*Orcinus orca*, Cetacea), the white shark is the latest iteration of an evolutionary succession of macrophagous apex predators since the Middle Triassic, about 245 mya, following ichthyosaurs, pliosaurs, marine crocodilians and mosasaurs (Fröbisch et al., 2013). Despite the prominence of great white sharks in the public sphere, only about 13% of modern selachians are pelagic (Materials and Methods).

As a historical archive of evolution, the fossil record may provide the most direct answer as to when selachians evolved pelagic lifestyles and what role pectoral fins had in this habitat expansion. Indeed, fossils demonstrate that sharks have expanded to new habitats in their extended history (Thies and Reif, 1985). Although selachians are known primarily from teeth in the fossil record, some preserved body forms, including pectoral fins, have suggested that sharks occupied different habitats (Kriwet and Klug, 2004; Vullo et al., 2021; 2024). For example, fossil evidence suggests that the Late Cretaceous shark, *Aquilolamna mircae*, used its highly elongated pectoral fins as stabilizers for swimming in the pelagic zone (Vullo et al., 2021). However, fossils that preserve fin shape are exceedingly rare and come from a small number of localities which were mostly formed in shallow water restricted marine environments (Schweigert et al., 1996; Kriwet and Klug, 2004; Friedman and Carnevale, 2018). Thus, there remains a very limited and poor understanding of the timing, anatomical changes, and ecological and evolutionary context of the expansion to pelagic habitats (Thies and Reif, 1985; Kriwet and Klug, 2004; Sorenson et al., 2014; Vullo et al., 2021; 2024).

The distribution of preferred habitats over a time-calibrated phylogeny, along with considerations of locomotor biomechanics of extant species, can offer important additional data on the timing and mechanism of habitat evolution in selachians. The evolution of shark locomotion has garnered considerable interest given that they are an ecologically and behaviorally diverse lineage from one of the oldest vertebrate clades (Lauder and Di Santo, 2016). In addition to their stiff integument used during locomotion (Wainwright et al., 1978), selachians are distinct in having a heterocercal caudal fin and

ventrolateral wing-like pectoral fins that remain extended laterally from the body during swimming (Maia et al., 2012; Lauder and Di Santo, 2016). Whereas benthic selachians often use their pectoral fins to generate negative lift (to stay on the substrate), the pectoral fins of pelagic selachians are actively adjusted in order to move vertically in the water column as they swim at relatively high speeds (Fish and Shannahan, 2000; Wilga and Lauder; 2000, 2001; Maia et al., 2012; Lauder and Di Santo, 2016). Given that moving quickly in water places substantial demands on the animal due to elevated drag (proportional to velocity^2), there should be strong selection on pectoral fin AR (Vogel, 1994; Fish and Lauder, 2017). Although recent work using 18 species of sharks found no significant impact of habitat on pectoral fin shape, a more robust approach with a much larger sample size is warranted (Hoffmann et al., 2020).

Here we present an ecomechanical (Higham et al., 2021) and ecophysiological perspective on the macroevolution of selachians, focusing on two primary hypotheses: 1) Given that the large majority of extant neoselachians (selachians and batoids) are benthic or benthopelagic, we hypothesized that selachians expanded into the pelagic zone from benthic ancestors; and 2) Based on predictions from pectoral fin functional morphology, we hypothesized that open-water sharks have pectoral fins with a higher AR than bottom-associated sharks, resulting from processes of adaptive evolution. Using a time-calibrated molecular phylogeny (Stein et al., 2018), we estimated the origin of pelagic selachians through ancestral state reconstructions, and then analyzed the evolutionary consequences of different marine habitats on biomechanically relevant pectoral fin shape with phylogenetic comparative methods for 490 species of extant selachians. Within the

context of historical sea-surface temperatures (Scotese et al., 2021) and inferred swimming performance, the early Late Cretaceous emerges as a decisive phase in the evolution of marine communities.

Materials and Methods

Morphological Trait Data and Measurements

Following the approaches in previous studies (Sternes and Shimada, 2020; Vanderwright et al., 2020; Vullo et al., 2021; Bigman et al., 2023; Iliou et al., 2023; Sternes et al., 2023; Siders et al., 2023; Vullo et al., 2024) we used the illustrations of every extant selachian shark species from *Sharks of the World: A Fully Illustrated Guide* by Ebert et al. (2013). The purpose of the book is to help readers in identifying sharks and it consists of nearly 500 shark species drawn in lateral view except for the order Squatiniformes which is drawn in dorsal view. Additionally, in this specific field guide, there is a scale bar for each illustration. Both Sternes and Shimada (2020) and Siders et al. (2023) have performed analyses comparing the illustrations from the book to real shark specimens to test for their accuracy and reliability. No major significant differences between the illustrations and preserved shark specimens were determined (Sternes and Shimada, 2020; Siders et al., 2023). As a guidebook, the pectoral fins are pointed ventrally (except Squatiniformes) to aid readers in comparing the shape of specimens to the illustrations for species identification. Therefore, the complete shape of the pectoral fin (e.g., area and fin length) are clearly drawn in a planar orientation. Since Squatiniformes are flattened sharks, they are presented in dorsal view but this still depicts

the full pectoral fin shape in a planar view. Each measurement taken from the illustrations is listed in **S2.1**. For fossil species, we used previously published images and museum specimens and each measurement is listed in **S2.2**. We used ImageJ to measure the precaudal length (PCL), total length (TL), pectoral fin length, and pectoral fin area. We calculated the aspect ratio (AR) of each fin defined as L^2/S, where L and S are the length and area of each fin, respectively.

Habitat Categorization

Species were coded as one of three habitat types, 'benthic', 'benthopelagic', or 'pelagic' based on their habitat descriptions from Ebert et al. (2021). We coded each species as 'benthic' based on habitat keywords of 'benthic,' 'on muddy bottom,' 'on sediment,' 'bottom on insular continental shelves.' Species were coded as 'benthopelagic' based on the key terms of 'demersal,' 'near bottom,' or 'near continental shelves.' Species were coded as 'pelagic' based on the keywords of 'pelagic,' 'epipelagic,' 'bathypelagic,' 'open ocean,' or 'oceanic' (note: functionally, water depth is not critical for classification of pelagic).

Phylogenetic Comparative Methods

We performed phylogenetic comparative methods on the basis of a dated taxon-complete tree for chondrichthyans with a pseudo-posterior distribution of 10,000 fully resolved trees (Stein et al., 2018). This tree was time-calibrated with treePL, informed by 10 calibration fossils and a soft bound on the root node of 422 mya. The backbone of our

analysis rests on the maximum clade credibility (MCC) tree, but we accounted for phylogenetic uncertainty as indicated below.

We estimated the evolutionary history of preferred habitat with stochastic character mapping (Bollback, 2006) implemented in the R (R Core Team, 2022) package "phytools" (Revell, 2012). We generated 1,000 trait mappings over the MCC tree with all-different transition rates (ARD), as this transition model appeared to be best supported in initial computations (see **S2.4**). To test the robustness of the root state estimate, we iterated the stochastic character mapping over a random sample of 1000 trees from the pseudoposterior distribution, generating 1000 trait mappings. We assessed the robustness of ancestral state estimates by comparing the proportions of inferred states.

To illustrate the phylogenetic and overall distribution of data on AR and PCL, we chose phylogenetic barplots and boxplots (**Figure 2.1**). As an initial exploratory tool, we assessed possible differences between different groups of preferred habitat with phylogenetic ANOVAs (Garland Jr. et al., 1993; implemented in "phytools'), in which the P-value is estimated through simulations (N=1,000) in a BM framework, the simplest evolutionary model of trait evolution. In addition, we applied a new version of phylogenetic ANOVA (RRPP), (Adams and Collyer, 2022). RRPP uses generalized least-square approaches with phylogenetic correlation to calculate the F-statistics and randomizes residuals in a permutation procedure instead of simulations.

Given that the patterns of AR and PCL are similar, we tested if AR scaled with PCL using phylogenetic generalized least-square regressions (Grafen, 1989). We assessed the support for different linear models, specifically, a simple, an intercept, and

an interaction model for linear fits using both a Brownian motion (BM) and an Ornstein-Uhlenbeck (OU) correlation structure, implemented in the "nlme" package (Pinheiro and Bates, 2000, 2022) for R. The simple model does not allow for differences across habitat groups and fits a single line to all data. The intercept model fits lines for each habitat group separately, but only the intercept is free to vary, the slope is forced to be equal for each group. The interaction model, finally, lets all slopes and intercepts vary. AIC scores and corresponding Akaike weights point to the BM interaction model as the best linear fit (see **S2.2**). P-values of this linear model reveal that if there is a correlation between AR and PCL it is only present in pelagic neoselachians. In addition, the bivariate scatterplot of AR and PCL illustrates the high variance of AR for given PCL (see **S2.1**). We therefore passed on AR and PCL to additional phylogenetic comparative methods and did not calculate residuals of AR (Wainwright et al., 2002).

To determine the mode of AR and PCL evolution and test for presence of adaptive signals in the data, we turned to evolutionary model fitting with mvMORPH (Clavel et al., 2015). We iterated the model fitting over a random subsample (N=100) from the pseudo-posterior tree distribution and specifically compared the fit of the following models of trait evolution:

- BM1, a BM model with a single rate for each trait;
- BMM, a BM model that allows different rates for each trait;
- EB, a model of trait evolution with initially fast rates that slow over time (early burst model);

- OU, an Ornstein-Uhlenbeck model of trait evolution with one selective regime for the whole tree (single peak OU model); and
- OUM, an Ornstein-Uhlenbeck model of trait evolution with multiple selective regimes for the tree, corresponding to pre-defined groups (multi-peak OU model). TO test fo hypotheses of evolutionary lag, i.e., with one trait trailing another, can be tested with asymmetrical alpha matrices (diagonal, upper, lower).

We determined the best fitting model via AIC scores and Akaike weights (see **S2.2** and **S2.3**). The OUM models emerged as the by far best supported models, yet there were no clear differences between the four OUM versions we tried (OUM, OUM diagonal, OUM upper, OUM lower). We therefore summarized the results of the basic OUM model (see **S2.4** and **S2.5**).

Next, we turned to an agnostic approach to characterize the adaptive landscape of AR evolution, a Bayesian implementation of the OU method (Uyeda and Harmon, 2014; Uyeda et al., 2022). We performed the bayou-analysis for the MCC tree, letting two reversible jump Markov Chain Monte Carlo (MCMC) simulations run for 6,000,000 generations. We used half-cauchy distributions for α and σ^2, a conditional Poisson distribution for the number of shifts (expected number of changes: 10, maximum number of changes: 50), and a normal distribution for θ, centered on the mean of AR with 1.5 standard deviations. We allowed one regime shift per branch, irrespective of branch length. After discarding the first 30% as burn-in, we checked whether the two independent MCMC chains had converged on similar regions in the parameter space with Gelman's R for log likelihood, σ^2, and α (see **S2.6**), and a bivariate plot of the posterior

probabilities for shifts along branches against each other (see **S2.7**). If convergence was reached, these posterior probabilities should fall along a line with a slope of one if convergence is reached. We considered shifts in the selective regime along a branch as well-supported if their respective posterior probabilities were far outside the main distribution of all probabilities (see **S2.8** and **S2.9**). With this approach, we conservatively identified 3 selective regime shifts, and confirmed that these branches received high support when we performed the bayOU analysis over a random subsample of 10 trees from the pseudo-posterior distribution.

We highlighted the position of these three very strongly supported selective regime shifts within an evolutionary traitgram of AR (Evans et al., 2009). The evolutionary traitgram (**Figure 2.2**; Evans et al., 2009) illustrates the inferred trait history, by plotting a projection of the phylogenetic tree in the space defined by AR. Unsurprisingly, the root ancestral state of AR is reconstructed near the average value of AR among extant neoselachians. The ancestral states are estimated by maximum likelihood, employing a BM model (the simplest evolutionary model), with no prior constraints on the root.

The early Late Cretaceous also emerges as an important time interval when calculating a subclade disparity through time plot (Harmon et al., 2003) with the R package “geiger” (Pennell et al., 2014). We obtained reproducible result when performing 10,000 simulations, and then iterated the disparity calculation over 100 random trees. The results from these 100 iterations allowed us to better understand when

subclade disparity began to exceed the subclade disparity expected under a BM model of trait evolution (**Figure 2.3**).

Estimates of Swimming Performance

We used the *in vitro* muscle data from Donley et al. (2007) to estimate the effects of historical changes in water temperature on the swimming performance of benthic and pelagic sharks. To do this, we used their data regarding the cycle frequency that resulted in maximum muscle power (PPF, or peak power frequency) over a range of temperatures in both mako sharks (*Isurus oxyrinchus*; 15 to 28°C) and leopard sharks (*Triakis semifasciata*; 15 to 25°C). Cycle frequency can be considered a proxy for tailbeat frequency, and tail beat frequency is correlated with swim speed. We ran linear regressions relating PPF to the temperatures used in their study, extracted the equations of the lines (see **S2.3**), and then used the historical sea surface temperature data from Scotese et al. (2021) to estimate the PPF for each species over time. The equation for mako sharks was PPF=0.16(temp)-2.24 and the equation for leopard sharks was PPF=0.04(temp)+0.02.

Results

Evolutionary History of Selachian Ecology

The majority of the 544 extant selachian species are benthic. We classified 490 extant species by their preferred occupied habitat (Materials and Methods). 342 species (70%) were predominantly benthic, 84 (17%) were benthopelagic, and 64 (13%) were

pelagic (see **S2.1**). Most extant pelagic selachians belong to only two orders, Lamniformes and Carcharhiniformes. Stochastic character mapping supports a non-pelagic origin of selachians (**Figure 2.1A**). For the root node, we found that only in 2.8% of the 1,000 iterations a pelagic state was inferred. In 46.3% and 50.9% of the iterations, a benthic or benthopelagic state was reconstructed, respectively. We hence have strong support for a non-pelagic origin, but it is unclear whether the origin was benthic or benthopelagic. The benthic to benthopelagic origin and the timing of the initial expansion to the pelagic zone are congruent with the fossil record and previous phylogenetic reconstructions (Thies and Reif, 1985; Sorenson et al., 2014). The initial expansion to open water occurred along the branch leading to the node defining the Lamniformes (**Figure 2.1A**), no later than the Early Cretaceous (122.6 mya, Barremian). Carcharhiniformes expanded their habitat into the pelagic zones next (98.3 to 82.4 mya, Cenomanian to early Campanian). Thus, the expansion to pelagic habitats in both Lamniformes and Carcharhiniformes, the two orders that contain most of the extant pelagic neoselachians date back to the Early to early Late Cretaceous. In total, we found selachians independently expanded into the pelagic zone at five different points. The other three shifts occurred later, including the small cookiecutter sharks (Squaliformes; 63.2 to 49.8 mya, early Paleogene) and, much more recently, the small spined pygmy shark (*Squaliolus laticaudus*) and the large and relatively slow whale shark (*Rhincodon typus*).

Evolution of Pectoral Fin AR

The distribution of pectoral fin AR across selachians is congruent with a pattern generated by adaptive evolution, as suggested by the results of evolutionary model fitting (Clavel et al., 2015) and the agnostic detection of selective regime shifts (Uyeda and Harmon, 2014; Uyeda et al., 2022). We fitted several evolutionary models to the data (Clavel et al., 2015; Materials and Methods) and found very strong support for an Ornstein-Uhlenbeck (OU) model with three adaptive peaks that reflect the different habitat categories. The inferred peaks agree well with the observed group means, especially for AR. Therefore, both AR and body size show signatures of adaptive evolution, but with AR experiencing stronger selection (median estimate of α for AR is 3.77 compared to 1.92 for PCL). However, there were considerable ranges of AR across all three groups as benthic selachians ranged from 1.1 to 4.3, mean=2.3, benthopelagic selachians ranged from 1.5 to 4.1, mean=2.5, and pelagic selachians ranged from 1.8 to 4.7, mean=3.3, respectively.

At least three major selective regime shifts of AR evolution are present within selachians, mostly congruent with the lamniform and carcharhiniform transition to pelagic habitats. Using an agnostic approach (Uyeda and Harmon, 2014; Uyeda et al., 2022; Methods) to characterize the adaptive landscape of AR, we found three very strongly supported shifts (**Figure 2.1A**). The oldest adaptive peak shift occurred with the origin of Lamniformes, directly coinciding with the initial shift to pelagic habitats no later than 122.6 mya (Barremian). Within Lamniformes, the adaptive peak for AR is estimated at 3.25, 1.52 times higher than the ancestral peak of 2.14. Two more selective

regime shifts occurred within the Carcharhiniformes, successively increasing the adaptive peak value for AR to 2.9 (127.9 to 103.6 mya, Hauterivian to Albian) and then 3.55 (60.8 to 54 mya, Paleocene to Eocene). The regime shifts in carcharhiniforms do not precisely line up with inferred shift towards pelagic habitats in this clade, as the older shift precedes the evolution of pelagic habitats and the more recent one lags behind. The support for selective regime shifts varies between analyses performed over a subsample of trees in the posterior distribution, but all three regime shifts identified for the consensus tree generally receive very strong support. The selective regime shift in lamniforms was strongly supported in 10 out of 10 iterations, the two shifts in carcharhiniforms in 7 out of 10. Estimates of the phylogenetic half-life indicate that it took less than 200,000 years for pectoral fin AR to evolve half-way towards a new peak.

Lamniforms and carcharhiniforms evolved high pectoral fin AR in succession, as suggested not only by the timing of the selective regime shifts but also visible in an evolutionary traitgram (Revell, 2012; Materials and Methods; **Figure 2.2**). The traitgram visualizes the shifts towards higher AR, by plotting a projection of the phylogenetic tree in the space defined by AR and time. In particular the branch leading to the lamniforms (node age 122.6 mya) and the branch leading to an early node within the carcharhiniforms (node age 103.6 mya) feature noticeable increases of AR. Given that the traitgram is based on ancestral state reconstruction of only living species, we superimposed fossil data (see **S2.2**) into this space. Late Jurassic sharks had low AR, while Late Cretaceous sharks achieved AR in the range of modern pelagic selachians,

reinforcing the view that selachians became pelagic during the Cretaceous (Thies and Reif, 1985; Kriwet and Klug, 2004; Sorenson et al., 2014; Vullo et al., 2021; 2024).

The evolutionary traitgram and the fossil record suggest an increase in the overall disparity of the pectoral fin aspect ratio during the early Late Cretaceous, and this pattern is confirmed with a subclade-disparity-through-time analysis. Selachian subclade disparity exceeds the null expectation at 93.7 mya (early Turonian), at which time the data deviate significantly from that expected under a Brownian motion (BM) model of trait evolution (**Figure 2.3B**). The timing of the deviation from the BM expectation overlaps with the Cretaceous Thermal Maximum (CTM), which featured global average sea surface temperatures (SST) of 28.2°C (Scotese et al., 2021). Upon exceeding the null expectation at 93.7 mya, the subclade disparity continued to rise, a trend that persisted even over the last 30 million years which experienced a substantial cooling of SST.

Evolution of swimming performance

Using *in vitro* muscle data from Donley et al. (2007) to estimate swimming performance between benthic and pelagic selachians we found that pelagic selachians likely had much higher swim speeds compared to benthic selachians during the CTM. Muscle performance data in mako and leopard sharks across a range of temperatures suggest that power output was significantly enhanced in the pelagic mako shark with temperatures up to 28ºC, whereas power output of the benthic leopard shark muscle declined slightly at the warmer temperatures (Scotese et al., 2021; **S2.3**). Muscle cycle frequency can be considered a proxy of tailbeat frequency, and therefore swim speed.

Thus, mako sharks can power swimming at greater sustained speeds than leopard sharks if their red muscle remains above 20ºC. Estimates of benthic and pelagic selachians muscle cycle frequency (that produces peak power) over the last 250 million years demonstrate that pelagic selachians consistently have higher predicted swim speeds compared to benthic selachians (**Figure 2.3A**). Differences in predicted swimming performance between benthic and pelagic selachians were pronounced during the early Late Cretaceous (**Figure 2.3A**).

Discussion

We found that selachians were benthic or benthopelagic in origin and expanded into the pelagic zone during the Early Cretaceous (by 122.6 mya) when sea surface temperatures were substantially higher than today. In alignment with the fossil record and a previous study, Lamniformes were the first to expand into the pelagic zone (Thies and Reif, 1985; Sorenson et al., 2014; Sternes and Shimada, 2020) where they experienced an increase in net diversification rates (Guinot and Cavin, 2016). Carcharhiniformes were the next group to expand into the pelagic zone where they also experienced an increase in net diversification rates (Guinot and Cavin, 2016). These independent expansions occurred during the Cretaceous, and Lamniformes and Carcharhiniformes to this day contain the overwhelming majority of the extant pelagic selachians.

As open-water long distance cruisers, all pelagic selachians experience similar physical requirements (Fish, 2023). Hydrodynamic demands associated with moving in open water likely resulted in the convergent evolution of the thunniform body shape

across a range of different vertebrates (Motani, 2002; Donley et al., 2004; Fish, 2023; Motani and Shimada, 2023). The anatomy of selachians, including body shape, caudal fin shape, and location of their dorsal and pectoral fins, likely reflects adaptive evolution in the context of different ecological lifestyles (Compagno, 1990; Sternes and Shimada, 2020). For example, oceanic species such as the blue shark (*Prionace glauca*) and oceanic white tip (*Carcharhinus longimanus*) have highly elongated pectoral fins most likely for fast cruising (Iosilevskii and Papastamatiou, 2016) compared to the benthic epaulette shark (*Hemiscyllium ocellatum*) that performs submerged walking with its short and rounded pectoral fins (Pridmore, 1994; Porter et al., 2022).

Pectoral fins are control surfaces that play critical roles in positioning and swimming in almost all species of fishes (Vogel, 1994; Wainwright et al., 2002; Weihs, 2002; Blake, 2004; Kane and Higham, 2012; Fish and Lauder, 2017). Like overall body form, pectoral fin morphology is considered to be closely related to ecology (Wainwright et al., 2002; Kane and Higham, 2012). Pectoral fin AR is routinely examined in fishes given its important role in swimming (Vogel, 1994; Wainwright et al., 2002; Weihs, 2002; Blake, 2004; Kane and Higham, 2012; Fish and Lauder, 2017). For example, among labrid fishes, species with higher AR pectoral fins swim fast whereas species with lower AR pectoral fins swim relatively slowly and frequently maneuver with their pectoral fins (Wainwright et al., 2002). For the limited shark species studied to date, there has been no clear quantitative difference in pectoral fin shape among species differing in ecology (Hoffmann et al., 2020). However, some empirical and theoretical evidence suggested that benthic selachians have short, rounded (i.e., low AR) pectoral fins,

whereas pelagic selachians have long and narrow (i.e., high AR) pectoral fins (Compagno, 1990; Pridmore, 1994; Vogel, 1994; Fish and Shannahan, 2000; Wilga and Lauder, 2000, 2001; Weihs, 2002; Blake, 2004; Maia et al., 2012; Iosilevskii and Papastamatiou, 2016; Lauder and Di Santo, 2016; Fish and Lauder, 2017; Porter et al., 2022).

We found evidence for adaptive evolution of pectoral fin AR. This suggests that habitat imposes a strong functional demand on pectoral fin morphology. For example, unlike benthic or benthopelagic selachians that can rest on the substrate, pelagic selachians are obligate ram ventilators that are constantly moving in the water column (Compagno, 1990; Maia et al., 2012; Iosilevskii and Papastamatiou, 2016; Lauder and Di Santo, 2016) which may be energetically demanding. Thus, the higher pectoral fin AR selected for in pelagic selachians may be a morphological adaptation to lower its energetic demands (Vogel, 1994; Fish and Shannahan, 2000; Maia et al., 2012; Iosilevskii and Papastamatiou, 2016; Lauder and Di Santo, 2016; Fish, 2023). In addition to higher pectoral fin AR, we found pelagic selachians were larger in body size compared to benthic and benthopelagic selachians (**Figure 2.2**). Having a larger body size has several benefits including increased buoyancy, increased energy storage, the ability to travel further distances, and having fewer predators (Kram and Taylor, 1990; Cohen et al., 1993; Iosilevskii and Papastamatiou, 2016). Pelagic selachians are known to perform long distance migrations and occupy high levels of the marine food web suggesting the larger body size is key a morphological adaptation for the pelagic zone (Compagno, 1990; Cortés, 1999; McCormack et al., 2022).

A Critical Phase in Shark Evolution

The Barremian to Cenomanian ages appear to be critical phases in selachian evolution (Guinot and Cavin, 2016). Our phylogenetic comparative analyses of extant species suggest that selachians had expanded to open-water habitat regions by the Barremian and pectoral fin AR had experienced two major increases prior to the Cenomanian (**Figures 2.1** and **2.2**). These results are congruent with the fossil record. Fossilized vertebral centra indicate that lamniform sharks had reached body sizes exceeding 6 m in total length by the Albian (Shimada, 1997a; Frederickson et al., 2015), a body size compatible with pelagic ocean cruisers. The Cenomanian features the evolution of the lamniform †*Cretoxyrhina mantelli*, the Cretaceous analogue to the modern great white shark (Shimada, 1997b). Commonly referred to as the ginsu shark, †*Cretoxyrhina mantelli* was the apex predator in a fauna that marks a global diversification event for actinopterygians and elasmobranchs (Shimada, 1997b; Friedman and Sallan, 2012; Guinot and Cavin, 2016). This taxonomic diversity peak coincides with high subclade disparity, which suggests that selachian lineages independently evolved similar AR (**Figure 2.3B**). Direct measurements of the AR in fossils suggest a possible mismatch between the evolutionary traitgram, which we use as a visualization but not an analytical tool, and the fossil record. In the deep parts of the tree, during the Late Jurassic, the majority of fossils have AR below the reconstructed values in the traitgram. The traitgram uses ancestral state reconstructions based on a BM process, and the computational approach based on BM favors the reconstruction of average values near

the root. The maximum likelihood root estimate is similar to a "weighted average" in which the weights are determined by the topology and branch lengths of the phylogenetic tree. Given that BM is a stochastic process, one would expect traits to evolve away from the starting point at the root, roughly evenly in both directions, toward larger and smaller AR values. The low fossil AR values could potentially mean that the ancestral state reconstructions in the traitgram are inaccurate, but two points are worth discussing in this context. First, ancestral state reconstructions based on extant species alone come with wide error margins in particular in the deep parts of a phylogenetic tree (see **S2.10**). While not necessarily inaccurate, it is important to keep the loose constraint of the reconstructions in the phenogram in mind. Second, bias in the fossil data towards low AR cannot be excluded. Preservation and sampling bias may partially have contributed to the predominance of low aspect ratios among Jurassic fossils. For example, many fossils in our data come from the Jurassic localities in Southern Germany (including Solnhofen), which formed in a shallow, restricted marine environment (Kriwet and Klug, 2004). The fossils from Cretaceous localities in both Lebanon and the Western Interior Seaway are slightly deeper and less restricted marine environments (Forey et al., 2003; Everhart, 2017) compared to the Jurassic localities in Southern Germany. The fossils from the Cretaceous localities tended to show higher AR compared to the Jurassic localities (see **S2.2**). The Eocene localities in Monte Bolca are also regarded as a shallow water habitat (Friedman and Carnevale, 2018) but unlike fossils from the Jurassic in Southern Germany fossil species with higher pectoral fin AR were present (see **S2.2**). While much remains to be learned about the fossil record of selachian shark evolution, the currently

available data suggest that AR >2.5 did not become common until the “mid-Cretaceous” (**Figure 2.3**).

Sea Surface Temperature, Swimming Performance, and Pectoral Fin Evolution

Given temperature has affected shark evolution and diversity during other periods (Friedman and Sallan, 2012; Guinot and Cavin, 2016; Condamine et al., 2019; Brée et al., 2022; Guinot and Condamine, 2023; Villafaña et al., 2023), it is perhaps unsurprising that we found the “mid-Cretaceous” was an important point for shark evolution as it was a period with a volatile climate such as ocean anoxic events and very warm SST (Scotese et al., 2021). For instance, global SST averaged 23°C during the Late Cretaceous with the Cretaceous Thermal Maximum (CTM) or Cenomanian-Turonian Thermal Maximum representing the warmest temperature (28.2°C global average SST) that has occurred in the last 200 million years (Scotese et al., 2021). We found the time that subclade disparity exceeded the BM expectation was during the CTM (**Figure 2.3**), and the high sea surface temperatures likely had a profound effect on the swimming performance of selachians.

Among ectotherms, warmer temperatures typically lead to increases in muscle-driven performance (Syme, 2006). Fishes are no exception, with swim speeds increasing with rising temperature (Dickson et al., 2002; Claireaux et al., 2006; Syme, 2006; Donley et al., 2007). For selachians, pelagic species can power swimming at greater sustained speeds, at temperatures above 20°C, compared to benthic species (Donley et al., 2007). However, muscle performance data in sharks is limited to two species (Donley et al., 2007). Thus, all hypotheses and discussion are constrained by the data from these two species. However, such a comparison is worthwhile as this provides us with a general

understanding of shark swimming performance across time. Nevertheless, when taking these limited performance data into consideration, benthic and pelagic selachians probably swam at different speeds under the range of temperatures they experienced for the last 250 million years. We investigated the history of selachian swim speeds by incorporating previously published data on muscle performance in sharks (Donley et al., 2007). Muscle performance data in mako and leopard sharks across a range of temperatures suggest that power output was significantly enhanced in the pelagic mako shark with temperatures up to 28°C, whereas power output of the benthic leopard shark muscle declined slightly at the warmer temperatures (Donley et al., 2007). Muscle cycle frequency can be considered a proxy of tailbeat frequency, and therefore swim speed, and Donley et al. (2007) found that mako may be able to power swimming at greater sustained speeds than leopard sharks if their red muscle remains above 20°C. Estimates of benthic and pelagic selachian muscle cycle frequency (that produces peak power) over the last 250 million years (Methods) demonstrate that pelagic sharks consistently have higher predicted swim speeds compared to benthic sharks (**Figure 2.3**). Differences in predicted swimming performance between benthic and pelagic selachians were pronounced during the early Late Cretaceous, a period of elevated water temperatures (**Figure 2.3**). Extant pelagic sharks are known to frequently exploit warmer waters, including those formed anthropogenically, for thermoregulation and as a strategy to increase swimming performance (Barash et al., 2023). Although pelagic selachians had greater sustained speeds compared to benthic selachians, that does not mean the pelagic selachians could tolerate the extremely warm tropical waters of the Late Cretaceous. For

example, fossil evidence shows the lamniform shark genus †*Cardabiodon* had an antitropical distribution (Cook et al., 2010) suggesting that even the Late Cretaceous tropical waters presented a limit of some selachian physiological tolerance.

Pelagic selachians swim faster than benthic selachians, which is likely associated with an increased cost of transport (COT), or the energy expended per unit body mass for a given distance travelled across varying speeds (Jahn and Seebacher, 2022). A high COT could negatively affect fitness (Irschick and Higham, 2016), so selection likely favored individuals that minimized COT via morphological changes. Increasing the lift-to-drag ratio of the pectoral fins by increasing fin AR is one mechanism (Vogel, 1994; Fish and Lauder, 2017). Thus, we hypothesize that an increase in global SST led to an increase in shark swim speeds (due to increased muscle performance) which, in turn, facilitated the expansion into the pelagic zone. Once in this new ecological zone, individuals that had higher AR pectoral fins were likely at an evolutionary fitness advantage, leading to higher AR fins in the pelagic species.

While the increase in SST may have been a key environmental factor for both the expansion to the pelagic zone and initial increase in AR subclade disparity, SST alone cannot explain the continued increased AR subclade disparity (**Figure 2.3B**). For example, even during the cooling phase over the last 30 my AR subclade disparity remains high (**Figure 2.3B**). This suggests that other factors must be important for the evolution of pectoral fin AR. For example, the continued appearance of coral reefs and changes in prey type over time have been linked to selachian evolution and

morphological specializations (Compagno, 1990; Sorenson, et al., 2014). This interesting paradigm warrants further research.

Conclusions

Our integrative study suggests temperature was one important factor in driving the evolution of selachian ecology and morphology. COT increases with swim speed, body size, and temperature, and all three of these are likely impacting the fitness of pelagic sharks at the maximum SST in the "mid-Cretaceous", jointly driving the selection of both more streamlined bodies (Vogel, 1994; Alexander, 2003; Fish, 2023) and high pectoral fin AR. The trifecta of swim speed, body size, and temperature and its impact on COT (Alexander, 2003; Hein and Keirsted, 2012; Jahn and Seebacher, 2022; Fish, 2023) may also explain how some pelagic sharks do not see an increase in AR - maybe these sharks are not swimming as fast, or are as large, or are active in cooler waters. The absence of well supported selective regime shifts for higher AR in the small cookiecutter sharks, the even smaller *Squaliolus laticaudus* (spined pygmy shark), and the slow-moving *Rhincodon typus* (whale shark) support such an interpretation. However, we want to clearly point out that other factors could potentially impact the evolution of pectoral fin AR. Our model fitting approach suggests that the most parameter-rich model explains the data best, and perhaps this complex model offers the only option that captures the full variability in the data. Other factors that could impact pectoral fin AR evolution might include reef habitats, which are known to impact carcharhinid diversification (Sorenson et al., 2014), feeding ecology (Bazzi et al., 2021), regional SST differences (O'Brien et al., 2017), or different locomotor physiology (Maia et al., 2012; Lauder and Di Santo, 2016).

Analyses of these factors is beyond the scope of this contribution, but we hope that future investigations will continue to explore the role of biotic and abiotic factors on shark evolution.

References

Adams DC, Collyer ML. 2022. Consilience of methods for phylogenetic analysis of variance. *Evolution* 76: 1406–1419.

Alfaro ME, Santini F, Brock C, Alamillo H, Dornburg A, Rabosky DL, Carnevale G, Harmon LJ. 2009. Nine exceptional radiations plus high turnover explain species diversity in jawed vertebrates. *Proceedings of the National Academy of Sciences USA* 106: 13410–13414.

Barash A, Schenin A, Bigal E, Shamir ZZ, Martinez S, Davidi A, Fadida Y, Pickholtz R, Tchernov D. 2023. Some like it hot: investigating thermoregulatory behavior of carcharhinid sharks in a natural environment with artificially elevated temperatures. *Fishes* 8: 428

Blake RW. 2004. Fish functional design and swimming performance. *Journal of Fish Biology* 65: 1193–1222.

Brée B, Condamine FL, Guinot G. 2022. Combining paleontological and neontological data shows a delayed diversification burst of carcharhiniform sharks likely mediated by environmental change. *Scientific Reports* 12: 21906.

Cook TD, Wilson M, Newbrey MG. 2010. The first record of the Late Cretaceous lamniform shark, Cardabiodon ricki, from North America and new empirical test for its presumed antitropical distribution *Journal of Vertebrate Paleontology* 30: 643–649.

Claireaux G, Couturier C, Groison A. 2006. Effect of temperature on maximum swimming speed and cost of transport in juvenile European sea bass (*Dicentrarchus labrax*). *Journal of Experimental Biology* 209: 3420–3428.

Clavel J, Escarguel G, Mereceron G. 2015. mvMORPH: an R package for fitting multivariate evolutionary models to morphometric data. *Methods in Ecology and Evolution* 6, 1311–1319.

Coates MI. 2003. The evolution of paired fins. *Theory of Biosciences* 122: 266–287.

Cohen JE, Pimm SL, Yodzis P, Saldaña J. 1993. Body sizes of animal predators and animal prey in food webs. *Journal of Animal Ecology* 1: 67–78.

Compagno LJV. 1977. Phyletic relationships of living sharks and rays. *American Zoologist* 17: 303–322.

Compagno LJV. 1990. Alternative life-history strategies of cartilaginous fishes in time and space. *Environmental Biology of Fishes* 28: 33–75.

Condamine FL, Romeiu J, Guinot G. 2019. Climate cooling and clade competition likely drove the decline of lamniform sharks. *Proceedings of the National Academy of Sciences USA* 116: 20584–20590.

Cortés E. 1999. Standardized diet compositions and trophic levels of sharks. *ICES Journal of Marine Science* 56: 707–717.

Dickson KA, Donley JM, Sepulveda C, Bhoopat L. 2002. Effects of temperature on sustained swimming performance and swimming kinematics of the chub mackerel Scomber japonicus. *Journal of Experimental Biology* 205: 969–980.

Donley JM, Sepulveda CA, Konstantindis P, Gembella S, Shadwick RE. 2004. Convergent evolution in mechanical design of lamnid sharks and tunas. *Nature* 429: 61–65.

Donley JM, Shadwick RE, Sepulveda CA, Syme DA. 2007. Thermal dependence of contractile properties of the aerobic locomotor muscle in the leopard shark and shortfin mako shark. *Journal of Experimental Biology* 210: 1194–1203.

Ebert DA, Dando M, Fowler S. 2021. *Sharks of the world: a complete guide*. Princeton, NJ: Princeton University Press.

Everhart MJ. 2017. *Oceans of Kansas: a natural history of the Western Interior Seaway, second edition.* Indiana University Press.

Fish FE. 2023. Aquatic locomotion: environmental constraints that drive convergent evolution. In Bels VL, Russell AP, eds. *Convergent evolution: animal form and function*. Berlin, Germany: Springer, 477–522

Fish FE, Lauder GV. 2017. Control surfaces of aquatic vertebrates: active and passive design and function. *Journal of Experimental Biology* 220: 4351–4363.

Forey PL, Yi L, Patterson CE, Davies CE. 2003. Fossil fishes from the Cenomanian (upper Cretaceous) of Namoura, Lebanon. *Journal Systematic Palaeontology* 4: 227–330.

Frederickson JA, Schaefer SN, Doucette-Frederickson JA. 2015. A gigantic shark from the Lower Cretaceous Duck Creek Formation of Texas. *PLoS ONE* 10: e0127162.

Friedman M, Carnevale G. 2018. The Bolca Lagerstätten: shallow marine life in the Eocene. *Journal of the Geological Society, London* 175: 569–579.

Friedman M, Sallan LC. 2012. Five hundred million years of extinction and recovery: a Phanerozoic survey of the large scale diversity patterns in fishes. *Palaeontology* 55: 707–742.

Fröbisch NB, Fröbisch J, Sander PM, Schmitz L, Rieppel O. 2013. Macropredatory ichthyosaur from the Middle Triassic and the origins of modern trophic networks. *Proceedings of the National Academy of Sciences USA* 110: 1393–1397.

Garland Jr. T, Dickerman AW, Janis CM, Jones JA. 1993. Phylogenetic analysis of covariance by computer simulation. *Systematic Biology* 42: 265–292.

Grogan ED, Lund R, Greenfest-Allen, E. 2012. The origin and early relationships of early chondrichthyans. In: Carrier JC, Musick JA, Heithaus MR, eds. *Biology of sharks and their relatives: second edition*. Boca Raton, FL: CRC Press, 3–30.

Guinot G, Cavin L. 2016. 'Fish' (Actinopterygii and Elasmobranchii) diversification patterns through deep time. *Biological Reviews* 91: 950–981.

Guinot G, Condamine FL. 2023. Global impact and selectivity of the Cretaceous-Paleogene mass extinction among sharks, skates, and rays. *Science* 379: 802–806.

Heinicke MP, Naylor GJP, Hedges SB. 2009. Cartilaginous fishes (Chondrichthyes). In Hedges SB, Kumar S, eds. *The timetree of life.* Oxford, UK: Oxford University Press, pp. 320–327.

Higham TE, Ferry LA, Schmitz L, Irschick DJ, Starko S, Anderson PS, Bergmann PJ, Jamniczky HA, Monteiro LR, Navon D, Messier J, Carrington E, Farina SC, Feilich KL, Hernandez LH, Johnson MA, Kawano SM, Law CJ, Longo SJ, Martin CH, Martone PT, Rico-GuevaraA, Santana SE, Niklas KJ. 2021. Linking

ecomechanical models and functional traits to understand phenotypic diversity. *Trends in Ecology & Evolution* DOI:https://doi.org/10.1016/j.tree.2021.05.009

Hoffmann SL, Buser TJ, Porter ME. 2020. Comparative morphology of shark pectoral fins. *Journal of Morphology* 281: 1501–1516.

Iosilevskii G, Papastamatiou YP. 2016. Relations between morphology, buoyancy and energetics of requiem sharks. *Royal Society Open Science* 3: 160406.

Irschick D, Higham T. 2016. *Animal athletes: an ecological and evolutionary approach.* Oxford University Press.

Jahn M, Seebacher F. 2022. Variations in cost of transport and their ecological consequences: a review. *Journal of Experimental Biology* 225: jeb243646.

Kane EA, Higham TE. 2012. Life in the flow lane: differences in pectoral fin morphology suggest transitions in station-holding demand across species of marine sculpin. *Zoology* 115: 223–232.

Kram R, Taylor C. 1990. Energetics of running: a new perspective. *Nature* 346: 265–267.

Kriwet J, Klug S. 2004. Late Jurassic selachians (Chondrichthyes, Elasmobranchii) from Southern Germany: re-evaluation on taxonomy and diversity. *Zitteliana* A44: 67–95.

Lauder GV. 2015. Flexible fins and fin rays as key transformations in ray-finned fishes. In: Dial KP, Shubin N, Brainerd, eds. *Great transformations in vertebrate evolution*. Chicago, IL: University of Chicago Press, 31–46.

Lauder GV, Di Santo V. 2016. Swimming mechanics and energetics of elasmobranch fishes. In: Shadwick RE, Farrell AP, Brauner CJ, eds. *Physiology of*

elasmobranch fishes: structure and environment. Cambridge, MA: Academic Press, 219–253.

Long JA, Gordon MS. 2004. The greatest step in vertebrate history: a paleobiological review of the fish tetrapod transition. *Physiological Biochemical Zoology* 77: 700–719.

Maia AMR, Wilga CAD, Lauder GV. 2012. Biomechanics of locomotion in sharks, rays, and chimaeras. In: Carrier JC, Musick JA, Heithaus MR, eds. *Biology of sharks and their relatives: second edition*. Boca Raton, FL: CRC Press, 125–151.

Maisey JG. 2012. What is an 'elasmobranch'? the impact of paleontology in understanding elasmobranch phylogeny and evolution. *Journal of Fish Biology* 80: 918–951.

Motani R. 2002. Scaling effects in caudal fin propulsion and the speed of ichthyosaurs. *Nature* 415: 309–312.

Motani R, Shimada K. 2023. Skeletal convergence in thunniform sharks, ichthyosaurs, whales, and tunas, and its possible ecological links through the marine ecosystem evolution. *Scientific Reports* 13: 16664.

Pridmore PA. 1994. Submerged walking in the epaulette shark Hemiscyllium ocellatum (Hemiscyllidae) and its implications for locomotion in rhipidistian fishes and early tetrapods. *Zoology* 98: 278–297.

Rayner JMV. 1988. The evolution of vertebrate flight. *Biological Journal of the Linnean Society* 34: 269–287.

Revell LJ. 2012. phytools: An R package for phylogenetic comparative biology (and other things). *Methods in Ecology and Evolution* 3: 217–223.

Romer AV. 1967. Major steps in vertebrate evolution. *Science* 158: 1629–1637.

Schweigert G, Dietl G, Kapitzke M, Rieter M, Hugger R. 1996. Libellen aus dem Nusplinger Plattenkalk (Obejura, Ober-Kimmeridgium, Baden-Württemberg). *Stuttgarter Beiträge zur Naturkunde (B)* 236: 1–12.

Scotese CR, Song H, Mills BJW, van der Meer DG. 2021. Phanerozoic paleotemperatures: the earth's changing climate during the last 540 million years. *Earth Science Reviews* 215: 103503.

Sorenson L, Santini F, Alfaro ME. 2014. The effect of habitat on modern shark diversification. *Journal of Evolutionary Biology* 27: 1536–1548.

Shimada K. 1997a. Gigantic lamnoid shark vertebra from the Lower Cretaceous Kiowa Shale of Kansas. *Journal of Vertebrate Paleontology* 71: 522–524.

Shimada K. 1997b. Paleoecological relationships of the Late Cretaceous lamniform shark, Cretoxyrhina mantelli (Agassiz). *Journal of Vertebrate Paleontology* 71: 926–933.

Shubin N, Tabin C, Carroll S. 2009. Deep homology and the origins of evolutionary novelty. *Nature* 457: 818–823.

Stein RW, Mull CG, Kuhn TS, Aschliman NC, Davidson LNK, Joy JB, Smith GJ, Dulvy NK. 2018. Global priorities for conserving the evolutionary history of sharks, rays and chimaeras. *Nature Ecology and Evolution* 2: 288–298.

Sternes PC, Shimada K. 2020. Body form in sharks (Chondrichthyes: Elasmobranchii) and their functional, ecological, and evolutionary implications. *Zoology* 140: 125799.

Stubbs TL, Benton MJ. 2016. Ecomorphological diversifications of Mesozoic marine reptiles: the role of ecological opportunity and extinction. *Paleobiology* 42: 547–573.

Syme DA. 2006. Functional properties of skeletal muscles. In Shadwick RE, Lauder GV, eds. *Fish physiology volume 23*. Cambridge, MA: Academic Press, 179–240.

Thies D, Reif WE. 1985. Phylogeny and evolutionary ecology of Mesozoic Neoselachii. *Neues Jahrbuch für Geologie und Paläontologie* 169: 333–361.

Uhen MD. 2007. Evolution of marine mammals: back to the sea after 300 million years. *The Anatomical Record* 290: 514–522.

Uyeda JC, Eastman J, Harmon L. 2022. bayou: Bayesian Fitting of Ornstein-Uhlenbeck Models to Phylogenies. R package version 2.2.0 (R Foundation for Statistical Computing, 2022).

Uyeda JC, Harmon LJ. 2014. A novel Bayesian method for inferring and interpreting the dynamics of adaptive landscapes form phylogenetic comparative data. *Systematic Biology* 63, 902–918.

Villafaña JA, Rivadneira MM, Pimiento C, Kriwet J. 2023. Diversification trajectories and paleobiogeography of Neogene chondrichthyans from Europe. *Paleobiology* 49: 329–341.

Vogel S. 1994. *Life in moving fluids: The physical biology of flow, second edition*. Princeton: Princeton University Press.

Vullo R, Frey E, Ifrim C, González González MA. 2021. Manta-like planktivorous sharks in Late Cretaceous oceans. *Science* 371: 1253–1256.

Vullo R, Villalobos-Segura E, Amadori M, Kriwet J, Frey E, González González A, Padila Gutiérrez JM, Ifrim C, Stinnesbeck ES, Stinnesbeck W. 2024. Exceptionally preserved shark fossils from Mexico elucidate the long-standing enigma of the Cretaceous elasmobranch *Ptychodus*. *Proceedings Royal Society B* 291: 20240262.

Wainwright PC, Bellwood DR, Westneat MW. 2002. Ecomorphology of locomotion in labrid fishes. *Environmental Biology of Fishes* 65: 47–62.

Wainwright SA, Vorsburgh F, Herbank JH. 1978. Shark skin: function in locomotion. *Science* 202: 747–749.

Weihs D. 2002. Stability versus maneuverability in aquatic locomotion. *Integrative Comparative Biology* 42: 127–134.

Wilga CD, Lauder GV. 2000. Three-dimensional kinematics and wake structure of the pectoral fins during locomotion in leopard sharks *Triakis semifasciata*. *Journal of Experimental Biology* 203: 2261–2278.

Wilga CD, Lauder GV. 2001. Functional morphology of the pectoral fins in bamboo sharks, *Chiloscyllium plagosium*: Benthic vs. pelagic station-holding. *Journal of Morphology* 249: 195–209.

Tables & Figures

Figure Legends

Figure 2.1. Ancestral state reconstructions of preferred habitat and visualization of pectoral fin aspect ratio (AR) and body size (log10 of precaudal length (PCL)). (A) Maximum clade credibility tree of the selachians in this study. Branches are colored by habitat and represent results of ancestral-state reconstructions obtained from stochastic character mapping (Methods). Posterior probabilities strongly suggest a non-pelagic origin of neoselachian sharks, irrespective of whether the ancestral state reconstructions are performed over the maximum clade credibility tree or over a random sample of 100 trees from the pseudoposterior distribution (histogram). The bar plots are aligned with the phylogeny and illustrate the distribution of AR and log10(PCL). Arrows indicate strongly supported selective regime shifts of AR. Select major lineages labelled. (B) Box plot of pectoral fin AR in benthic, benthopelagic, and pelagic sharks. (C) Box plot of log10(PCL) in benthic, benthopelagic, and pelagic sharks. Silhouettes of angel, dogfish, and carcharhinid sharks were downloaded from www.phylopic.org (all downloaded images were available for reuse under the Public Domain Dedication 1.0 license).

Figure 2.2. Traitgram projections of pectoral fin aspect ratio (AR) using time calibrated phylogeny. Gray shapes represent measured fossil specimen pectoral fin aspect ratios (Appendices). Arrows indicate strongly supported selective regime shifts of AR. Silhouettes were downloaded from www.phylopic.org (all downloaded images were available for reuse under the Public Domain Dedication 1.0 license).

Figure 2.3. Muscle cycle frequency comparing benthic (orange line) and pelagic (blue line) shark species is shown in A. Muscle cycle frequency can be considered a proxy for tailbeat frequency, therefore swim speed. Subclade disparity (solid black line) over time is show in B. The dashed line represents the average subclade disparity expected under a Brownian Motion (BM) model of trait evolution. The grey area represents 95% confidence interval for average subclade disparity under BM. Red line shows average global sea surface temperatures (SST) from Scotese et al. (2021). Average subclade disparity exceeds the BM confidence interval during the early Late Cretaceous (dashed blue line). The blue region represents the phylogenetic uncertainty of when subclade disparity began to exceed the subclade disparity expected under a BM model of trait evolution (Materials and Methods). Shark images were downloaded from https://commons.wikimedia.org/wiki/Main_Page (both downloaded images were available for reuse under Creative Commons Attribution-Share Alike 3.0 Unported license).

Figure 2.1. Ancestral state reconstructions of preferred habitat and visualization of pectoral fin aspect ratio (AR) and body size (log10 of precaudal length (PCL)).

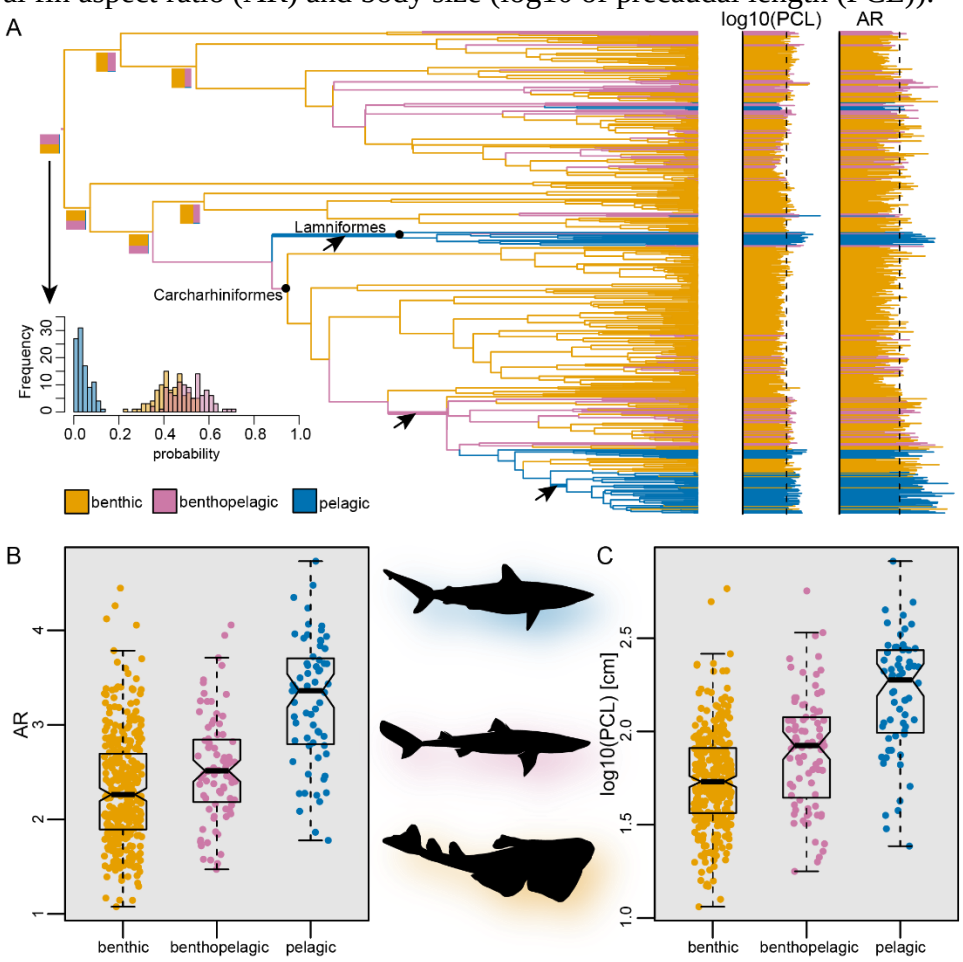

Figure 2.2. Traitgram projections of pectoral fin aspect ratio (AR) using time calibrated phylogeny.

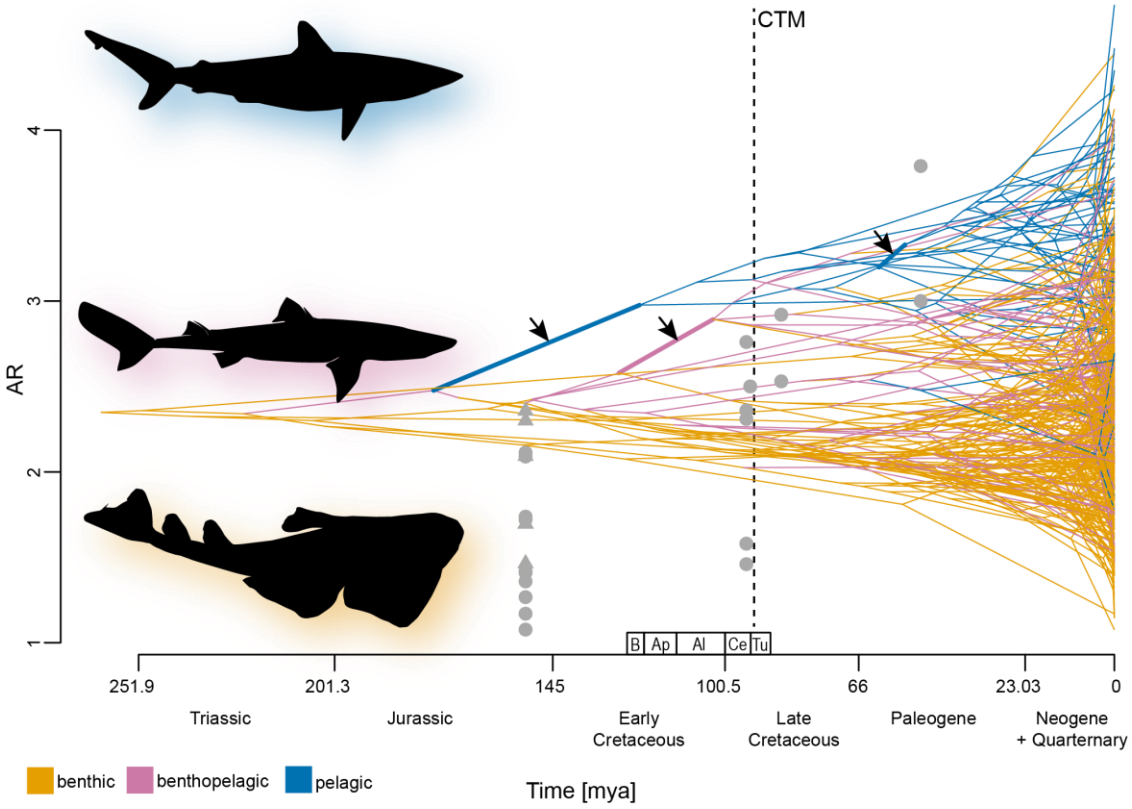

Figure 2.3. Selachian swimming performance and subclade disparity of AR from the past 252 million years.

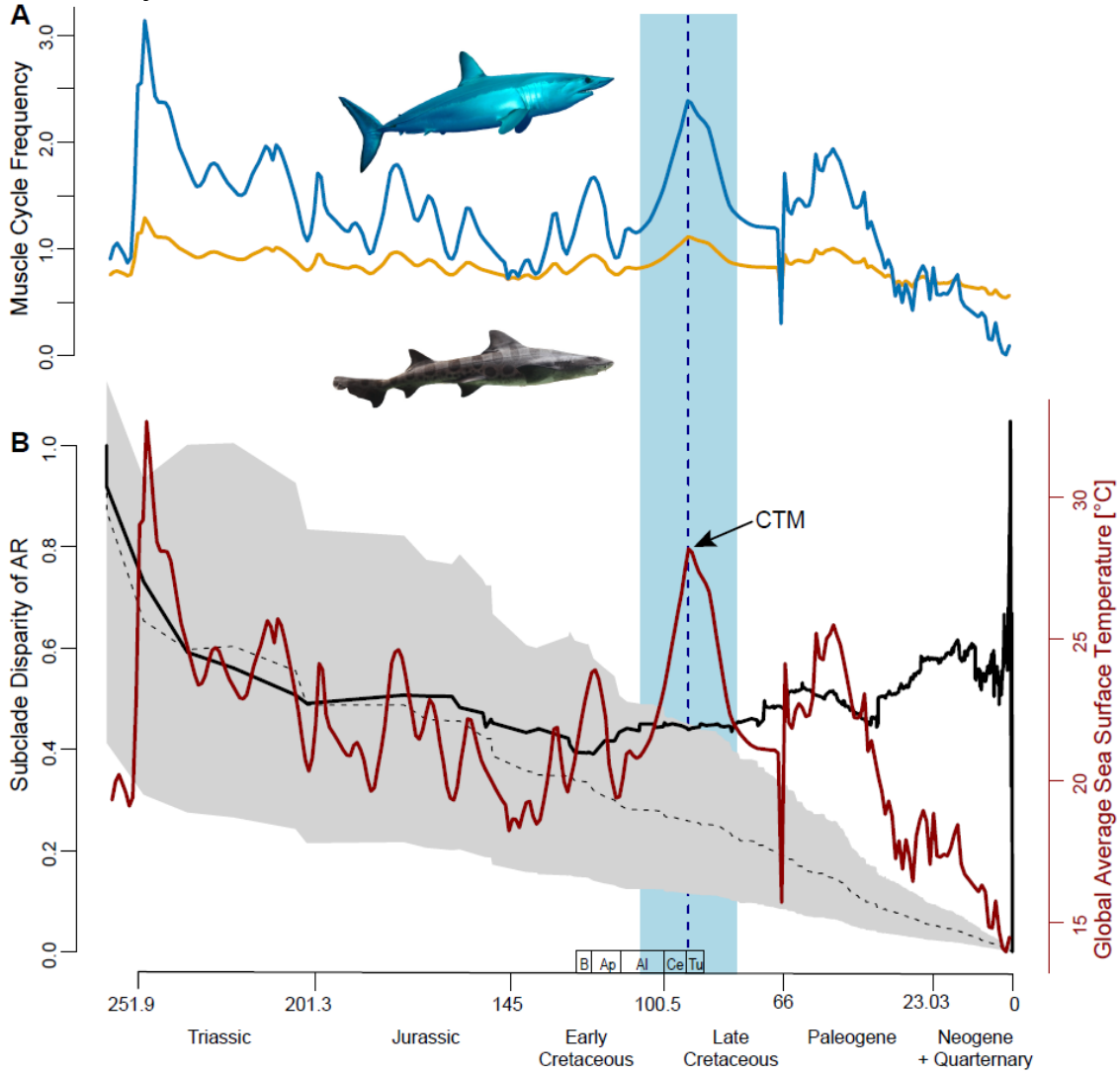

CHAPTER 3

Pelagic Shark Pectoral fins Generate lift During Steady Swimming

Abstract

Sharks are among the oldest vertebrate lineages to possess paired fins. Yet, there is a paucity of information on the functional performance of pelagic shark pectoral fins. The historical view, based on older work, is that shark pectoral fins act as lift generating appendages during steady swimming. Interestingly, data from contemporary studies show that shark pectoral fins do not generate lift during steady swimming. However, these have focused on benthic shark species that differ in both morphology and behavior compared to pelagic sharks. Using a freely accessible 3D generated model of a pelagic shark, the shortfin mako (*Isurus oxyrinchus*), we used computational fluid dynamics (CFD) to investigate the functional performance of the isolated pectoral fin. We examined the pectoral fin across a wide range of attack angles that have been observed in freely-swimming sharks in nature. We found that the pectoral fins of the pelagic mako shark produces lift during steady swimming, including when moving horizontally. Additionally, we found the pectoral fins performed most efficiently when angled in positions for rising (+11°) and sinking (-11°) behavior. Overall, it appears that pelagic and benthic sharks exhibit differences in pectoral fin function that strongly align with their natural swimming behavior. Specifically, pelagic shark fins generate lift during steady swimming whereas benthic sharks use their pectoral fins for vertical and turning maneuvers.

Introduction

Sharks (Elasmobranchii: Selachii) are representatives of one of the oldest vertebrate lineages to possess paired fins (Compagno, 1977; Coates, 2003; Heinicke et al., 2009; Maisey, 2012; Whitenack et al., 2022). Yet, there are surprisingly few studies on the functional morphology, biomechanics, and/or hydrodynamics of shark paired fins, specifically the pectoral fins. Shark pectoral fins have long been thought to generate lift anterior to the shark's center of mass and, therefore, balance the torque generated by the undulation of the asymmetrical caudal fin (i.e., heterocercal tail) (Harris, 1936; Affleck, 1950; Alexander, 1965; Simons, 1970; Thomson, 1976). However, empirical studies on shark pectoral fins have revealed that, during steady horizontal swimming, the angle of attack of the pectoral fins, as well as vorticity patterns in their wake, suggest that negligible lift is produced (Wilga and Lauder, 2000, 2001). Rather than being a lift producer during steady swimming, contemporary studies suggest that shark pectoral fins act as critical control surfaces for maneuvering in the water column (Wilga and Lauder, 2000, 2001; Hoffmann and Porter, 2019; Paig-Tran et al., 2022)

Given that sharks vary considerably in their movement ecology and body shape (Thomson and Simanek, 1977; Compagno, 1990; Grubbs, 2010; Sternes and Shimada, 2020; Paig-Tran et al., 2022; Abel and Grubbs, 2023; Renshaw et al., 2023), the generality of this hypothesis remains unclear. Both species (bamboo and leopard sharks) used in the empirical studies for steady swimming are considered benthic and benthopelagic, respectively (Compagno, 1990; Ebert et al., 2021; Abel and Grubbs, 2023; Chapter 2). Recently, Sternes et al. (Chapter 2) investigated shark pectoral fin

morphology in relation to ecology and determined that an overwhelming majority (~87%) of sharks are regarded as benthic or benthopelagic, whereas the remaining 13% of shark species are in the pelagic zone. Additionally, there is a strong relationship between pectoral fin shape and ecology. For example, pelagic sharks have significantly higher pectoral fin aspect ratios compared to all other sharks (Sternes et al., Chapter 2). Consequently, the role of the pectoral fins may differ between pelagic and benthic sharks.

No empirical data exist on the hydrodynamics of pelagic shark pectoral fins. This is most likely due to the extreme challenges in capturing, handling and maintaining large pelagic shark species in a laboratory setting (Graham et al., 1990; Lowe, 1996; Donley et al., 2005). Instead, Fish and Shannahan (2000) filmed various shark species, including two pelagic species, in a large public aquarium and suggested that, based on their orientation during steady swimming, pectoral fins may serve as lift generating appendages. Iosilevskii and Papastamatiou (2016) used a theoretical framework and found that pelagic sharks have an optimal span and area of the pectoral fins to lower their cost of transport. In addition, Sternes et al. (Chapter 2) hypothesized that pelagic sharks have higher aspect ratio pectoral fins to increase the lift-to-drag ratio and, therefore, lower the cost of transport. Furthermore, cross-sectional morphology of the pectoral fins of some pelagic shark species supports the idea that they produce lift during steady horizontal swimming (Hoffmann et al., 2020). When taking pelagic shark morphology, life history, and previous studies into account, pelagic shark pectoral fins may have differences in function related to lift generation capacity and efficiency compared to other sharks.

The shortfin mako shark (*Isurus oxyrinchus* Rafinesque, 1810), here-after referred to as mako, is a large pelagic apex predator with a worldwide distribution and is regarded as the fastest and most active shark in the world (Stevens, 2008; Ebert et al., 2021; Waller et al., 2023). It routinely performs long-distance migrations with some individuals travelling nearly 4000 km in a single year (Casey and Kohler, 1992; Block et al., 2011; Vaudo et al., 2016a). In addition, the mako frequently performs vertical movements in the water column, diving as deep as 1000 m and returning to the surface (Vaudo et al., 2016b; Andrzejaczek et al., 2022; Santos et al., 2021; Saraiva et al., 2023; Vaudo et al., 2024). The high performance of mako sharks is likely tied to their physiological adaptations (Bernal et al., 2001; Bernal et al., 2003a, b), although performing at such high capacities in the pelagic environment still imparts a high energetic cost (Bernal et al., 2012; Irschick and Higham, 2016).

We hypothesize that the pelagic mako shark will have clear hydrodynamic differences compared to benthic/benthopelagic species studied. We predict that the mako will generate lift during steady swimming. We employed computational fluid dynamics (CFD) to evaluate the hydrodynamics of the shortfin mako's pectoral fins over a wide range of angles of attack (AoA). Computational fluid dynamics is a mathematical modelling technique to simulate fluid flows by numerically solving the continuity and momentum conservation equations and has been frequently used to understand swimming capabilities in vertebrates (Liu et al., 1996; Hazekamp et al., 2010; Harada et al. 2021; Hocking et al., 2021; Masud and Dabnichki, 2022) including sharks (Diez et al., 2015; Gaylord et al., 2020; Sumikawa et al., 2023; Obayashi et al., 2024).

Materials and Methods

Mako shark model

A 3D surface model of a subadult mako shark from an online repository was used. This model, was derived from a combination of photographs and video as well as complete 3D photogrammetry scan (Irschick et al., 2022). This freely accessible model was generated by DigitalLife3D team, who aimed to keep the reconstruction as anatomically correct as possible (Irschick et al., 2022). It consists of a Blender file containing low-resolution triangulated mesh surfaces of the shark. Because of the rough triangulation, many sharp corners existed in the mesh, especially at regions with high curvature such as the edges of the pectoral fins (**Figure 3.1A**). To enable the subsequent operations and CFD, the mesh was refined and smoothed, using program Geomagic Wrap 2017 (3D Systems Inc., Rock Hill, USA). This inevitably resulted in rounding of sharp and thin-edged structures, and consequently shortening of the tip of the original pectoral fin (**Figure 3.1B** versus **3.1A**). However, the shape and size of spanwise sections of the pectoral fin was preserved reasonably well along approximately ¾ of the original span with the highest matching accuracy at the base (**Figure 3.1C, D**). This overall fin shape is highly representative of most pelagic shark pectoral fins. Next, the left pectoral fin and part of its attachment to the body were isolated and retained for CFD analysis. To facilitate force data extraction at different locations along the long-axis of the fin, the mesh was subdivided into ten equally thin strips (numbered 1 at the base to 10 at the tip) and converted into patches of adjacent non-uniform rational B-spline surfaces using

Geomagic (Fig. 1E). As the DigitalLife model had dorsal and ventral surfaces of the pectoral fin that were approximately in parallel to the rostrocaudal axis of the animal (and hence aligned to the incoming flow in the simulations), the original fine posture was defined as the 0° angle of attack.

CFD model and validation

To ensure the validity of the computed drag and lift forces for a wing-like structure, our CFD model design and settings, including turbulence model and mesh settings, were first validated for a wing shape for which experimental data exist (see also Hocking et al. (2021) for a similar validation approach using the same turbulence model). We chose to use the NACA2412 profile (**Figure 3.2A**) for comparison with wind tunnel data at a Reynolds number (*Re*; calculated using chord length as the characteristic linear dimension) of $5.7\ 10^6$ from Abbott and Von Doenhoff (1959).

The NACA outline was imported into the geometry building environment (DesignModeler) of ANSYS 2019 R1 (ANSYS Inc., Canonsburg, PA, USA). A rectangular flow domain of 10 m long (1.5 m in front and 8.5 m behind the wing) and 2 m high was created. The NACA2412 was scaled to a chord length of 20 cm to approximate the absolute dimensions of the mako shark's pectoral fin. The mesh size was controlled at three levels: at the wing surface (selected mesh edge length = 0.75 mm), at a bounding box of 0.2 m high by 3 m long surrounding the wing and its wake (maximal mesh edge length = 4 mm), and at the outer edges of the flow domain (maximal mesh edge length = 50 mm). Inflation layers (maximally 20 layers) were used to optimize

the solution accuracy of the boundary layer (first layer height = 0.075 mm; growth rate = 1.15). A growth rate of 1.1 was enforced to transition between the mesh size targets in the rest of the domain. The mesh was created in ANSYS Meshing.

The mesh was imported into the CFD-solver ANSYS Fluent (version 2019R1). Reynolds-averaged Navier-Stokes equations were solved numerically with the addition of the 2-equation shear-stress transport (SST) k-ω model for turbulence (Menter, 1994). This turbulence model is widely used, for example in wind turbine research (e.g. Costa-Rocha et al., 2014), and provides reliable results at relatively low *Re* (e.g. for aerofoils at *Re* = 120 000; Aftab et al., 2016). It utilizes the original k-ω model of Wilcox (Wilcox, 1988) in the sublayer of the boundary layer because of its simplicity, numerical stability, and accuracy, and switches to a k-ε behaviour in the free-stream to avoid the standard k-ω model's high sensitivity to turbulence properties of the incoming flow. The SST k-ω model in ANSYS Fluent uses a y^+ insensitive wall treatment to improve the accuracy with varying mesh element dimensions in the boundary layer.

As boundary conditions for the NACA2412 simulations, the two side walls were assigned the 'symmetry' boundary condition. The front face is defined as a 'velocity inlet' (using the default turbulence intensity of 10% and viscosity ratio of 10), the back face as a 'pressure outlet' (zero pressure difference due to flow over the lizard and branch imposed). The top and bottom boundary sides are modelled as impermeable boundaries ('walls') that move along with the fluid flow. The wing is modelled as smooth 'walls' for which the no-slip condition is enforced. The ANSYS Fluent 2019R1 default solver settings were retained (SIMPLE scheme for solving the pressure-velocity coupling; least

squared cell based gradient discretization; second order discretization for pressure and momentum; first order upwind method for discretization of turbulent kinetic energy and dissipation rate). Iterative convergence was checked by monitoring the scaled equation residuals (drop below 0.001) and drag and lift forces (remaining approximately constant). The fluid in the model had a water density of 998.2 kg m^{-3} and a dynamic viscosity of 1.001 Pa s. Calculations were run on a computer with 36 processor cores.

First, simulations were performed at a *Re* close to that of the shark fin (water flow speed 2.51 m s^{-1}; *Re* = 500 000) when performing a mesh convergence analysis, and hence at the *Re* of the wind tunnel data for validation (water flow speed 28.6 m s^{-1}; Re = 5.7 10^6). After selecting a mesh size setting of a simulation appearing on the plateau region of the convergence plots for drag and lift coefficients (**Figure 3.2B**), the model was compared against wind tunnel data for a range of angles of attack (**Figure 3.2C, D**). Lift force was predicted accurately (**Figure 3.2C**). Drag force showed modestly lower values in CFD, for example 8.3% lower minimal drag (**Figure 3.2D**). These differences were considered acceptable given the purpose of our study to evaluate the hydrodynamic role of the pectoral fins.

Shark fin CFD

Mesh properties and geometry of the flow domain were kept identical to those from the NACA2412 validations, except for using a semi-cylindrical side wall of the channel (diameter 2 m) (**Figure 3.2E**). Tetrahedral cells were used during meshing to fit the more complex shape. The final mesh consisted of approximately 40 million cells.

We chose to simulate a water velocity of 1.86 m s^{-1} as it is within the estimated cruising speeds and within the total range of measured speeds of free swimming mako sharks (Klimley et al., 2002; Sepulveda et al., 2004; Watanabe et al., 2015; Saraiva et al., 2023; Waller et al., 2023;). We ran each simulation 6500 times to reach the appropriate convergence. We ran a total of 25 simulations with angles of attack ranging from -25°to +25°. Lift and drag coefficients were then calculated from each simulation's lift and drag forces (sum of pressure forces and viscous forces along, respectively, the ventrodorsal axis and the rostrocaudal axis, $C_{L,D} = 2F_{D,L} / \rho U^2 A$.). We also performed a qualitative assessment of the pectoral fin at optimal angles of attack, including diagrams of velocity, pressure, and vorticity patterns.

Results

Lift coefficients ranged from -1.139 to 1.457 whereas drag coefficients ranged from 0.072 to 0.465 (**Figure 3.3A, B, Table 3.1**). The greatest positive lift was generated at +19°angle of attack whereas the greatest negative lift was generated at -11°angle of attack (**Figure 3.3A, Table 3.1**). Drag was highest at +25° angle of attack and lowest at -1° angle of attack (**Figure 3.3B, Table 1**). The greatest lift-to-drag ratios of the pectoral fins occurred at -11° and +11° angle of attack, with optimal values being -9.62 and 6.68, respectively (**Figure 3.3C, D, Table 1**).

For the angles with the highest efficiency (+11° AoA and -11° AoA) we performed a qualitative assessment of the flow patterns (**Figure 3.4**). The basic flow patterns are mostly mirrored for these two angles of attack. Flow separation can be

observed close to the trailing edge, leaving a narrow wake with low recirculation velocities (**Figure 3.4A, D**). Lift forces result predominantly from negative pressure on the lee-side, which are strongest close to the leading edge of the distal half of the fin (**Figure 3.4B, E**). Negative pressure in this zone are slightly higher in magnitude for the negative AoA (-11°) compared to the +11° AoA (**Figure 3.4E** lower right panel vs Figure **3.4B** lower left panel). Plots of the flow zones with dominating vorticity (**Figure 3.4C, F**) show a clear vortex starting from the fin tip. Seen in the flow direction, the left fin's tip vortex is counterclockwise for the +11° simulation, and clockwise in the -11° simulation. Two counterrotating spanwise vortices are present just downstream of the trailing edge. Vortices also start from the base of the fin with a structure differing between the two described simulations (**Figure 3.4C, F**)

Discussion

Pelagic shark pectoral fins during steady swimming

During steady swimming, pelagic mako shark pectoral fins generate lift (**Figure 3.3A, Table 3.1**), supporting the classical hypothesis of shark pectoral fin function (Harris, 1936; Affleck, 1950; Alexander, 1965; Simons, 1970; Thomson, 1976). This is based on an angle of attack between +9 to+10°, which was observed during horizontal swimming in pelagic sharks by Fish and Shannahan (2000). This range of AoAs resulted in positive lift coefficients of 0.7-0.9 (**Figure 3.3A, Table 3.1**). Although the mako was not one of the two pelagic species studied by Fish and Shannahan (2000), we assume that the orientations were similar given the similar pectoral fin shapes among the species

(Sternes et al., Chapter 2). Additionally, these angles of attack result in high efficiency (**Figure 3.3C**), further supporting the idea that the pectoral fins are producing lift effectively.

Unlike benthic sharks that have a flat ventral body surface, pelagic sharks have a ventral body that is much more rounded. This led Lingham-Soliar (2005) to suggest that the pectoral fins must be responsible for lift generation. Fish and Shannahan (2000) also suggested that, based on video analyses of shark species swimming in a large aquarium, the pectoral fins might act as lift-generating surfaces. Additionally, Iosilevskii and Papastamatiou (2016) used a theoretical approach to explore the relationship between morphology, buoyancy, and energetics of requiem sharks, and determined that the pectoral fin span of pelagic species is optimal for lowering the cost of transport. Sternes et al. (Chapter 2) hypothesized that the invasion of the pelagic zone increased the selective pressure for increased pectoral fin aspect ratio to help lower their cost of transport. Our results support this hypothesis, in that pelagic sharks generate more lift to lower the cost of transport.

Although contemporary studies on shark pectoral fin function found that negligible lift was produced during steady swimming, the species used in those studies were benthic and benthopelagic species (Wilga and Lauder, 2000, 2001). In terms of morphology, both the overall shape and cross-sectional morphology of benthic/benthopelagic sharks differ compared to pelagic sharks (Hoffmann et al., 2020; Sternes et al., Chapter 2). Ecologically, benthic and benthopelagic sharks are drastically different as they are non-obligate ram ventilators that frequently rest on the bottom and

are usually non-migratory whereas pelagic sharks are obligate ram ventilators with known long-distance migrations (Compagno, 1990; Ebert et al., 2021; Abel and Grubbs, 2023). Thus, it is unsurprising that our investigation of a pelagic shark reveals new functional aspects of shark pectoral fins.

Pelagic shark pectoral fins during vertical movements

In benthic and benthopelagic species, the pectoral fins generate positive lift during rising behavior and negative lift during sinking behavior (Wilga and Lauder, 2000, 2001; Paig-Tran et al., 2022). For example, the leopard shark generated small, but significant, lift forces for rising (+14° AoA) and sinking (-22° AoA) and the bamboo shark also generated lift forces for rising (+20° AoA) and sinking (-14° AoA; Wilga and Lauder, 2000, 2001). Therefore, the pectoral fin range of angles of attack exhibited for rising in the water column are from +14° to +20°and -14° to -22° angle of attack for sinking. In our analyses, the largest amount of lift produced for positive and negative angles of attack was +20° and -13°, respectively (**Table 3.1**, **Figure 3.3A**). Both values are near or within range of those reported in previous species examined, suggesting the mako will most likely orient its fins in this manner to produce the maximum amount of positive or negative lift for vertical movement in the water column.

For pelagic sharks, vertical movements in the water column are a critical aspect of their ecology (Andrzejaczek et al., 2022). Vertical behavior is hypothesized to be driven by optimizing the energetic costs of locomotion, foraging, and thermoregulation (Nakumara et al., 2011; Iosilevskii et al., 2012; Andrzejaczek et al., 2018; Watanabe et

al., 2021). Like other pelagic sharks, the mako shark frequently performs vertical movements in the water column (Vaudo et al., 2016b; Santos et al., 2021; Andrzejaczek et al., 2022; Saraiva et al. 2023; Vaudo et al., 2024). During vertical movements, pelagic sharks will rise up in the water column then enter a descending 'gliding' phase where tail beat frequency stops also called "yo-yo swimming" (Klimley et al., 2002; Shepard et al., 2006; Nakumura et al., 2011; Iosilevskii et al., 2012; Andrzejaczek et al., 2018; Saraiva et al., 2023; Waller et al., 2023). This would implicate the critical importance of the pectoral fins as control surfaces during such behavior (Fish and Lauder, 2017).

We found the pelagic mako shark generates considerably more lift compared to benthic and benthopelagic shark species (Wilga and Lauder, 2000, 2001). Wilga and Lauder (2000) recorded forces of 0.06 and 0.09 N for leopard shark pectoral fins during rising and sinking behavior whereas the mako generated a force of 18.56 N during rising behavior (**Table 3.1**). Although a limited number of shark species have been sampled, we can compare to other vertebrates with convergent morphology and ecology. The appendages of pinnipeds, cetaceans, and penguins all share a similar morphology to the mako shark (Weber et al., 2009; Harada et al., 2021; Hocking et al., 2021; Masud and Dabichnki, 2022), and we found the pelagic shark pectoral fins perform similar if not better than these groups. For example, the mako achieved a lift coefficient of 1.4 (**Table 3.1**) (comparable to cetaceans and penguins), whereas pinnipeds are only capable of achieving a lift coefficient of 0.75 (Weber et al., 2009; Harada et al., 2021; Hocking et al., 2021; Masud and Dabichnki, 2022).

Conclusions

Our findings reveal a difference in pectoral fin function between benthic and pelagic shark, with the latter generating lift during steady horizontal swimming. Benthic and benthopelagic shark species use their pectoral fins exclusively for turning maneuvers and rising/sinking behaviors (Wilga and Lauder, 2000, 2001; Hoffmann and Porter, 2019; Paig-Tran et al., 2022). Pelagic sharks can use their pectoral fins for the same functions as benthic and benthopelagic sharks, but also use their pectoral fins as lift-generating appendages to help the shark maintain position in the water column during steady swimming (Affleck, 1950; Alexander, 1965; Harris, 1936; Simons, 1970; Thomson, 1976; Fish and Shannahan, 2000). This additional lift generation from the pectoral fins optimizes their cost of transport (Iosilevskii and Papastamatiou, 2016; Sternes et al., Chapter 2).

Although we focus on one pelagic species, future studies should examine other pelagic sharks that have pectoral fins with higher aspect ratios than the mako such as the blue shark (*Prionace glauca*) or oceanic white tip (*Carcharhinus longimanus*) (Sternes et al., Chapter 2). Additionally, we acknowledge that future studies based on empirical data may be helpful to fully understand pectoral fin performance during swimming. For example, shark pectoral fins vary considerably in their skeletal support which may affect the overall stiffness of the fin (Compagno, 1988; Tomita et al., 2014; Hoffmann et al., 2020; Silva et al., 2023). However, given the logistical challenges in using pelagic sharks for performance studies (Graham et al., 1990; Lowe, 1996; Donley et al., 2005) this data may be difficult to obtain. Our CFD approach can be used to explore important aspects of

pectoral fin function and can also be used to explore the functional consequences of morphological diversity.

References

Abbott IH, von Doenhoff AE. 1958. *Theory of wing sections*. Dover.

Abel DC, Grubbs RD. 2023. *The lives of sharks: a natural history of shark life.* Princeton, NJ: Princeton University Press.

Affleck RJ. 1950. Some points in the function, development, and evolution of the tail in fishes. *Proceeding of the Zoological Society of London* 120: 349–368.

Aftab SMA, Rafie ASM, Razak NA, Ahmad KA. 2016. Turbulence model selection for low Reynolds number flows. *PLoS ONE* 11: e0153755.

Alexander RM. 1965. The lift produced by the heterocercal tails of Selachii. *Journal of Experimental Biology* 43: 131–138.

Andrzejaczek S, Gleiss AC, Jordan LKB, Pattiaratchi CB, Howey LA, Brooks EJ, Meekan MG. 2018a. Temperature and the vertical movements of oceanic whitetip sharks, *Carcharhinus longimanus*. *Scientific Reports* 8: 8351.

Andrzejaczek S, Lucas TCD, Goodman MC, Hussey, NE, Armstrong AJ, Carlisle A, Coffey DM, Gleiss, AC, Huveneers C, Jacoby DMP, et al. 2022. Diving into the vertical dimension of elasmobranch movement ecology. *Science Advances* 8: eabo1754.

Bernal D, Dickson KA, Shadwick RE, Graham JB. 2001. Review: Analysis of the evolutionary convergence for high performance swimming in lamnid sharks and tunas. *Comparative Biochemistry and Physiology Part A Molecular Integrative Physiology* 129: 695–726.

Bernal D, Sepulveda C, Mathieu-Costello O, Graham JB. 2003a. Comparative studies of high performance swimming in sharks. I Red muscle morphometrics, vascularization and ultrastructure. *Journal of Experimental Biology* 206: 2831–2843.

Bernal D, Smith D, Lopez G, Weitz D, Grimminger T, Dickson K, Graham JB. 2003b. Comparative studies of high performance swimming in sharks II. Metabolic biochemistry of locomotor and myocardial muscle in endothermic and ectothermic shark. *Journal of Experimental Biology* 206: 2845–2857.

Bernal D, Carlson JK, Goldman KJ, Lower CG. 2012. Energetics, metabolism, and endothermy in sharks and rays. In Carrier JC, Musick JA, Heithaus MR, eds. *Biology of sharks and their relatives, second edition*. Boca Raton, FL: CRC Press, p. 211–237.

Block BA, Jonsen ID, Jorgensen SJ, Winship AJ, Shaffer SA, Bograd SJ, Hazen EL, Foley DG, Breed, GA, et al. 2011. Tracking apex marine predator movements in a dynamic ocean. *Nature* 475: 86–90.

Casey JG, Kohler NE. 1992. Tagging studies on the shortfin mako shark (*Isurus oxyrinchus*) in the Western North Atlantic. *Australian Journal of Marine and Freshwater Research* 43:45–60.

Coates MI. 2003. The evolution of paired fins. *Theory of Biosciences* 122: 266–287.

Compagno LJV. 1977. Phyletic relationships of living sharks and rays. *American Zoologist* 17: 303–322.

Compagno LJV. 1988. *Sharks of the order Carcharhiniformes*. Princeton, NJ: Princeton University Press.

Compagno LJV. 1990. Alternative life-history strategies of cartilaginous fishes in time and space. *Environmental Biology of Fishes* 28: 33–75.

Costa Rocha PA, Barbosa Rocha HH, Moura Carneiro FO, Vieira da Silva ME, Valenta Bueno A. 2014. *k–ω* SST (shear stress transport) turbulence model calibration: A case study on a small scale horizontal axis wind turbine. *Energy* 65: 412–418.

Díez G, Soto M, Blanco JM. 2015. Biological characterization of the skin of shortfin mako shark Isurus oxyrinchus and preliminary study of the hydrodynamic behavior through computational fluid dynamics. *Journal of Fish Biology* 87: 123–137.

Donley JM, Shadwick RE, Sepulveda CA, Konstantinidis P, Gembella S. 2005. Patterns of red muscle strain/activation and body kinematics during steady swimming in a lamnid shark, the shortfin mako (*Isurus oxyrinchus*). *Journal of Experimental Biology* 208: 2377–2387.

Ebert DA, Dando M, Fowler S. 2021. *Sharks of the world: a complete guide*. Princeton, NJ: Princeton University Press.

Fish FE, Lauder GV. 2017. Control surfaces of aquatic vertebrates: active and passive design and function. *Journal of Experimental Biology* 220: 4351–4363.

Fish FE, Shannahan LD. 2000. The role of the pectoral fins in body trims of sharks. *Journal of Fish Biology* 56: 1062–1073.

Gaylord MK, Blades EL, Parsons GR. 2020. A hydrodynamics assessment of the hammerhead shark cephalofoil. *Scientific Reports* 10: 14495.

Graham JB, Dewar H, Lai NC, Lowell WR, Arce SM. 1990. Aspects of shark swimming performance determined using a large water tunnel. *Journal of Experimental Biology* 151: 175–192.

Grubbs RD. 2010. Ontogenetic shifts in movements and habitat use. In: Carrier JC, Musick JA, Heithaus MR, eds. *Sharks and their relatives II: Biodiversity, adaptive physiology, and conservation*. Boca Raton, FL: CRC Press, 319–350.

Harada N, Oura T, Maeda M, Shen Y, Kikuchi DM, Tanaka H. 2021. Kinematics and hydrodynamics analyses of swimming penguins: wing bending improves propulsion performance. *Journal of Experimental Biology* 224: jeb242140.

Harris JE. 1936. The role of the fins in the equilibrium of the swimming fish. I. Wind-tunnel tests on a model of *Mustelus canis* (Mitchell). *Journal of Experimental Biology* 13: 476–493.

Hazekamp AAH, Mayer R, Osinga N. 2009. Flow simulation along a seal: the impact of an external device. *European Journal of Wildlife Research* 56: 131–140.

Heinicke MP, Naylor GJP, Hedges SB. 2009. Cartilaginous fishes (Chondrichthyes). In Hedges SB, Kumar S, eds. *The timetree of life.* Oxford, UK: Oxford University Press, pp. 320–327.

Hoffmann SL, Porter ME. 2019. Body and pectoral fin kinematics during routine yaw turning in bonnethead sharks. (*Sphyrna tiburo*). *Integrative Organismal Biology* 1: obz014.

Hoffmann SL, Buser TJ, Porter ME. 2020. Comparative morphology of shark pectoral fins. *Journal of Morphology* 281: 1501–1516.

Iosilevskii G, Papastamatiou YP. 2016. Relations between morphology, buoyancy and energetics of requiem sharks. *Royal Society Open Science* 3: 160406.

Irschick DJ, Christiansen F, Hammerschlag N, Martin J, Madsen PT, Wyneken J, Brooks A, Gleiss A, Fossette S, Siler C, et al. 2022. 3D visualization processes for recreating and studying organismal form. *iScience* 25: 104867.

Irschick D, Higham T. 2016. *Animal athletes: an ecological and evolutionary approach.* Oxford University Press.

Klimley AP, Beavers SC, Curtis TH, Jorgensen SJ. 2002. Movements and swimming behavior of three species of shark in La Jolla Canyon, California. *Environmental Biology of Fishes* 63: 117–135.

Lingham-Soliar T. 2005. Caudal fin allometry in the white shark *Carcharodon carcharias*: Implications for locomotory performance and ecology. *Naturwissenschaften* 92: 231–236.

Liu H, Wassersug RJ, Kawachi K. 1996. A computational fluid dynamics study of tadpole swimming. *Journal of Experimental Biology* 199: 1245–1260.

Lowe CG. 1996. Kinematics and critical swimming speed of juvenile scalloped hammerhead sharks. *Journal of Experimental Biology* 199: 2605–2610.

Maisey JG. 2012. What is an 'elasmobranch'? the impact of paleontology in understanding elasmobranch phylogeny and evolution. *Journal of Fish Biology* 80: 918–951.

Masud MH, Dabnichki P. 2022. Aerodynamic performance analysis of penguin-inspired biomimetic aircraft wing. In: Karakoc TH, Das R, Ekmekci I, Dlakiran A, Ercan AH, eds. *Green approaches in sustainable aviation: proceedings of international symposium on sustainable aviation 2022*. Berlin, Germany: Springer. p. 115–120.

Menter FR. 1994. Two-equation eddy-viscosity turbulence models for engineering applications. *AIAA Journal* 32: 1598–1605.

Nakamura I, Watanabe YY, Papastamatiou YP, Sato K, Meyer CG. 2011. Yo-yo vertical movements suggests a foraging strategy for tiger sharks *Galeocerdo cuvier*. *Marine Ecology Progress Series* 424: 237–246.

Obayashi Y, Sumikawa H, Miyoshi T. 2024. The hammerhead shark's cephalofoil reduces fluid moments during turning motion. *Ichthyological Research* https://doi.org/10.1007/s10228-024-00966-0

Paig-Tran EWM, Porter ME, Ferry LA, Whitenack LB. 2022. How to build a sharks: biomechanics and bioinspiration. In In Carrier JC, Simpfendorfer CA, Heithaus MR, Yopak KE, eds. *Biology of sharks and their relatives, third edition*. Bocar Raton, FL: CRC Press, pp. 59–103.

Renshaw S, Hammerschlag N, Gallagher AJ, Lubitz N, Sims DW. 2023. Global trackin of shark movements, behaviour, and ecology: a review of the renaissance years of satellite tagging studies, 2010–2020. *Journal of Experimental Marine Biology and Ecology* 560: 151841.

Santos CC, Domingo A, Carlson J, Natanson LJ, Travassos P, Macías D, Cortés E, Miller P, Hazin F, Mas F et al. 2021. Movements, habitat use, and diving behavior of shortfin mako in the Atlantic Ocean. *Frontiers in Marine Science* 8: 686343.

Saraiva BM, Macena BLM, Solleliet-Ferreira S, Afonso P, Fontes J. 2023. First insights into the shortfin mako shark (*Isurus oxyrinchus*) fine-scale swimming behaviour. *Royal Society Open Science* 10: 230012.

Sepulveda CA, Kohin S, Chan C, Vetter R, Graham JB. 2004. Movement patterns, depth preferences, and stomach temperatures of free-swimming juvenile mako sharks, Isurus oxyrinchus, in the Southern California Bight. *Marine Biology* 145: 191–199.

Shepard ELC, Ahmed MZ, Southall EJ, Witt MJ, Metcalfe JD, Sims DW. 2006. Diel and tidal rhythms in diving behaviour of pelagic sharks identified by signal processing of archival tagging data. *Marine Ecology Progress Series* 328: 205–213.

Silva JPCB, Shimada K, Datovo A. 2023. The importance of the appendicular skeleton fo the phylogenetic reconstruction of lamniform sharks (Chondrichthyes: Elasmobranchii). *Journal of Morphology* 284: e21585.

Simons JR. 1970. The direction of thrust produced by the heterocercal tails of two dissimilar elasmobranchs: the Port Jackson shark, *Heterodontus portusjacksoni* (Meyer), and the piked dogfish, *Squalus megalops* (MacLeavy). *Journal of Experimental Biology* 52: 95–107.

Sternes PC, Shimada K. 2020. Body form in sharks (Chondrichthyes: Elasmobranchii) and their functional, ecological, and evolutionary implications. *Zoology* 140: 125799.

Stevens JD. 2008. The biology and ecology of the shortfin mako shark, *Isurus oxyrinchus*. In: Camhi MD, Pikitch EK, Babcock EA, eds. Sharks of the Open Ocean: Biology, Fisheries and Conservation. Hoboken, NJ: Blackwell Publishing, pp. 87–94.

Sumikawa H, Naraoka Y, Obayashi Y, Fukue T, Miyoshi T. 2023. Fluid dynamic properties of shark caudal fin morphology and its relationship to habitats. Ichthyological Research https://doi.org/10.1007/s10228-023-00933-1

Thomson KS. 1976. On the heterocercal tail in sharks. *Paleobiology* 2: 19–38.

Thomson KS, Simanek DE. 1977. Body form and locomotion in sharks. *American Zoologist* 17: 343–354.

Tomita T, Tanaka S, Sato K, Nakaya K. 2014. Pectoral fin of the megamouth shark: skeletal and muscular systems, skin histology, and functional morphology. *PLoS ONE* 9: e86205.

Vaudo JV, Byrne ME, Wetherbee BM, Harvey GM, Shivji MS. 2016a. Long-term satellite tracking reveals region-specific movements of a large pelagic predator, the shortfin mako shark, in the western North Atlantic Ocean. *Journal of Applied Ecology* 54: 1765–1775.

Vaudo JV, Dewar H, Byrne ME, Weatherbee BM, Shivji MS. 2024. Integrating vertical and horizontal movements of shortfin mako sharks *Isurus oxyrinchus* in the eastern North Pacific Ocean. *Marine Ecology Progress Series* 732: 85–99.

Vaudo JV, Wetherbee BM, Wood AD, Weng K, Howey-Jordan LA, Harvey GM, Shivji MS. 2016b. Vertical movements of shortfin mako sharks in the Western North Atlantic Ocean are strongly influenced by temperature. *Marine Ecology Progress Series* 54: 163–175.

Waller MJ, Queiroz N, da Costa I, Cidade T, Loureiro B, Womersley FC, Fontes J, Afonso P, Macena BCL, Loveridge A et al. 2023. Direct measurement of cruising and burst swimming speeds of the shortfin mako shark (*Isurus oxyrinchus*) with estimates of field metabolic rate. *Journal of Fish Biology* https://doi.org/10.1111/jfb.15475

Watanabe YY, Goldman KJ, Caselle JE, Chapman DD, Papastamatiou YP. 2015. Comparative analyses of animal-tracking data reveal ecological significance of endothermy in fishes. *Proceedings of the National Academy Sciences USA* 112: 6104–6109.

Watanabe YY, Nakamura I, Chiang W. 2021. Behavioral thermoregulation linked to foraging in blue sharks. *Marine Biology* 16: 161.

Weber PW, Howle LE, Murray MM, Fish FE. 2009. Lift and drag performance of odontocete cetacean flippers. *Journal of Experimental Biology* 212: 2149–2158.

Whitenack LB, Kim SL, Sibert EC. 2022. Bridging the gap between paleobiology and biology. In Carrier JC, Simpfendorfer CA, Heithaus MR, Yopak KE, eds. *Biology*

of sharks and their relatives, third edition. Bocar Raton, FL: CRC Press, pp. 1–29.

Wilcox DC. 1988. Reassessment of the scale-determining equation for advanced turbulence models. *AIAA Journal* 26:1299–1310.

Wilga CD, Lauder GV. 2000. Three-dimensional kinematics and wake structure of the pectoral fins during locomotion in leopard sharks *Triakis semifasciata*. *Journal of Experimental Biology* 203: 2261–2278.

Wilga CD, Lauder GV. 2001. Functional morphology of the pectoral fins in bamboo sharks, *Chiloscyllium plagosium*: Benthic vs. pelagic station-holding. *Journal of Morphology* 249: 195–209.

Tables & Figures

Table 3.1 List of all angles of attack and corresponding lift force, drag force, lift coefficient, drag coefficient, and efficiency.

Angle of Attack (°)	Lift (N)	Drag (N)	Lift Coefficient	Drag Coefficient	Efficiency (Lift/Drag)
-25	-19.79	-18.56	-0.57	0.54	-1.07
-23	-19.32	16.98	-0.56	0.49	-1.14
-21	-21.34	15.40	-0.62	0.45	-1.39
-19	-25.47	13.26	-0.74	0.38	-1.92
-17	-24.98	11.75	-0.72	0.34	-2.13
-15	-26.76	9.84	-0.78	0.29	-2.72
-13	-45.44	6.06	-1.32	0.18	-7.50
-11	-39.31	4.09	-1.13	0.12	-9.62
-9	-31.96	4.06	-0.93	0.12	-7.87
-7	-26.00	3.48	-0.75	0.10	-7.47
-5	-18.63	2.97	-0.54	0.09	-6.26
-3	-12.85	2.67	-0.37	0.08	-4.82
-1	-5.83	2.49	-0.17	0.07	-2.34
+1	0.64	2.54	0.02	0.07	0.25
+3	7.22	2.74	0.21	0.08	2.63
+5	14.47	3.04	0.42	0.09	4.77
+7	20.5	3.52	0.59	0.10	5.82
+9	26.74	4.17	0.77	0.12	6.41
+11	31.57	4.79	0.91	0.14	6.68
+13	37.44	5.70	1.08	0.17	6.57
+15	42.31	6.56	1.22	0.19	6.45
+17	46.61	7.82	1.35	0.22	5.96
+19	50.32	9.12	1.46	0.26	5.52
+21	50.27	9.09	1.47	0.2	5.53
+23	31.71	14.36	0.92	0.42	2.21
+25	32.58	16.04	0.94	0.46	0.46

Figure Legends

Figure 3.1 Mako shark pectoral fin model geometry. A, Original reconstruction by DigitalLife3D. B, Processed surface model with smooth and refined mesh. C-D, Comparison of pectoral fin section outlines from lateral view at three locations along the span of the fin (shown in the dorsal view on the shark) for the original model (C) and cleaned model (D). E, Final left fin surface model made out of spline surface segments and used for CFD.

Figure 3.2 CFD validation test results on NACA2412 wing profile. A, Outline of the NACA2412 with angle of attack sign definition. B, Results of the mesh convergence analysis at 0° angle of attack and Re = 5.0 10^5. The arrows indicate the mesh size that was used in subsequent simulations. C, Comparison of lift coefficient (Cl) in function of angle of attack for wind tunnel data (Abbott and Von Doenhoff 1959) with the SST k-□ model and settings used in this study, and (D) a similar comparison in a drag polar plot. E, Geometry of the flow domain and boundary conditions for the pectoral fin CFD.

Figure 3.3 Results of CFD analyses. A, Lift coefficient versus angle of attack. B, Drag coefficient versus angle of attack. C, Efficiency (Lift/Drag) versus angle of attack. D, Lift coefficient by drag coefficient.

Figure 3.4 Hydrodynamics of the pelagic shark pectoral fin at the optimum drag-to-lift ratio positions for positive +11° (A-C) and negative -11° (D-F) angles of attack. Incoming flow velocity is 1.86 m s^{-1} in the z-axis direction (Re = 3.7 10^5). In A and D, 3D flow velocity magnitudes are shown on a parasagittal plane halfway the span of the fin as indicated on the top right corner. In B and E, pressure patterns on the fin surface are shown from a lateral view (top), dorsal view (lower left), and ventral view (lower right). In C and F, areas in the flow field where the vorticity dominates are shown by isosurfaces of the Q-criterion set at 100 s^{-1}. To indicate the direction of the vortical flows, the isosurfaces are colored by spanwise flow velocities, with hot colors indicating flow from tip to base and cool colors from base to tip.

Figure 3.1 Mako shark pectoral fin model geometry.

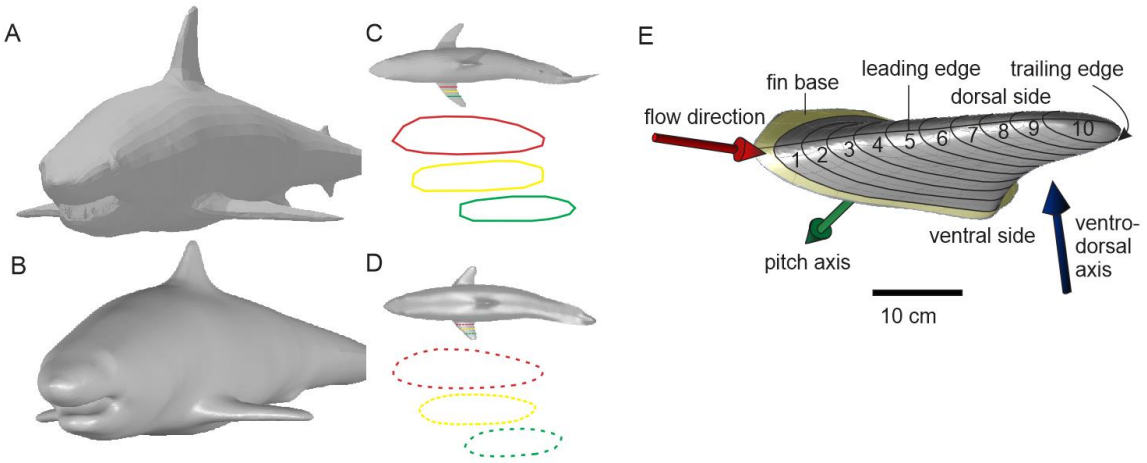

Figure 3.2 CFD validation test results on NACA2412 wing profile.

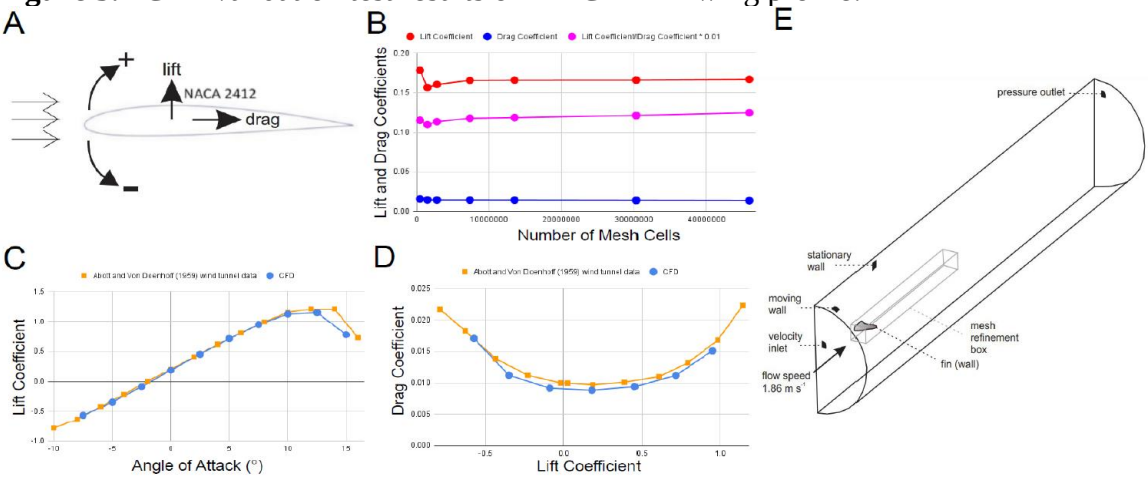

Figure 3.3 Results of CFD analyses.

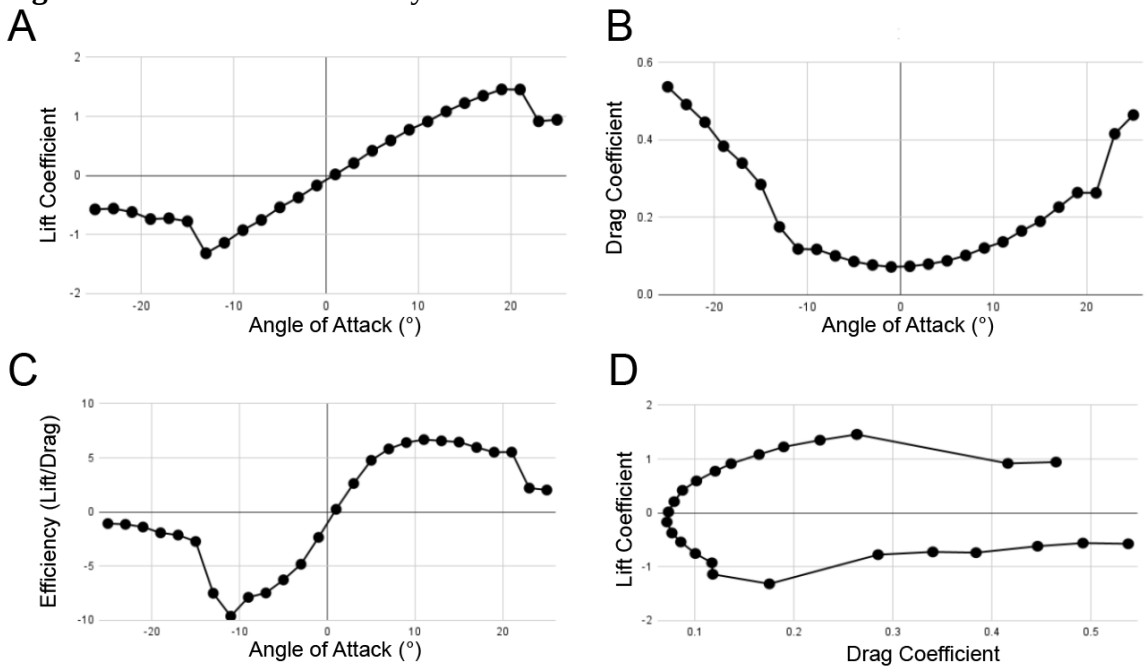

Figure 3.4 Velocity, pressure, vorticity, diagrams of pectoral fin at +11° and -11° AoA.

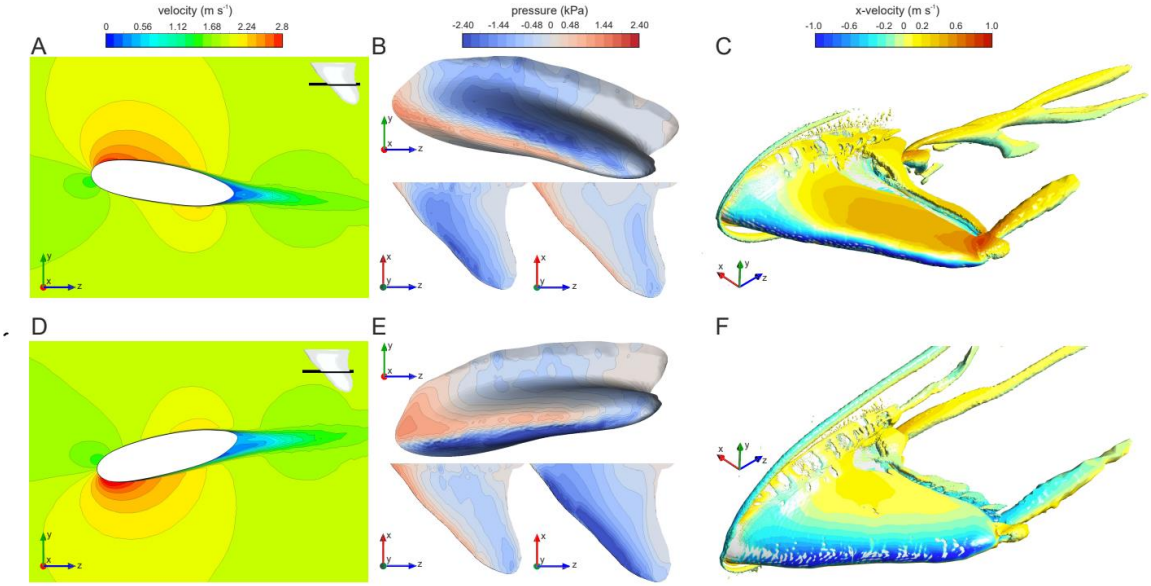

CHAPTER 4

Ontogenetic Scaling of Morphology in Sharks is Partially Explained by Ecological Shifts

Abstract

Patterns of scaling among organisms can be related to a myriad of changes that occur throughout an animal's life, including physiological, behavioral, functional, and ecological. Understanding these drivers of shape change in organisms is important for understanding phenotypic diversity. Among sharks, allometric niche shifts have been proposed as one driver of allometric changes in morphology, whereas biomechanical demands to maintain locomotory capabilities might also result in allometry. Despite a number of studies, we lack a broad comparison of species that vary in ecology, size, and life history. We collected extensive morphological data on four species of shark found off the coast of California and combined this with six species from other studies. We addressed the question of whether lifestyle (benthic, benthopelagic, or pelagic) was a key driver of scaling relationships. We found that both ecological and functional demands likely drive allometry in sharks and indicate other factors that might also play roles. Our results indicate the complex interactions between shape, behavior, ecology, and function. Given the large number of extant shark species, this opens the door to more extensive analyses of the diversity of shark scaling relationships.

Introduction

Almost every aspect of an animal's life is impacted by body size (Schmidt-Nielsen, 1984). Both how the environment influences the organism and the capacity of an organism to perform in its environment can be influenced by ontogenetic changes in size and shape (Higham et al., 2021). Although maintaining geometric similarity (isometric growth) can be beneficial, there can often be negative consequences (Schmidt-Nielsen, 1984). For example, the increase in forces applied to the bones of terrestrial mammals (proportional to mass) rises faster than those resisting the force (proportional to cross-sectional area) as they get larger (Biewener, 1989). Aquatic organisms experience unique challenges given that water is drastically more viscous and denser than air. Larger animals experience great increases in pressure drag forces, favoring more streamlined bodies and fins (Fish, 2023). Thus, studies of scaling are best when there is a wide range in body sizes (Schimdt-Nielsen, 1984). Sharks are a perfect group for this approach given their extremely wide range of body sizes (20 cm to 800 cm) and variety of ecological niches occupied (Ebert et al., 2021; White et al., 2022).

Sharks (Elasmobranchii: Selachii), with over 540 species (Ebert et al., 2021; White et al., 2022), can be classified into two different body groups based on their ecology (Sternes and Shimada, 2020). For example, benthic sharks tend to be elongated, ‘shallow-bodied’, with a posteriorly placed first dorsal fin along the body axis, whereas pelagic sharks are stout, ‘deep-bodied’, with a more anteriorly placed first dorsal fin along the body axis (Thomson and Simanek, 1977; Sternes and Shimada, 2020).

However, some shark species undergo habitat shifts during ontogeny (Grubbs 2010; Abel and Grubbs 2023), suggesting the possibility of allometric changes in morphology.

Recent studies examining the scaling of shark body form have found several interesting patterns (Sternes and Higham, 2022; Bellodi et al., 2023; Gayford et al., 2023a, b; Yun and Watanabe, 2023; Gayford et al., 2024; Seamone et al., 2024). Gayford et al. (2023b) proposed the allometric niche shift hypothesis which states that pressures associated with long-distance movements, along with changes in diet, can drive changes in morphology. For example, scalloped hammerheads exhibit considerable allometric changes in shape as they shift from a coastal shallow water habitat to a pelagic deep-water habitat as they grow larger (Sternes and Higham, 2022). Specifically, larger individuals found in the pelagic habitat had increased fin aspect ratios which lower their cost of transport. Among the other instances, it was demonstrated that shifts in ecology coincided with major changes in scalloped hammerhead body shape such as a more streamlined body for improved hydrodynamics during open ocean long distance migrations (Sternes and Higham, 2022). On the other hand, benthic nurse sharks with the same habitat and no major diet shifts throughout life exhibit isometric growth in morphology (Irschick and Hammerschlag, 2015). Alternatively, Seamone et al. (2024) investigated the shape of pelagic blue sharks and found they exhibited allometric growth despite no change in prey type or habitat. Seamone et al. (2024) suggested allometric growth may be required to maintain similar functions across increasing size. For example, blue sharks become more neutrally buoyant as they grow larger which in turn

would shift the caudal fin from acting as a lift and thrust generating appendage to one that only generates thrust.

Approximately 43 different species of sharks have been reported off the California coastline (over 1,100 miles) of the United States which varies in water temperatures due to differing currents and seasonal changes (Ebert, 2003). Among the 43 reported species, those commonly found include: horn sharks (*Heterodontus francisci*), swellsharks (*Cephaloscyllium ventriosum*), tope sharks (*Galeorhinus galeus*), and leopard sharks (*Triakis semifasciata*) (**Figure 4.1**) (Ebert, 2003; Ebert et al., 2021). Horn sharks and swellsharks are benthic with very similar habitats and small home ranges that commonly overlap whereas tope sharks and leopard sharks are regarded as stronger swimming and benthopelagic, with much larger home ranges (Ebert, 2003; Ebert et al., 2021). Additionally, tope sharks and leopard sharks will give birth in shallow water bays and estuaries and larger individuals may be found farther offshore in deeper habitats (Ebert, 2003; Ebert et al., 2021).

Horn sharks and swellsharks display clear differences in both overall body morphology and ecology in comparison to tope and leopard sharks (Thomson and Simanek, 1977; Compagno, 1990; Ebert, 2003; Sternes and Shimada, 2020; Ebert et al., 2021). However, it is unknown how the morphology of all four species scales with body size. Horn sharks experience a diet shift through ontogeny but they remain benthic throughout life (Ebert, 2003; Ebert et al., 2021). Swellsharks have the same general ecology and habitat throughout their life, whereas tope and leopard sharks exhibit major shifts in habitat and diet (Ebert, 2003; Ebert et al., 2021). Given the allometric niche shift

hypothesis for sharks (Gayford et al., 2023b), we predict that the body and fin morphology of horn sharks and swellsharks will scale with isometry whereas tope sharks and leopard sharks should exhibit allometric changes in morphology that relate to changes in ecology. Here we assessed the scaling of body and fin shape in horn sharks, swellsharks, tope sharks, and leopard sharks using both linear and area measurements over a large size range for all four species. In addition, we used shark scaling data from other previous studies allowing us to have a dataset of 10 sharks with varying ecologies. Since we compared species using data from live and museum specimens, body shape would be difficult to compare due to the possibility of deformity and shrinkage in the museum specimens. Therefore, we focused on scaling patterns in three key fins for locomotion: the caudal, pectorals, and dorsal. We hypothesized that allometric scaling would be prevalent in those species that exhibited ontogenetic habitat shifts. In light of previous work (e.g., Gayford et al., 2023b and Sternes and Higham, 2023), we predicted positive allometric relationships in those species that shift to a pelagic lifestyle after a certain body size is reached, such as in the scalloped hammerhead.

Materials and methods

Samples

We examined preserved specimens of horn sharks (*H. francisci*): $N = 41$ (15–91 cm TL), swellsharks (*C. ventriosum*): $N = 28$ (19–79 cm TL), tope sharks (*G. galeus*): $N = 20$ (32–176 cm TL), and leopard sharks (*T. semifasciata*): $N = 29$ (21–102 cm TL) from

the Natural History Museum of Los Angeles County (LACM), Los Angeles, CA, USA and the Scripps Institute of Oceanography (SIO), University of California, San Diego, CA, USA.

In addition, to the data collected here, we included data from six other species from previously published studies. These include nurse sharks (*Ginglyostoma cirratum*), blacktip sharks (*Carcharhinus limbatus*), bull sharks (*Carcharinus leucas*), tiger sharks (*Galeocerdo cuvier*), scalloped hammerheads (*Sphyna lewini*), and blue sharks (*Prionace glauca*).

Morphological measurements

We followed the previous methods of Irschick and Hammerschlag (2015) and Sternes and Higham (2022) to document shape changes in the four species. We used a standard metric tape measure (accurate to 1 mm) to quantify the following measurements: (1) the head size (EE): distance between the inner part of the eyes; (2) lateral span (LS): the distance from (i.e. around the curved dorsal side of the shark) from the insertion point of the anterior edge of one pectoral fin to the insertion point of the other pectoral fin; (3) frontal span (FS): the distance (i.e. around the curved dorsal side of the shark) from the insertion point of the anterior edge of the dorsal fin to a line oriented parallel to the horizontal plane of the pectoral fin; (4) proximal span (PS): the distance spanning (i.e. around the curved dorsal side of the shark) from the insertion point of the posterior edge of the dorsal fin to a line oriented parallel to the horizontal plane of the pectoral fin; (5) caudal keel circumference (CKC): total circumference at the base of the tail as measured

at the caudal keel; (6) pectoral fin length (PFL): the linear distance from the insertion of the pectoral fin at the distal edge to the tip of the pectoral fin when fully extended; (7) dorsal fin 1 (DF1): distance from the anterior insertion point of the dorsal fin to the tip of the dorsal fin; (8) dorsal fin 2 (DF2): distance from the tip of the dorsal fin to the posterior insertion point of the dorsal fin; (9) dorsal fin 3 (DF3): distance horizontally across the shark body between the anterior and posterior insertion points of the dorsal fin; (10) caudal fin 1 (CF1): the linear distance from the dorsal insertion of the caudal fin to the dorsal tip of the caudal fin; (11) caudal fin 2 (CF2): the linear distance from the dorsal tip of the caudal fin to the ventral tip of the bottom part of the caudal fin; (12) caudal fin 3 (CF3): the linear distance from the bottom anterior edge of the caudal fin to the bottom posterior edge of the caudal fin; and (13) pre-caudal length (PCL): the linear distance from the tip of the snout to the pre-caudal pit, which is a longitudinal notch on the caudal peduncle directly on the anterior side of the caudal fin.

In addition to linear measurements, we obtained digital images of the head, first dorsal fin, pectoral fin, and the caudal fin. We used ImageJ to calculate the area of the various fins and head. Subsequently, we calculated aspect ratio (AR) of each fin, defined as L^2/S, where L and S are the length and area of the fin, respectively.

Scaling and statistical analysis

Following Sternes and Higham (2022) we determined the scaling relationships using the power-law function $y=mx^b$, where in this case, x=PCL (body length in cm), y is the variable of interest, and b is the scaling exponent. All data were Log_{10} transformed prior to analyses. Linear and area measurements have expected isometric slopes of 1.0

and 2.0, respectively. For the comparisons using all 10 species, we examined all 10 species for linear measurements but we only examined, horn sharks, swellsharks, tope sharks, leopard sharks, scalloped hammerheads, and blue sharks. To compare the scaling exponents to those expected from isometry, the 95% confidence interval of the slope was first calculated. If the expected value fell within the confidence interval, the relationship was considered isometric, but an exponent below or above the expected value was considered negative or positive allometry, respectively.

Results

Table 4.1 lists the average and range of measurements for the four species in our study. For scaling, all morphological variables were significantly correlated with body length. **Table 4.2** lists the observed slopes and standard error of the slopes.

Horn shark

For the horn shark, eye-to-eye distance, lateral span, frontal span, caudal keel circumference, pectoral fin area, dorsal fin 1, dorsal fin 2, dorsal fin area, caudal fin 1, caudal fin 2, caudal fin 3, caudal fin upper area, caudal fin lower area, and caudal fin total area all scaled with negative allometry. Pectoral fin aspect ratio scaled with positive allometry. Head area, proximal span, pectoral fin length, dorsal fin 3 all scaled with isometry.

Swellshark

For the swellshark, lateral span, proximal span, dorsal fin 3, caudal fin 3, caudal fin lower area all scaled with isometry. Eye-to-eye, caudal keel circumference, caudal fin

1, caudal fin 2, caudal fin upper area, and caudal fin total area all scaled with negative allometry. Head area, pectoral fin length, pectoral fin area, dorsal fin 1, dorsal fin 2, and dorsal fin area all scaled with positive allometry.

Tope shark

For the tope shark, head area, lateral span, caudal keel circumference, pectoral fin area, pectoral fin aspect ratio, dorsal fin 1, dorsal fin 2, dorsal fin 3, dorsal fin area, caudal fin 2, caudal fin lower area, and caudal fin total area all scaled with isometry. Frontal span, proximal span, pectoral fin length, caudal fin 3, all scaled with positive allometry. Eye-to-eye and caudal fin 1 scaled with negative allometry.

Leopard shark

For the leopard shark, head area, lateral span, frontal span, pectoral fin area, dorsal fin 1, dorsal fin 2, dorsal fin 3, dorsal fin area, caudal fin 1, caudal fin upper area, caudal fin lower area, and caudal fin total area all scaled with isometry. Proximal span, pectoral fin length, and caudal fin 3 all scaled with positive allometry. Eye-to-eye, caudal keel circumference, and caudal fin 2 all scaled with negative allometry.

Comparison across all 10 species

The length of the upper lobe of the caudal fin (caudal fin 1) scaled with negative allometry in nearly all species (**Figure 4.2A**) whereas the lower lobe (caudal fin 3) showed a mix of positive allometry, negative allometry, and isometry (**Figure 4.2B**). Likewise, the pectoral fin length also showed a mix of allometry and isometry (**Figure 4.2C**). Scaling of the length of the pectoral fin scaled isometrically for benthopelagic sharks, whereas benthic and pelagic sharks exhibited allometry (**Figure 4.3A**). The

dorsal fin height (dorsal fin 2) scaled with positive allometry, negative allometry, and isometry depending on the species (**Figure 4.2D**), whereas dorsal fin area was near isometry in most cases (**Figure 4.3B**).

Discussion

All shark species examined in this study exhibited varying degrees of allometric growth. The Allometric Niche Shift hypothesis suggests that sharks undergoing major ecological shifts as they get larger should display allometric growth. In contrast, sharks remaining in a single habitat (with a similar diet) throughout their lives should grow isometrically. On the other hand, it has been suggested sharks must grow allometrically in certain cases to maintain function (i.e., locomotory capabilities) with increasing mass (Seamone et al., 2024). Surprisingly, we found that several traits grew allometrically in sharks that tend to have a constant habitat and diet throughout life. Below we discuss these results and what factors drive allometry in sharks.

Caudal fin shape in relation to ecology and function

The caudal fin is the primary propulsor in sharks and is responsible for thrust generation (Alexander, 1965; Wilga and Lauder, 2002; Paig-Tran et al., 2022). Sharks generally exhibit heterocercal tails, with a larger upper lobe and a much smaller ventral lobe, although there are some specializations that are likely related to ecology and phylogenetic history (Thomson, 1976; Sternes and Shimada, 2020). For example, pelagic sharks have a more symmetrical tail and, in some instances, a lunate shaped tail, whereas

benthic sharks have a much more asymmetrical tail shape (Thomson, 1976; Sternes and Shimada, 2020). Tail shape appears to be linked with swim speed as sharks with more symmetrical, higher aspect ratio caudal fins swim faster than sharks with lower aspect ratio, asymmetrical fins (Iliou et al., 2023; Sumikawa et al., 2023). Some shark species exhibit a more symmetrical tail fin shape as they grow larger (Fu et al., 2016; Anhelt et al., 2020; Yun and Watanabe, 2023) especially when shifting their ecology from a benthic to more pelagic lifestyle (Sternes and Higham, 2022; Gayford et al., 2023b).

The growing number of shark scaling studies (Irschick and Hammerschlag, 2015; Sternes and Higham, 2022; Gayford et al., 2023b; Seamone et al., 2024), offers an opportunity to compare scaling trends across multiple species with varying ecologies. Using the four species from our dataset along with six species from other previous studies, we compared the scaling slopes of the caudal fin upper and lower lobe lengths (**Figure 4.2A, B**). Interestingly, for the upper lobe length (caudal fin 1) we generally observed negative allometry regardless of ecology (**Figure 4.2A**). In fact, there are no cases of positive allometry among the 10 species. The lower lobe (caudal fin 3) exhibited mixed results, including positive (tope, leopard, scalloped hammerhead) and negative (horn, blacktip, bull, tiger) allometry, as well as isometry (swell, nurse).

The negative allometry of the upper lobe, which is larger than the lower lobe, across nearly every species indicates that shark caudal fins become more symmetrical with increasing size. These results may support the idea that, as sharks increase in mass, a more symmetrical caudal fin may be necessary for locomotion (Seamone et al., 2024). Hydrodynamically, a more symmetrical fin may improve the lift to drag ratio indicating

increased efficiency (Vogel, 1994; Alexander, 2003). Additionally, models of shark fins with various shapes have shown that more symmetrical fins will displace water more backwards compared to the traditional asymmetrical (heterocercal) caudal fin that displaces water downwards and backwards (Flammang et al., 2011). Indeed, some species in our study shift their ecology throughout life (i.e., hammerhead, tope, leopard) supporting the idea that the ANS may explain allometry. However, some species have constant ecology throughout life and still show changes in tail shape. Therefore, locomotor demands may play a key role in explaining allometric patterns. However, additional experimental or modeling studies are needed to fully understand the functional changes that occur as sharks get larger.

Pectoral fin shape in relation to ecology and function

In sharks, pectoral fins are control surfaces critical for turning maneuvers, vertical movement, pelagic station holding, and in some cases submerged walking (Pridmore, 1994; Wilga and Lauder, 2000, 2001; Hoffmann and Porter, 2019; Paig-Tran et al., 2022). Pectoral fins exhibit a clear ecological signal as benthic sharks have lower aspect ratio pectoral fins compared to pelagic sharks (Sternes et al., Chapter 2). Additionally, it has been noted when species undergo strong ecological shifts throughout life, their pectoral fin shape may change in response (Sternes and Higham, 2022; Gavford et al., 2023b). For example, scalloped hammerhead shift from a restricted shallow water habitat to a deep-water open ocean habitat when reaching larger body sizes (Duncan and Holland, 2006; Hoyos-Padilla et al., 2014). The pectoral fins tend to become longer and

narrower indicating an increase in aspect ratio, improving the lift to drag ratio and swimming efficiency (Sternes and Higham, 2022).

Across the ten species, we see various cases of positive allometry, negative allometry, and isometry in the pectoral fin length (**Figure 4.2C**). Considering fin length is an isolated linear measurement, we further explored fin shape by comparing pectoral fin area across six of the 10 and still recovered mixed results of allometry and isometry (**Figure 4.3A**). This raises questions on the exact drivers of the pectoral fin scaling in sharks. For example, shifts from nearshore to offshore habitats in the tope, leopard, and scalloped hammerhead may serve as the driver for pectoral fin shape change (Ackerman et al., 2000; Ebert, 2003; Ebert et al., 2021; Nosal et al., 2021; Sternes and Higham, 2022). However, benthic horn and swell sharks exhibit allometry in their pectoral fins despite having a bottom dwelling ecology throughout life. One thing to consider is benthic sharks may encounter areas of higher flow and current and need to generate negative lift or simply hold their place in the substrate using their pectoral fin (Wilga and Lauder, 2001). One possibility is, due to their larger body size which will encounter greater forces of flow (Vogel, 1994), the pectoral fins must change in shape to help larger sharks remain in place. Comparatively, in pelagic sharks with a constant habitat, it has been suggested smaller pectoral fins might be important to reduce drag as the sharks grow in size (Seamone et al., 2024), thus lowering the cost of transport (Vogel, 1994; Alexander, 2003). Future research should explore additional species, and incorporate modeling or experimental approaches to connect shape changes and functional demands.

Dorsal fin shape in relation to ecology and function

The dorsal fin is known to serve as both a stabilizer and as an additional thrust generating appendage (Lingham-Soliar, 2005; Maia et al., 2017). However, this depends on the location of the dorsal fin as fins placed more anteriorly along the body axis are better as stabilizers whereas those located more posteriorly along the body axis will better act as thrust generators Sharks exhibit a clear ecomorphological signal in the position of their dorsal fin as benthic sharks a have more posteriorly located dorsal fin compared to pelagic sharks (Sternes and Shimada, 2020) which in turn suggests clear dorsal fin functional differences between benthic and pelagic sharks.

Across all ten species, the dorsal fin height (dorsal fin 2) exhibits allometry in most cases (**Figure 4.2D**) whereas dorsal fin area shows a mix of allometry and isometry. For benthic shark species, the allometry of the dorsal fin may be related to increased thrust generation (Maia et al., 2017) whereas it has been suggested that allometry in the dorsal fin of pelagic blue sharks may enhance roll stability (Seamone et al., 2024). Interestingly, the benthopelagic sharks mostly displayed isometry, although slight positive allometry was present in the dorsal fin height of the tope shark (**Figure 4.2D, 4.3A, Table 4.2**). Considering benthopelagic sharks can be found either on the bottom or swimming in the open water perhaps there are conflicting ecological forces acting on the dorsal fin. Thus, the dorsal fin may be scaling with isometry due to these conflicting pressures.

Head and body shape in relation to ecology and function

Sharks possess a variety of head and body shapes, but they can generally be categorized as either ‘shallow-bodied’ or ‘deep-bodied’ fusiform sharks (Sternes and Shimada, 2020). Body shape has been greatly influenced by ecology and phylogeny but there remains a paucity of data on the influence of feeding and locomotion on head shape in sharks (Irschick and Hammerschlag, 2015; Fu et al., 2016; Gaylord et al., 2020; Sternes and Shimada, 2020; Paig-Tran et al., 2022). However, ontogenetic changes in ecology, including migratory patterns and diet, have both been proposed as the drivers of allometry in both body and head morphology (Summers et al., 2004; Lowry et al., 2007; Kolmann and Huber, 2009; Fu et al., 2016; Anhelt et al., 2020; Sternes and Higham, 2022; Bellodi et al., 2023; Gayford et al., 2023a, b; Gayford et al., 2024; Seamone et al., 2024). Given that our data set had a mix of live sharks and museum specimens, leading to potential shape changes during preservation, we focus on the California shark species in our discussion below.

The several cases of negative allometry in body and head shape of horn sharks most likely relate to the fact that they hide in caves in crevices (Ebert, 2003). This allows them to exploit these habitats despite increasing in overall body size. However, the negative allometry in the head might be related to a diet shift. Horn sharks prefer worms and small clams as juveniles whereas adults eat snails, crabs, shrimps, sea stars, and sea urchins (Ebert, 2003). Horn sharks are capable of consuming hard prey as adults due to increased mineralization in the jaws and positive allometry of their jaw adducting muscles (Summers et al., 2004; Kolmann and Huber, 2009). This pattern has been

observed in other species such as blacktips (*Carcharhinus limbatus*) and leopard sharks where a narrower head and increased musculature will increase bite performance (Huber et al., 2006; Lowry et al., 2007). Thus, the allometry in the head shape is unsurprising in horn sharks. Swellsharks are unique in that they inflate themselves when under predation pressure (Ebert, 2003; Ebert et al., 2021). Swellsharks will swim into crevices on reefs and inflate themselves to keep themselves lodged in the crevice while hiding from predators (Ebert, 2003). The positive allometry may imply a large body size to help the shark remain lodged in crevices but at the same time a larger body would also small crevices inaccessible.

Tope and leopard sharks both had cases of positive allometry in their body shape which may be related to an increasing liver size. A larger liver can store larger amount of lipids which would in turn improve buoyancy (i.e., increase hydrostatic lift). A similar pattern has been observed in both brown smoothhound sharks and blue sharks (Gayford et al., 2023a; Seamone et al., 2024). Thus, a larger liver with increased hydrostatic benefits would then take the pressure off the caudal fin for generating lift (Flammang et al., 2011), which appears to be the trend in sharks (see caudal fin discussion above). As tope sharks grow larger, their heads become relatively narrower. Similar to the blacktip shark (Huber et al., 2006), the narrowing head of the head may be related to performance differences to be able to consume different prey through ontogeny (Ebert 2003). In both a previous study (Lowry et al., 2007) and our own, the leopard shark head narrows which may be related to bite performance differences through ontogeny (Huber

et al., 2006). Leopard sharks also show a change in diet through ontogeny and like other patterns seen in shark species, a narrower head may be beneficial.

Conclusion

We found that allometric changes in morphology arise from a number of possible reasons, indicating that a single hypothesis, such as the ANS hypothesis, is simply not suitable to make broad scale inferences. For example, some sharks may benefit from a more symmetrical caudal fin as they grow larger, regardless of ecology. In this case, behavioral changes, or changes in functional demand due to increased body size, may necessitate changes in shape. The caudal fin of some sharks may shift from producing both a lift and thrust to exclusively generating thrust as a larger animal. Positive allometry of the liver, which enhances buoyancy (assuming oil content scales with liver mass), among sharks (Bone and Roberts, 1969) would support this idea, since less lift needs to be generated with increases in body size. On the other hand, there are morphological traits, such as those related to the pectoral fin, that likely exhibit allometry due to the drastic changes in habitat such as shifting from a shallow water nearshore habitat to a deepwater open ocean habitat. These two hypotheses are just that. Behavioral changes, physiological changes, and other factors may play key roles in determining how sharks change shape as they grow larger. Future studies should continue to collect data on not only sharks but also other chondrichthyan fishes to perform even broader scale comparisons.

References

Abel DC, Grubbs RD. 2023. *The lives of sharks: a natural history of shark life*. Princeton (NJ): Princeton University Press.

Ackerman JT, Kondratieff MC, Matern SA, Cech Jr. JJ. 2000. Tidal influences on spatial dynamics of leopard sharks, *Triakis semifasciata*, in Tomales Bay, California. *Environmental Biology of Fishes* 58: 33–43.

Alexander RM. 1965. The lift produced by the heterocercal tails of Selachii. *Journal of Experimental Biology* 43: 131–138.

Alexander RM. 2003. *Principles of animal locomotion*. Princeton, NJ: Princeton University Press.

Anhelt H, Sauberer M, Ramler D, Koch L, Pogoreutz C. 2020. Negative allometric growth during ontogeny in the large pelagic filter-feeding basking shark. *Zoomorphology* 139: 71–83.

Bellodi A, Mulas A, Daniel L, Cau A, Porcu C, Carbonara P, Follesa MC. 2023. Ontogenetic shifts in body morphology of demersal sharks' species (Order: Squaliformes) inhabiting the Western-Central Mediterranean Sea, with implications for their bio-ecological role. *Biology* 12: 1150.

Biewener AA. 1989. Scaling body support in mammals: limb posture and muscle mechanics. *Science* 245: 45–48.

Bone Q, Roberts BL. 1969. The density of elasmobranchs. *Journal of Marine Biological Association United Kingdom* 49: 913–937.

Compagno LJV. 1990. Alternative life-history strategies of cartilaginous fishes in time and space. *Environmental Biology of Fishes* 28: 33–75.

Duncan KM, Holland, KN. 2006. Habitat use, growth rates and dispersal patterns of juvenile scalloped hammerhead sharks *Sphyrna lewini* in a nursery habitat. *Marine Ecology Progress Series* 312: 211–221.

Ebert DA. 2003. *Sharks, rays, and chimaeras of California*. Berkeley (CA): University of California Press.

Ebert DA, Dando M, Fowler S. 2021. *Sharks of the world: a complete guide*. Princeton (NJ): Princeton University Press.

Fish FE. 2023. Aquatic locomotion: environmental constraints that drive convergent evolution. In Bels VL, Russell AP, eds. *Convergent evolution: animal form and function*. Berlin, Germany: Springer, pp. 477–522.

Flammang BE, Lauder GV, Troolin DR, Strand T. 2011. Volumetric imaging of shark trail hydrodynamics reveals a three-dimensional dual-ring vortex wake structure. *Proceedings Royal Society B* 278: 3670–3678.

Fu AL, Hammerschlag N, Lauder GV, Wilga CD, Kuo CY, Irschick DJ. 2016. Ontogeny of head and caudal fin shape of an apex marine predator: the tiger shark (*Galeocerdo cuvier*). *Journal of Morphology* 277:556–564.

Gayford JH, Godfrey H, Whitehead DA. 2023a. Ontogenetic morphometry of the brown smoothhound shark *Mustelus henlei* with implications for ecology and evolution. *Journal of Morphology* 284: e21608.

Gayford JH, Whitehead DA, Ketchum JT, Field DJ. 2023b. The selective drivers of allometry in sharks (Chondrichthyes: Elasmobranchii). *Zoological Journal of the Linnean Society* 198: 257–277.

Gayford JH, Whitehead DA, Jaquemet S. 2024. Ontogenetic shifts in the body form in the bull shark (*Carcharhinus leucas*). *Journal of Morphology* 285: e21673.

Gaylord MK, Blades EL, Parsons GR. 2020. A hydrodynamics assessment of the hammerhead shark cephalofoil. *Scientific Reports* 10: 14495.

Grubbs RD. 2010. Ontogenetic shifts in movements and habitat use. In: Carrier JC, Musick JA, Heithaus MR, eds. *Sharks and their relatives II: Biodiversity, adaptive physiology, and conservation*. Boca Raton, FL: CRC Press, 319–350.

Higham TE, Ferry LA, Schmitz L, Irschick DJ, Starko S, Anderson PSL, Bergmann PJ, Jamniczky HA, Monteiro LR, Navon D, et al. 2021. Linking ecomechanical models and functional traits to understand phenotypic diversity. *Trends in Ecology and Evolution* 36: 860–873.

Hoffmann SL, Porter ME. 2019. Body and pectoral fin kinematics during routine yaw turning in bonnethead sharks (*Sphyrna tiburo*). *Integrative Organismal Biology* 1:obz014.

Hoyos-Padilla EM, Ketchum JT, Klimley AP, Galván-Magaña F. 2014. Ontogenetic migration of a female scalloped hammerhead shark *Sphyrna lewini* in the Gulf of California. *Animal Biotelemetry* 2: 17.

Huber DR, Weggelaar CL, Motta PJ. 2006. Scaling of bite force in the blacktip shark *Carcharhinus limbatus*. *Zoology* 109: 109–119.

Iliou et al. AS, Vanderwright W, Harding L, Jacoby DMP, Payne NL, Dulvy NK. 2023. Tail shape and the swimming speed of sharks. *Royal Society Open Science* 10: 231127.

Irschick DJ, Hammerschlag N. 2015. Morphological scaling of body form in four shark species differing in ecology and life history. *Biological Journal of the Linnean Society* 114: 126–135.

Kolmann MA, Huber DR. 2009. Scaling of feeding biomechanics in the horn shark *Heterodontus francisci*: ontogenetic constraints on durophagy. *Zoology* 112: 351–361.

Lingham-Soliar T. 2005. Dorsal fin in the white shark, *Carcharodon carcharias*: a dynamic stabilizer for fast swimming. *Journal of Morphology* 263: 1–11.

Lowry D, Motta PJ, Heuter RE. 2007. The ontogeny of feeding behavior and cranial morphology in the leopard shark *Triakis semisfasciata* (Girard 1854): a longitudinal perspective. *Journal of Experimental Marine Biology and Ecology* 341: 153–167.

Maia A, Lauder GV, Wilga CD. 2017. Hydrodynamic function of dorsal fins in spiny dogfish and bamboo sharks during steady swimming. *Journal of Experimental Biology* 220: 3967–3975.

Nosal AP, Cartamil DC, Long JW, Lührmann M, Wegner NC, Graham JB. 2013. Demography and movement patterns of leopard sharks (*Triakis semifasciata*) aggregating near the head of a submarine canyon along the open coast of southern California, USA. *Environmental Biology of Fishes* 96: 865–878.

Nosal AP, Cartamil DP, Ammann AJ, Bellquist LF, Ben-Aderet NJ, Blincow KM, Burns ES, Chapman ED, Freedman RF, Klimley AP, Logan RK, Lowe CG, Semmens BX, White CF, Hastings PA. 2021. Triennial migration and philopatry in the critically endangered soupfin shark *Galeorhinus galeus. Journal of Applied Ecology* 58: 1570–1582.

Paig-Tran EWM, Porter ME, Ferry LA, Whitenack LB. 2022. How to build a sharks: biomechanics and bioinspiration. In Carrier JC, Simpfendorfer CA, Heithaus MR, Yopak KE, eds. *Biology of sharks and their relatives, third edition*. Bocar Raton, FL: CRC Press, pp. 59–103.

Pridmore PA. 1994. Submerged walking in the epaulette shark *Hemiscyllium ocellatum* (Hemiscyllidae) and its implications for locomotion in rhipidistian fishes and early tetrapods. Zoology 98: 278–297.

Schmidt-Nielsen K. 1984. *Scaling: why is animal size so important?* Cambridge, UK: Cambridge University Press.

Seamone SG, Sternes PC, McCaffrey TM, Tsao NK, Syme DA. 2024. Growing out of the fins: implications of isometric and allometric scaling of morphology relative to increasing mass in blue sharks (*Prionace glauca*). Zoology (in revision).

Sternes PC, Shimada K. 2020. Body forms in sharks (Chondrichthyes: Elasmobranchii) and their functional, ecological, and evolutionary implications. *Zoology* 140: 125799.

Sternes PC, Higham TE. 2022. Hammer it out: shifts in habitat are associated with changes in fin and body shape in the scalloped hammerhead (*Sphyrna lewini*). *Biological Journal of the Linnean Society* 136: 201–212.

Sumikawa H, Naraoka Y, Obayasi Y, Fukue T, Miyoshi T. 2023. Fluid dynamics of shark caudal fin morphology and its relationship to habitats. *Ichthyological Research* https://doi.org/10.1007/s10228-023-00933-1

Summers AP, Ketcham RA, Rowe T. 2004. Structure and function of the horn shark (*Heterodontus francisci*) cranium through ontogeny: Development of a hard prey specialist. Journal of Morphology 260: 1–12.

Thomson KS. 1976. On the heterocercal tail in sharks. *Paleobiology* 2: 19–38.

Thomson KS, Simanek DE. 1977. Body form and locomotion in sharks. *American Zoologist* 17: 343–354.

Vogel S. 1994. *Life in moving fluids: The physical biology of flow, second edition*. Princeton: Princeton University Press.

White WT, O'Neill HL, Naylor GJP. 2022. Taxonomy and diversity of extant elasmobranchs. In Carrier JC, Simpfendorfer CA, Heithaus MR, Yopak KE, eds. *Biology of sharks and their relatives, third edition*. Bocar Raton, FL: CRC Press, pp. 31–57.

Wilga CD, Lauder GV. 2000. Three-dimensional kinematics and wake structure of the pectoral fins during locomotion in leopard shark *Triakis semifasciata*. *Journal of Experimental Biology* 203: 2261–2278.

Wilga CD, Lauder GV. 2001. Functional morphology of the pectoral fin in bamboo sharks, *Chiloscyllium plagosium*: benthic vs. pelagic station-holding. *Journal of Morphology* 249: 195–209.

Wilga CD, Lauder GV. 2002. Function of the heterocercal tail in sharks: quantitative wake dynamics during steady horizontal swimming and vertical maneuvering. *Journal of Experimental Biology* 205: 2365–2374.

Yun C, Watanabe YY. 2023. Allometric growth of the enigmatic deep-sea megamouth shark *Megachasma pelagios* Taylor, Compagno, and Struhasker, 1983 (Lamniformes, Megachasmidae). *Fishes* 8: 300.

Tables & Figures

Table 4.1 Mean morphological (±1 SE) values for 23 variables. Parentheses = ranges

	Horn shark	Swellshark	Tope shark	Leopard shark
Total length	51.9 ± 3.3 (15.0–91.1)	45.3 ± 4.3 (18.6–79.4)	78.1 ± 10.7 (32.0–175.8)	42.2 ± 3.6 (20.9–102.3)
Pre-caudal length	40.0 ± 2.7 (10.2–74.1)	35.0 ± 3.4 (13.3–63.3)	60.6 ± 8.5 (24.5–139.9)	32.6 ± 2.7 (17–78.9)
Eye-to-Eye	4.2 ± 0.2 (1.1–6.9)	4.3 ± 0.4 (2–7.4)	6.7 ± 0.8 (3.1–13.9)	3.6 ± 0.2 (2.2–7.7)
Head area	83.0 ± 11.5 (4.0–287.8)	84.3 ± 14.8 (9.0–244.0)	140.4 ± 32.8 (17.2–459.9)	43.0 ± 10.6 (11.2–304.3)
Lateral span	15.5 ± 1.1 (4.5–29.0)	11.3 ± 1.2 (4.2–23.0)	16.7 ± 2.4 (5.7–38.4)	8.8 ± 0.7 (4.6–20.7)
Frontal span	15.6 ± 1.1 (4.0–32.2)	15.3 ± 1.7 (4.8–29)	19.8 ± 3.1 (5.8–47.3)	9.9 ± 0.9 (4.5–24.7)
Proximal span	15.0 ± 1.1 (3.2–31.8)	9.2 ± 0.9 (3.3–16.1)	18.4 ± 2.9 (4.4–42.3)	7.7 ± 0.8 (3.2–21.8)
Caudal keel circumference	6.5 ± 0.3 (3.1–10.4)	5.6 ± 0.4 (2.9–9.8)	9.0 ± 1.2 (3.3–19.5)	4.4 ± 0.3 (2.9–9.8)
Pectoral fin length	10.9 ± 0.7 (2.3–20.4)	6.2 ± 0.7 (1.7–12.9)	10.1 ± 1.7 (2.4–24.4)	5.5 ± 0.6 (2.3–13.3)
Pectoral fin area	72.6 ± 7.0 (6.4–168.3)	27.6 ± 4.9 (2.9–82.1)	60.9 ± 14.8 (5.3–193.6)	18.8 ± 3.4 (3.9–79.9)
Pectoral fin AR	1.9 ± 0.1 (0.7–3.0)	1.7 ± 0.1 (0.9–2.4)	2.1 ± 0.2 (0.9–3.6)	1.9 ± 0.1 (0.7–2.7)
Dorsal fin 1	6.7 ± 0.4 (1.8–10.6)	4.4 ± 0.5 (1.2–8.9)	7.2 ± 1.0 (2.5–14.6)	5.2 ± 0.5 (2.6–11.9)
Dorsal fin 2	5.4 ± 0.3 (1.7–8.8)	2.8 ± 0.3 (0.8–6.2)	5.1 ± 0.8 (1.5–12.9)	3.4 ± 0.3 (1.6–8.5)
Dorsal fin 3	3.7 ± 0.3 (0.8–9.2)	3.7 ± 0.4 (1.4–7.1)	6.5 ± 1.0 (1.7–14.2)	4.5 ± 0.4 (2.2–10.2)

Dorsal fin area	21.7 ± 2.0 (1.6–51.8)	10.1 ± 1.8 (0.96–28.0)	32.2 ± 8.6 (2.5–134.6)	12.1 ± 2.1 (2.6–49.1)
Dorsal fin aspect ratio	1.5 ± 0.1 (1.0–2.2)	1.0 ± 0.1 (0.5–1.9)	1.11 ± 0.05 (0.8–1.3)	1.1 ± 0.1 (0.5–2.6)
Caudal fin 1	12.0 ± 0.7 (3.8–19.4)	9.6 ± 0.8 (4.3–16.1)	17.3 ± 2.2 (6.2–36.3)	9.0 ± 0.8 (4.6–22.3)
Caudal fin 2	9.6 ± 0.5 (3.2–15.7)	7.9 ± 0.6 (3.7–13.9)	15.2 ± 2.0 (5.3–32.8)	7.6 ± 0.6 (4.1–17.8)
Caudal fin 3	4.0 ± 0.3 (1.3–7.2)	2.5 ± 0.3 (0.6–4.9)	5.9 ± 0.9 (1.7–11.8)	2.0 ± 0.2 (0.4–5.8)
Caudal fin upper area	36.6 ± 3.7 (3.5–87.5)	20.2 ± 3.0 (3.4–52.2)	87.8 ± 21.2 (10.9–336.1)	16.7 ± 2.8 (3.8–62.1)
Caudal fin lower area	21.8 ± 2.4 (2.9–59.1)	13.3 ± 2.2 (1.3–41.6)	30.8 ± 9.1 (2.6–166.8)	7.8 ± 1.4 (1.4–30.0)
Caudal fin total area	58.4 ± 6.1 (5.5–146.7)	33.5 ± 5.2 (4.7–93.8)	118.6 ± 30.0 (14.8–502.)	24.6 ± 4.2 (5.2–92.1)
Caudal fin aspect ratio	1.8 ± 0.03 (1.6–2.5)	2.3 ± 0.1 (1.7–4.0)	2.6 ± 0.1 (1.9–3.2)	2.8 ± 0.08 (2.2–3.4)

Table 4.2 Scaling coefficients and standard errors from regressions between 21 morphological variables versus PCL. Positive and negative allometry values bolded.

	Horn shark	Swellshark	Tope shark	Leopard shark
Eye-to-Eye	0.84 ± 0.03	0.94±0.04	0.85±0.04	0.74±0.03
Head area	1.90 ± 0.07	2.13±0.05	1.89±0.08	1.90±0.11
Lateral span	0.88 ± 0.03	0.98±0.07	1.07±0.04	0.95±0.03
Frontal span	0.93 ± 0.03	1.17±0.03	1.22±0.06	1.01±0.05
Proximal span	1.06 ± 0.05	0.98±0.04	1.26±0.08	1.11±0.05
Caudal keel Circ.	0.67 ± 0.03	0.73±0.05	0.94±0.05	0.76±0.03
Pectoral fin length	0.94 ± 0.04	1.24±0.03	1.24±0.04	1.13±0.06
Pectoral fin area	1.63 ± 0.09	2.22±0.07	2.05±0.06	1.96±0.09
Pectoral fin AR	0.24 ±0 .12	0.26±0.06	0.42±0.07	0.30±0.14
Dorsal fin 1	0.78 ± 0.04	1.17±0.07	1.00±0.04	1.06±0.05
Dorsal fin 2	0.69 ± 0.04	1.19±0.06	1.14±0.05	1.04±0.07
Dorsal fin 3	0.77 ± 0.12	1.01±0.04	1.07±0.05	0.98±0.05
Dorsal fin area	1.45 ± 0.7	2.22±0.10	2.14±0.08	1.86±0.08
Dorsal fin AR	-0.01 ± 0.24	0.17±0.11	0.13±0.07	0.22±0.15
Caudal fin 1	0.84 ± 0.03	0.85±0.03	0.91±0.03	0.98±0.03
Caudal fin 2	0.81 ± 0.03	0.81±0.03	0.98±0.05	0.93±0.03
Caudal fin 3	0.88 ± 0.03	1.16±0.08	1.15±0.06	1.39±0.13
Caudal fin upper area	1.58 ± 0.05	1.63±0.07	1.91±0.08	1.89±0.06
Caudal fin lower area	1.71 ± 0.06	1.84±0.11	2.00±0.13	1.92±0.09
Caudal fin total area	1.63 ± 0.05	1.70±0.08	1.93±0.08	1.89±0.06

Caudal fin AR	-0.01 ± 0.04	-0.09±0.06	0.04±0.06	-0.03±0.07

Figure Legends

Figure 4.1 Images of the four study species. A, horn shark, B, swellshark, C, tope shark, D, leopard shark. Images were taken as follows: horn shark (Wikimedia commons, by Ed Bierman (own work) [https://creativecommons.org/licenses/by/2.0/deed.en]), swellshark (Wikimedia Commons, by Cliff [https://creativecommons.org/licenses/by/2.0/deed.en]), tope shark (Wikimedia Commons, by AshlieJMcivor (own work) [https://creativecommons.org/licenses/by-sa/4.0/deed.en]), leopard shark (Wikimedia Commons, by Matthew Field (own work) [https://creativecommons.org/licenses/by-sa/3.0/deed.en]).

Figure 4.2 Comparison of shark fin length scaling trends with varying species ecology. A, caudal fin 1 scaling trends. B, caudal fin 3 scaling trends. C, pectoral fin length scaling trends. D, dorsal fin 2 scaling trends. Orange color=benthic ecology, pink color=benthopelagic ecology, blue color=pelagic ecology.

Figure 4.3 Comparison of shark fin area scaling trends with varying species ecology. A, pectoral fin area. B, dorsal fin area.

Figure 4.1 Species used in this study

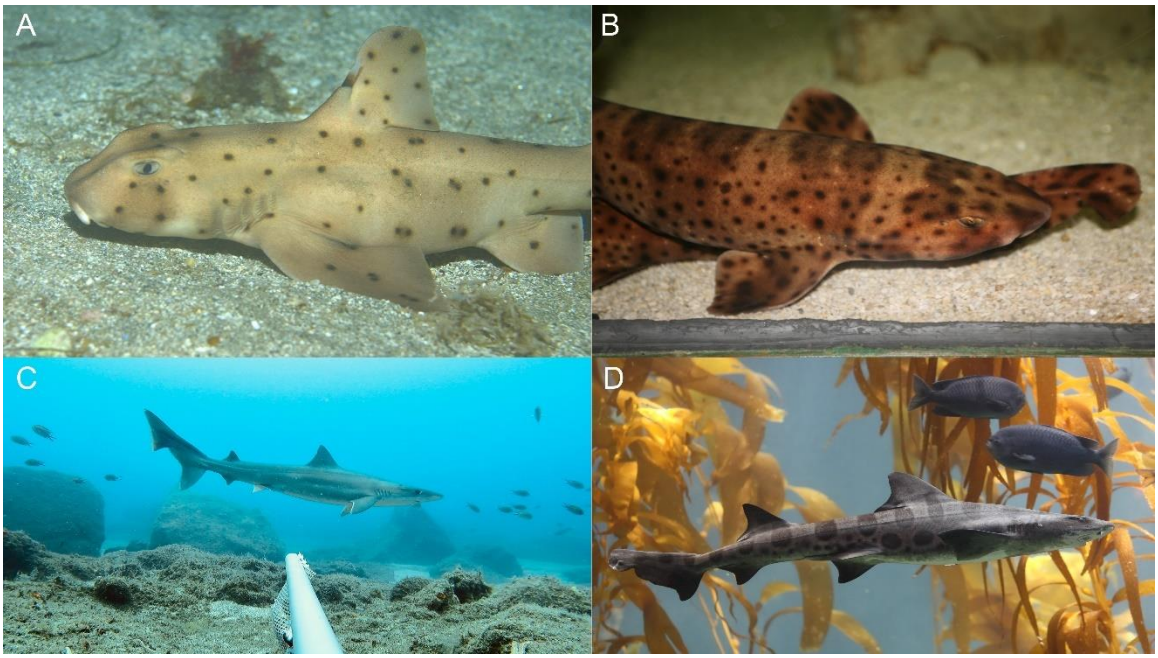

Figure 4.2 Scaling trends of shark fin lengths

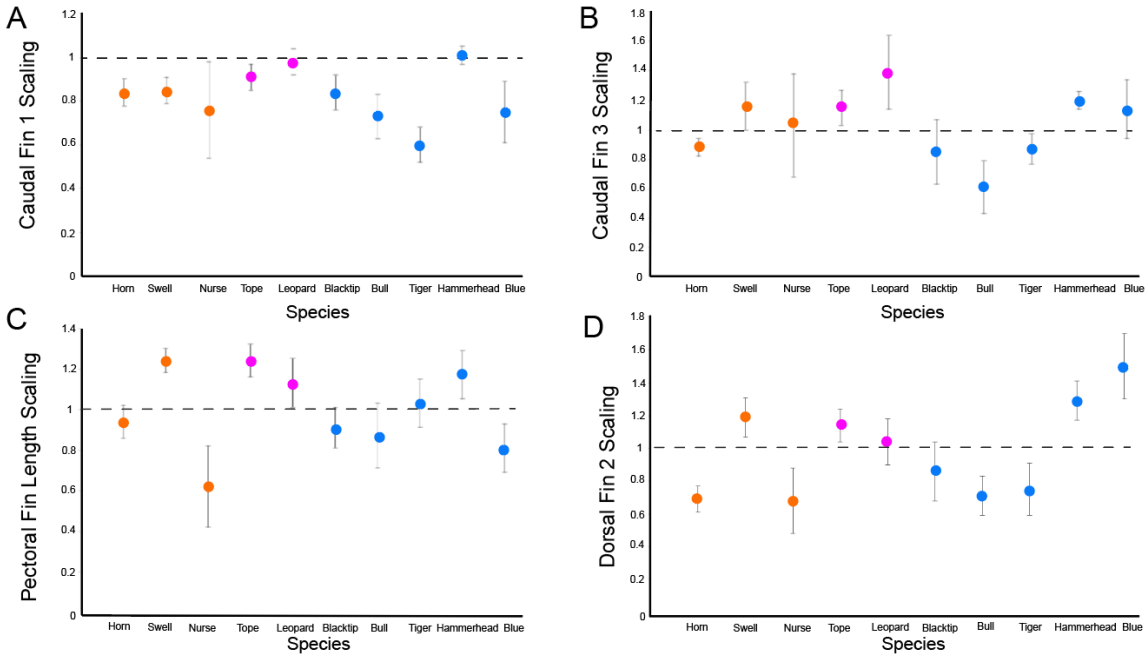

Figure 4.3 Scaling trends of shark fin areas

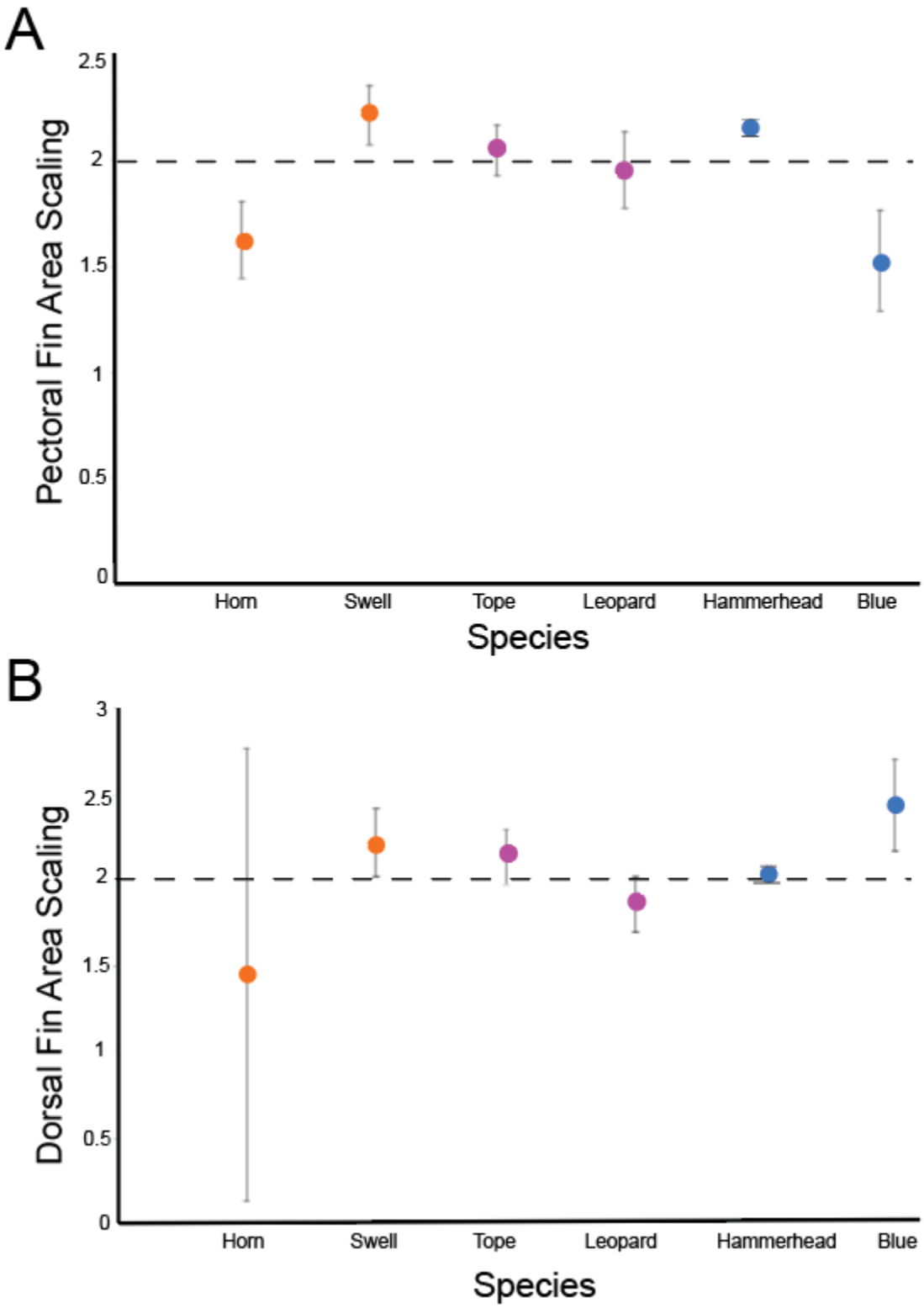

CONCLUSION

The origin and evolution of pectoral fins remains one of the key interests for biologists to understand vertebrate evolution. The evolution of shark pectoral fins provides us a better understanding of how these critical control structures will change both over time and an in response to various ecological changes in the environment. My dissertation provides a vast amount of new information on this interesting subject.

Chapter 1 demonstrated that shark pectoral fins can change in shape in response to change in life history. The scalloped hammerhead, *Sphyrna lewini*, begins its early life in shallow water near shore habitats. However, as the shark grows larger it will leave this near shore habitat and move into deeper oceanic waters performing long distance migrations. The vastly different ecological habitats probably have different functional demands and our study shows that the scalloped hammerhead seems to have pectoral fin shape change to increase its performance in a different habitat.

Chapter 2 focused on the diversity and evolution of shark pectoral fin shape. This integrative study showed that shark pectoral fins have evolved when changing habitats. In this case, sharks began on the seafloor with lower aspect ratio pectoral fins but when invading the open water, pelagic zone shark pectoral fins increased in aspect ratio. In addition, we also determined changes in Sea Surface Temperatures (SST) likely had a major impact on shark swimming and therefore evolution.

Chapter 3 helped addressed a lingering question from not only chapter 2 but also for shark swimming in general. We used a computational fluid dynamics (CFD) approach and determined that the pectoral fins of a pelagic shark produced lift during steady

swimming. Considering pelagic sharks differ in pectoral fin shape and just overall ecology, this was unsurprising. However, given the logistical challenges in trying to obtain this quantitative data this study has provided new major information to understand not only shark pectoral fin function but pectoral fin function in general.

Chapter 4 was a follow up to the hypotheses proposed in Chapter 1. Chapter 1 examined one species of shark to see how shifts in ecology affected its pectoral fins and chapter 4 tested this hypothesis on four species of sharks found off the coast of California as well as six additional species. We found there is additional complexity to the drivers of pectoral shape change in response to ecological shifts throughout life. Future studies on more species may offer a broader perspective on the exact drivers of pectoral fin shape change across both increasing body size and ecology.

APPENDICES

Chapter 1

S1.1. List of specimens examined in this study.

Specimen	PCL	TL	Sex
CAS 2253	31	44.1	F
CAS 82911	41.2	59.5	M
CAS 191993	24.8	36.6	F
CAS 14260	34	48.8	M
CAS 68163	41.5	60.1	M
CAS 30815	31.4	45	F
CAS 30678	35.4	50.7	F
CAS Uncat. #	40.5	58.2	M
CAS 224410	38	54.9	F
CAS 58050	43.3	62.5	M
CAS 22440	59.8	86.4	F
CAS 1957	55	79.4	F
CAS 157-8	71.5	103.5	F
CAS 107	64	93.2	F
CAS 40919	66.2	95.8	M
CAS 2563	58.1	83.9	M
FMNH 63092	41	53.4	M
FMNH 90921	21.8	33.1	M
FMNH 89838	23.9	32.8	F
LACM 7024	31.5	43.6	F
LACM 5427.001	47.1	74.6	F
LACM 33555-1	34	48.7	M
LACM 34189-1	83.5	130	F
LACM 2250	47	73.4	F
LACM 38116.026	42.3	60.6	F
LACM 36277-5	28	42.6	F
LACM 42300-1	34.2	46.4	F
LACM 3130-48	32.4	48.1	M
LACM 9407.022	41.5	54	F
LACM 48404.001	36.5	51.3	M
LACM 3288(1)	28.5	43	M
LACM 3288(2)	28	41.5	F
LACM 3288(3)	29.2	45.2	F
SIO 69-386	32.2	46.2	F
SIO H52-394-5	32.1	46.1	M
SIO 15-77(1)	38.5	55.3	M
SIO 15-77(2)	39.1	56.6	M
SIO 15-77(3)	33	47.3	F
SIO 81-152	31.8	45.7	M
SIO 61-267	72.5	105.4	M

SIO 87-120	52	75	M
SIO 62-48	54.5	77.3	F
SIO 65-83-183-53	67.7	85.7	M
SIO 19-119	31.2	44.7	F
SIO 98-39(1)	41.5	59.8	F
SIO 98-39(2)	40.5	58.3	M
SIO 93-191	39.5	59.1	F
SIO 93-171	38.3	55.1	M
SIO 10-119	29.4	41	F
SIO 10-57	44.2	63.7	F

APPENDICES

Chapter 2

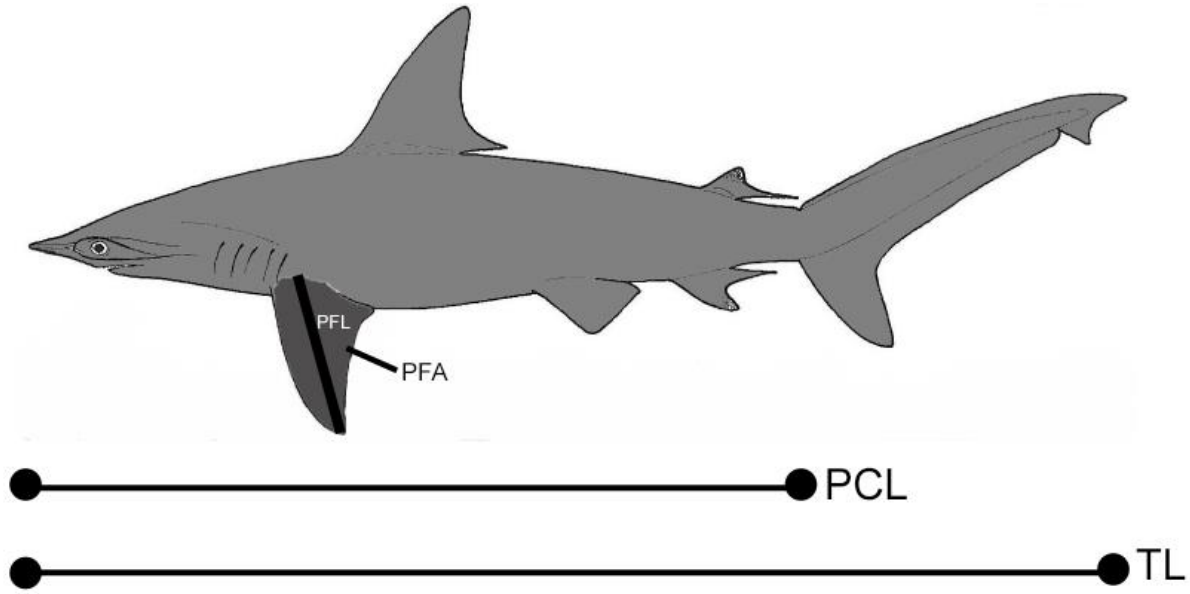

S2.1. Diagram of scalloped hammerhead with measurements in this study. PFL, pectoral fin length; PFA, pectoral fin area; PCL, precaudal-length; TL, total length.

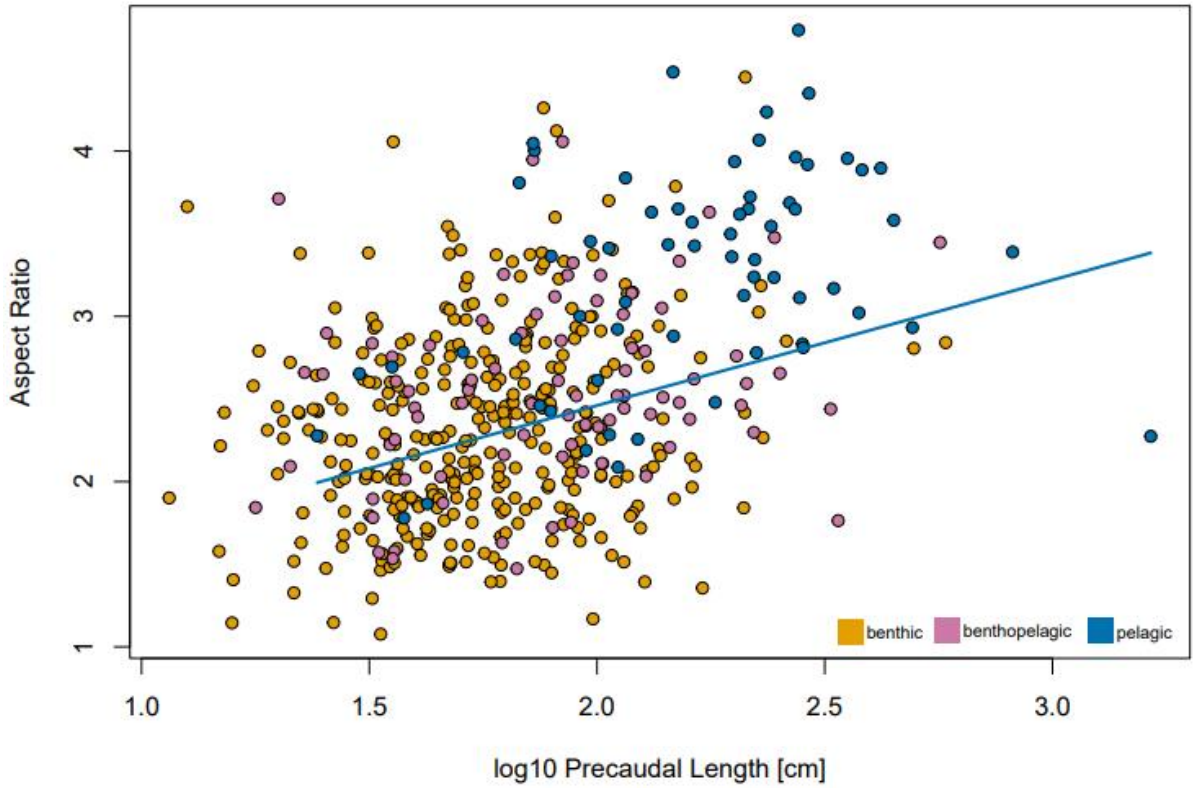

S2.2. Plot of pectoral fin aspect ratio (AR) against the logarithm (base=10) of precaudal length (cm) for N=490 selachian shark species. For given precaudal length, AR varies widely. This pattern is corroborated with an R^2 of 0.43, based on the likelihood of observing the data. Results from phylogenetic generalized least square regression models further suggest that precaudal length impacts the AR of only pelagic sharks, which make up 13% of the data. The slope of the fitted line for pelagic neoselachians is 0.73.

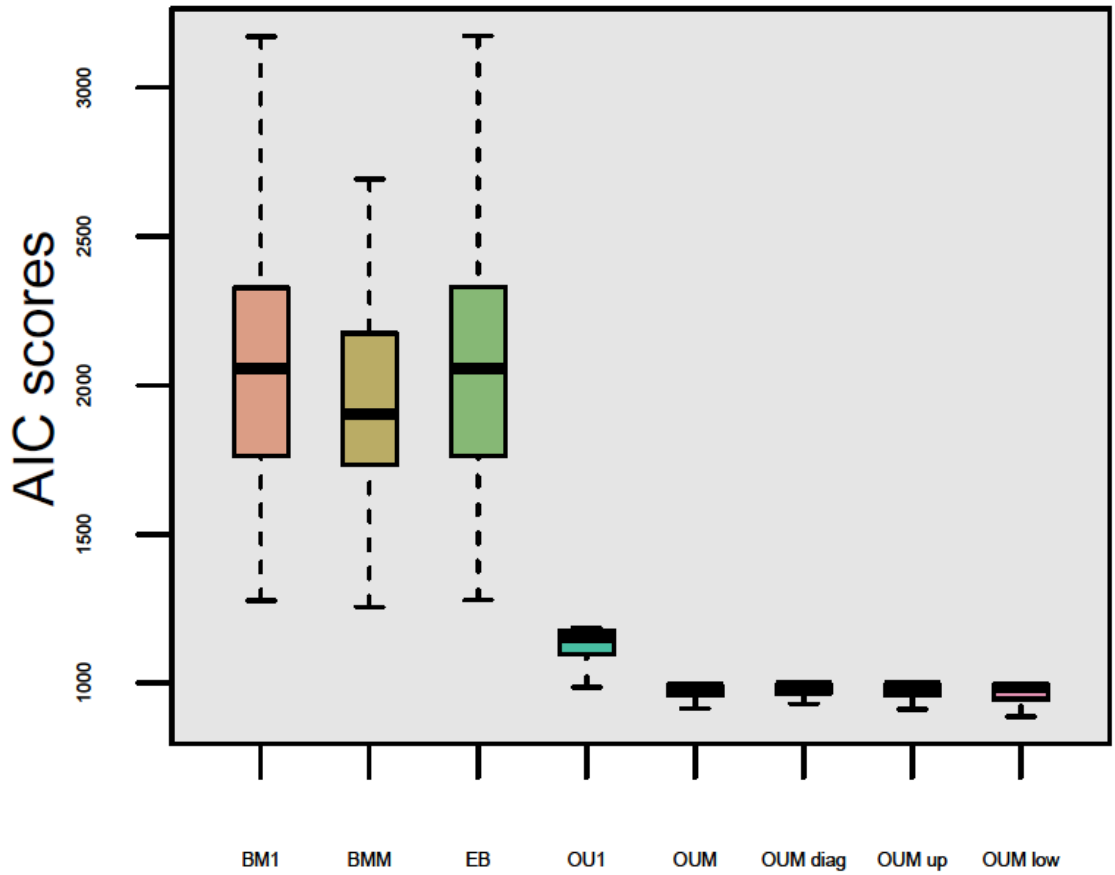

S2.3. Box plots of the AIC scores of the evolutionary models fitted to pectoral fin aspect ratio and precaudal length (log10-transformed). These boxplots summarize 100 iterations of mvMORPH model fitting over a random subsample of 100 trees from the pseudo-posterior distribution. The thick horizontal lines represent the median, and the boxes contain 50% of the AIC scores for each group. The whiskers represent 1.5 times the interquartile range. We specifically compared the fit of the following models of trait evolution: BM1 (single rate BM model), BMM (multi-rate BM model), EB (early burst model), OU (single peak OU model), and OUM (OU models with multiple peaks, including OUM, OUM diagonal, OUM upper, and OUM lower). The OUM models are by far the best supported models, yet there were no clear differences between the four OUM versions we tried.

.

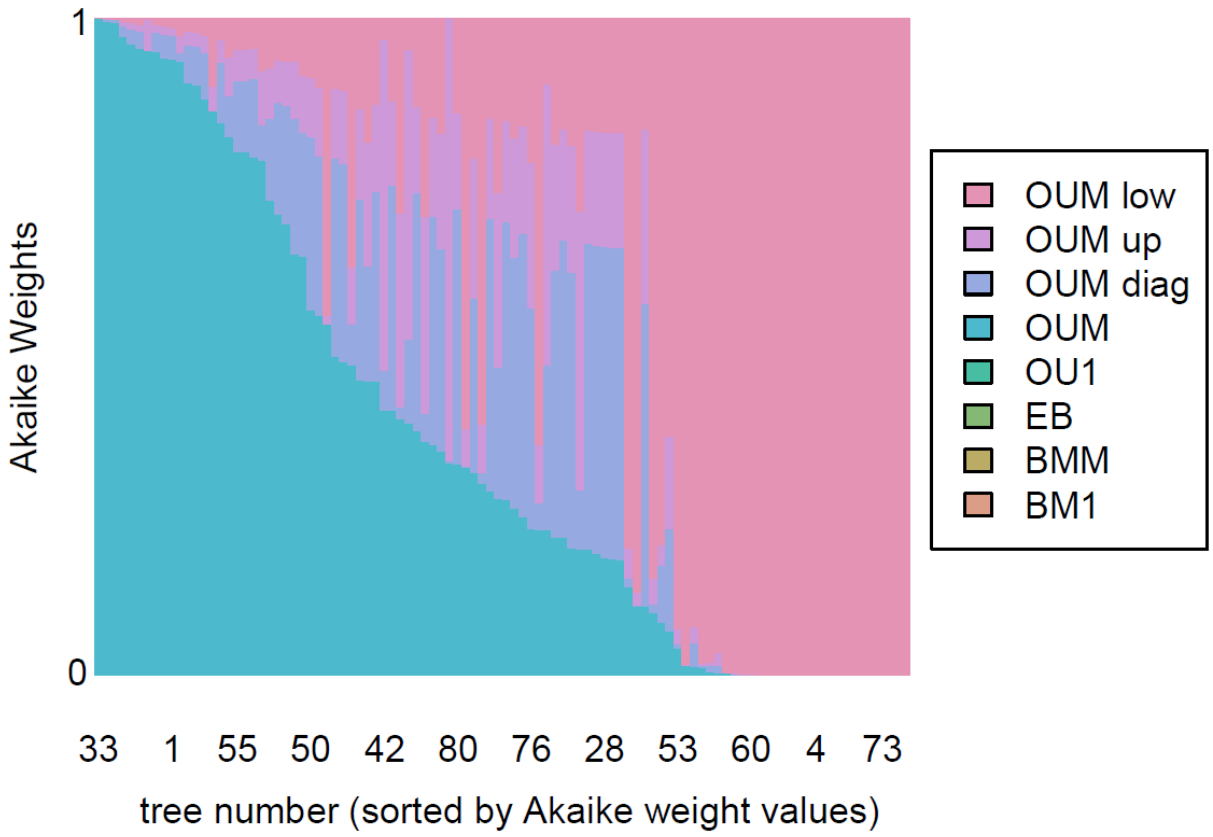

S2.4. Stacked barplots of the Akaike weights over 100 iterations of evolutionary model fitting of pectoral fin aspect ratio and precaudal length (log10-transformed). These barplots summarize results over a random subsample of 100 trees from the pseudo-posterior distribution. The OUM models received high Akaike weights, while the Akaike weights of BM1, BMM, EB, and OU1 models are zero. However, the Akaike weights for the OUM models vary considerably by tree choice, hence there is no clear support for any specific OUM model.

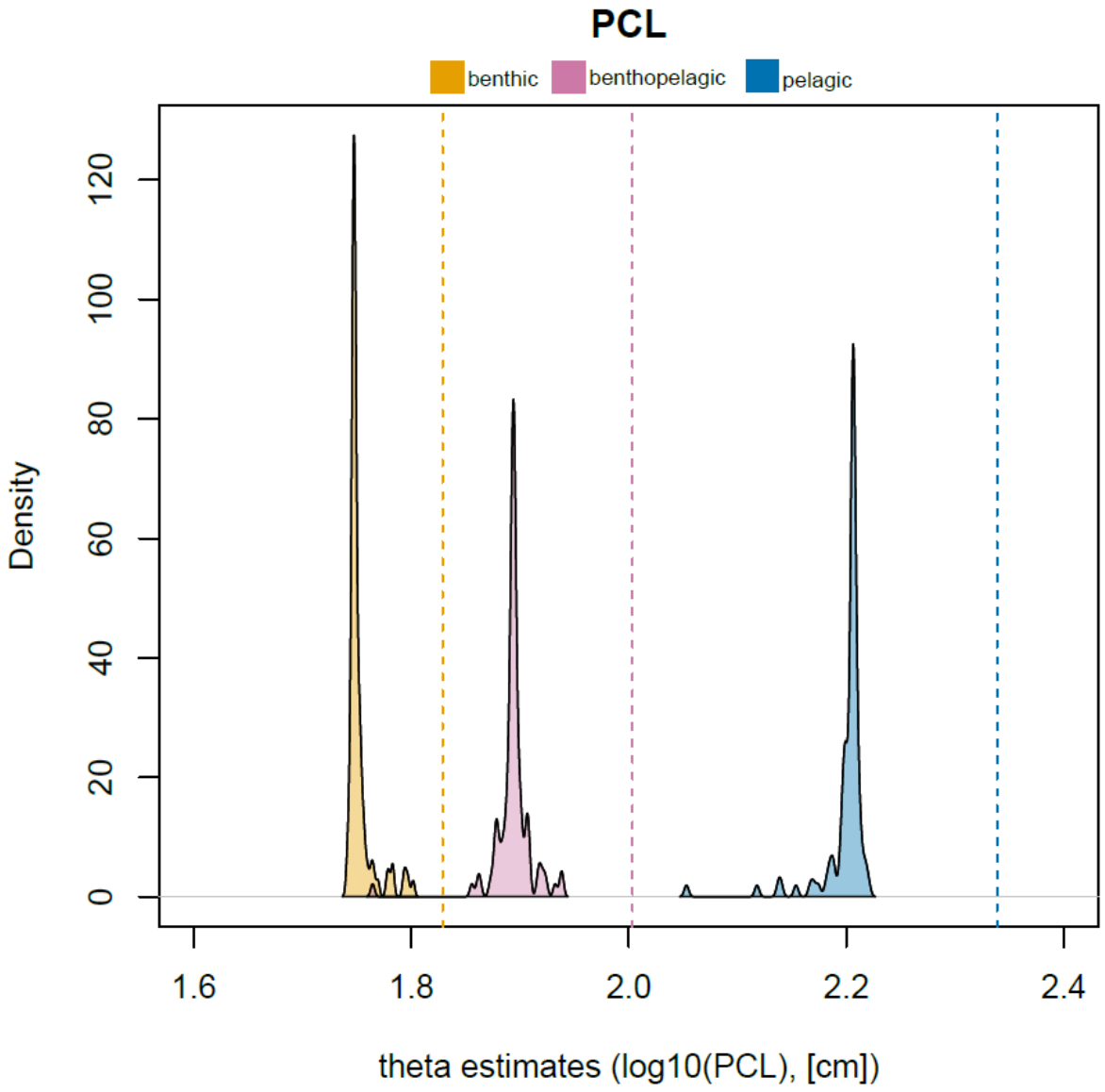

S2.5. Density distribution of θ estimates for the logarithm (base=10) of precaudal length, summarizing 100 iterations of OUM model fitting to the data. The θ estimates, which represent the 'optimal' value in the Ornstein-Uhlenbeck model of trait evolution, are lowest for benthic selachians (yellow) and highest for pelagic selachians (blue), matching the sequence seen for the respective group means, which are superimposed as vertical dashed lines, matched in color to the density curves. However, the θ estimates are consistently lower than the observed means.

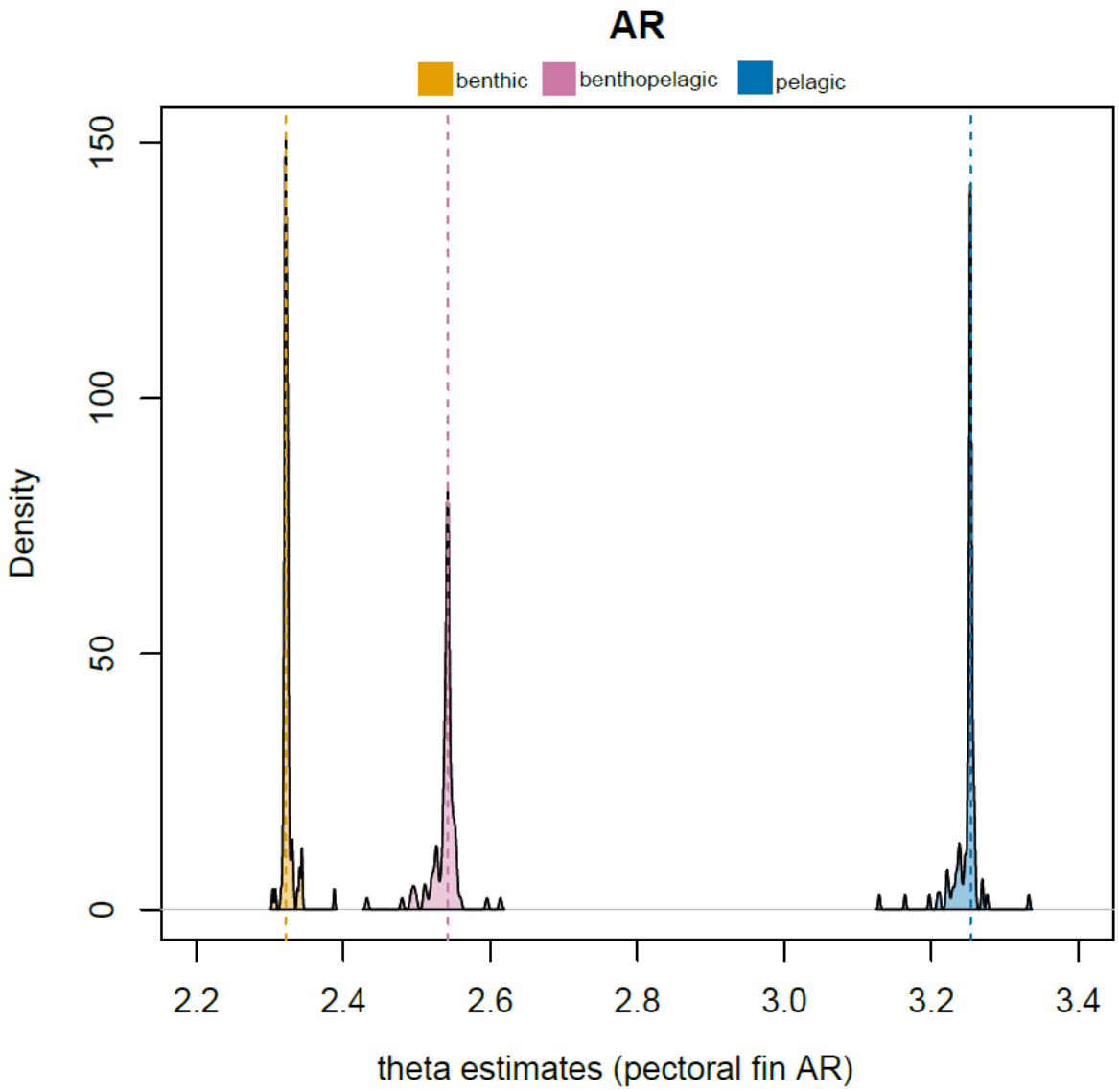

S2.6. Density distribution of θ estimates for the pectoral fin aspect ratio, summarizing 100 iterations of OUM model fitting to the data. The θ estimates, which represent the 'optimal' value in the Ornstein-Uhlenbeck model of trait evolution, are lowest for benthic selachians (yellow) and highest for pelagic selachians (blue), matching the sequence seen for the respective group means, which are superimposed as vertical dashed lines, matched in color to the density curves. The peaks of the density distributions of θ are very close to the observed means.

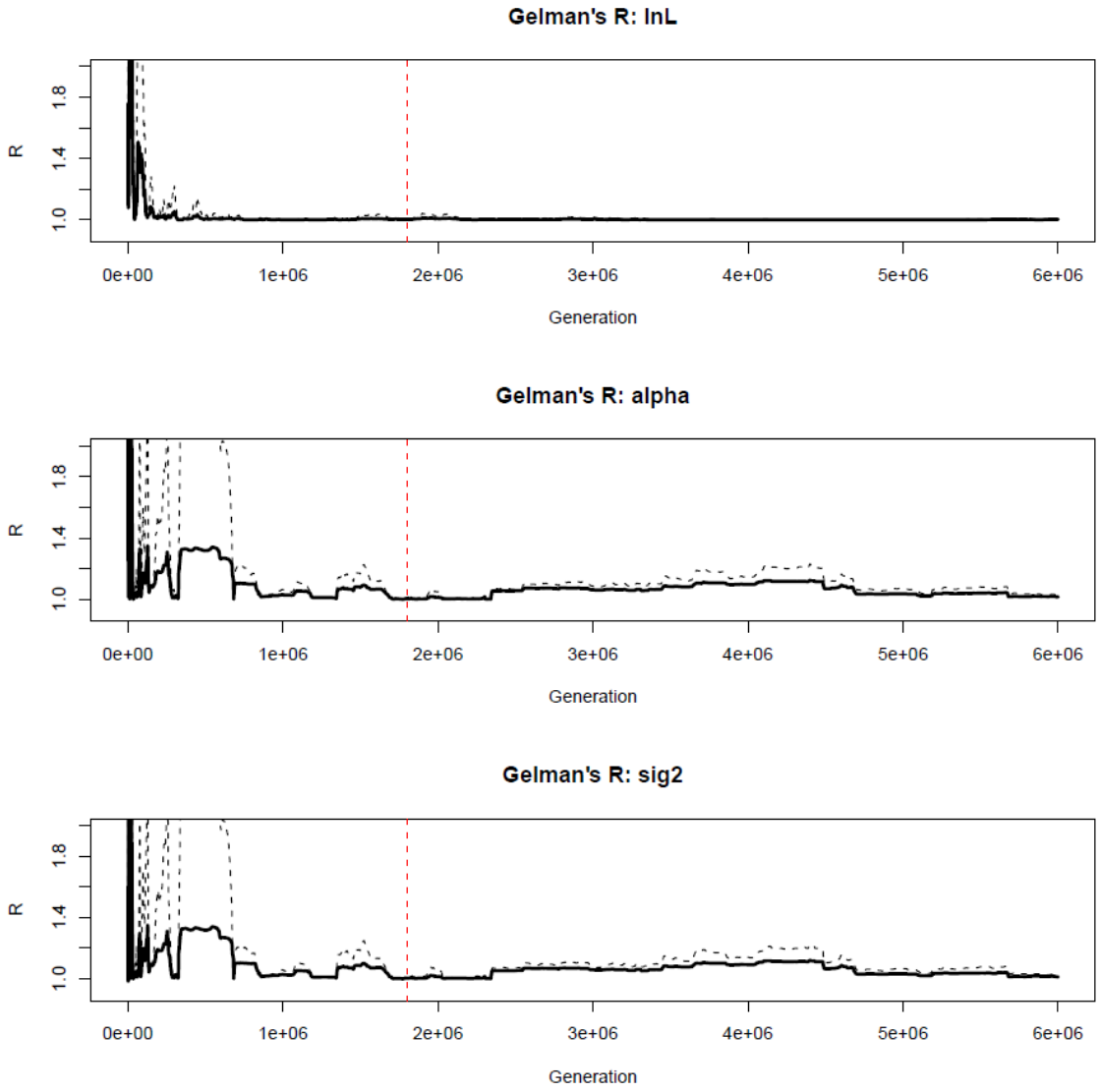

S2.7. Plots of Gelman's R for the natural logarithm of likelihood (lnL), α, and σ^2 estimates from bayOU, carried out for the pectoral fin aspect ratio and the maximum clade credibility tree. Full convergence of the two independent MCMC chains is achieved when the two lines overlap. The dashed red line is the cut-off for burnin, which means that the results from all chains to the left of the dashed red line were discarded.

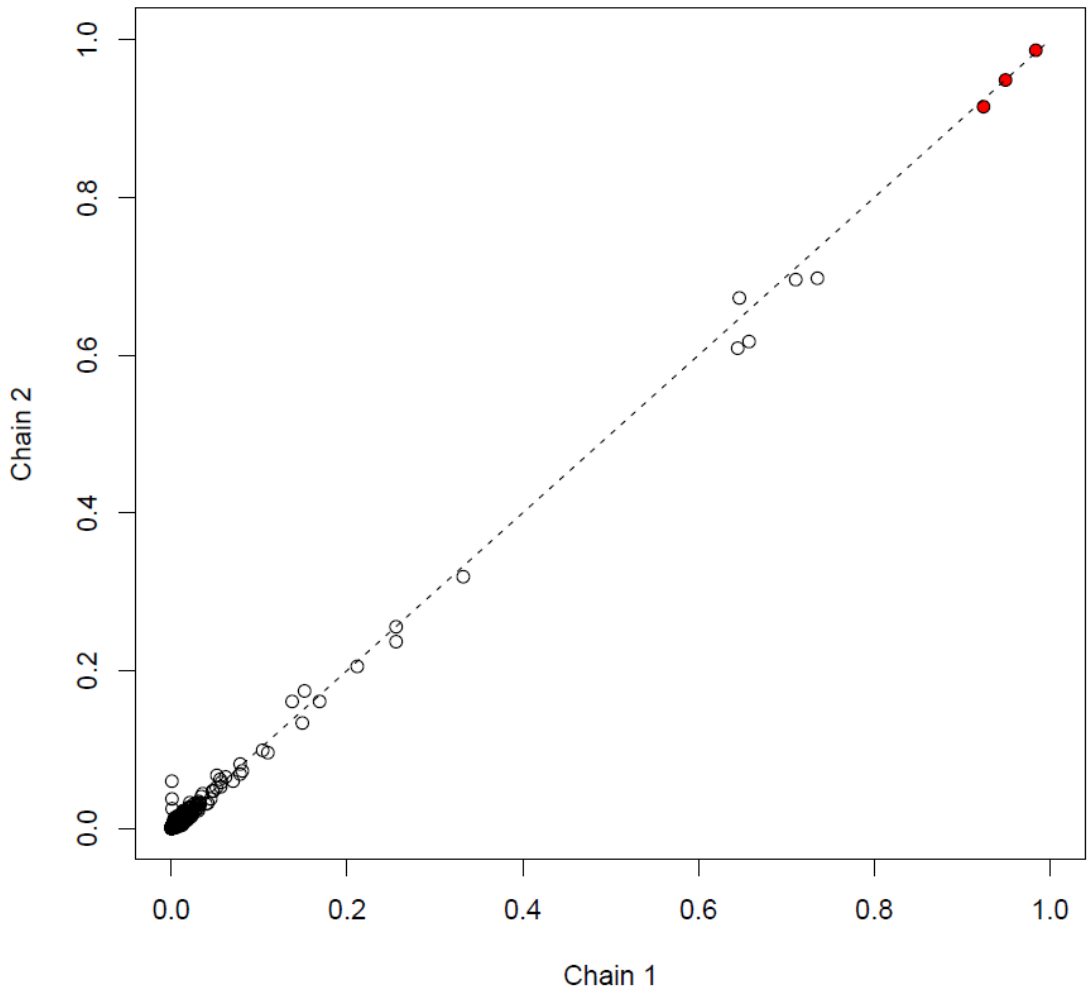

S2.8. Scatterplot of the posterior probabilities obtained from MCMC chains 1 and 2**.** Most points fall along a line with a slope of 1 (dashed line), a strong sign of convergence of the MCMC chains.Red fill color identifies strongly supported selective regime shifts.

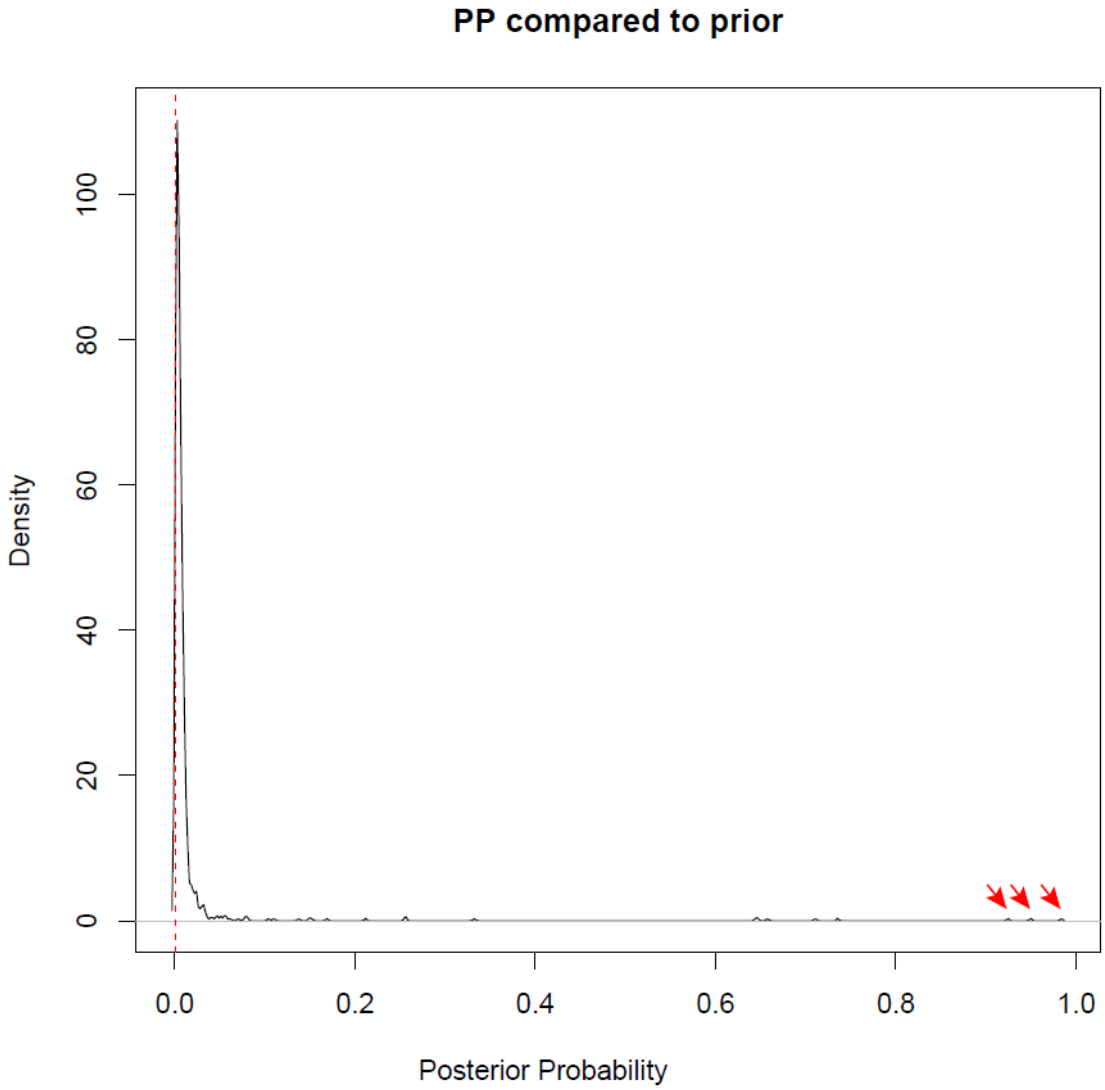

S2.9. Density distributions of the posterior probabilities of selective regime shifts of pectoral fin aspect ratio (MCMC chain 1), based on the maximum clade credibility tree. Three branches (red arrows; posterior probability > 0.9) stand out from all others, indicating very strong support for selective regime shifts along those branches. The dashed red line indicates the prior probability of a shift to occur along each individual branch in the phylogeny. Red arrows identify strongly supported selective regime shifts.

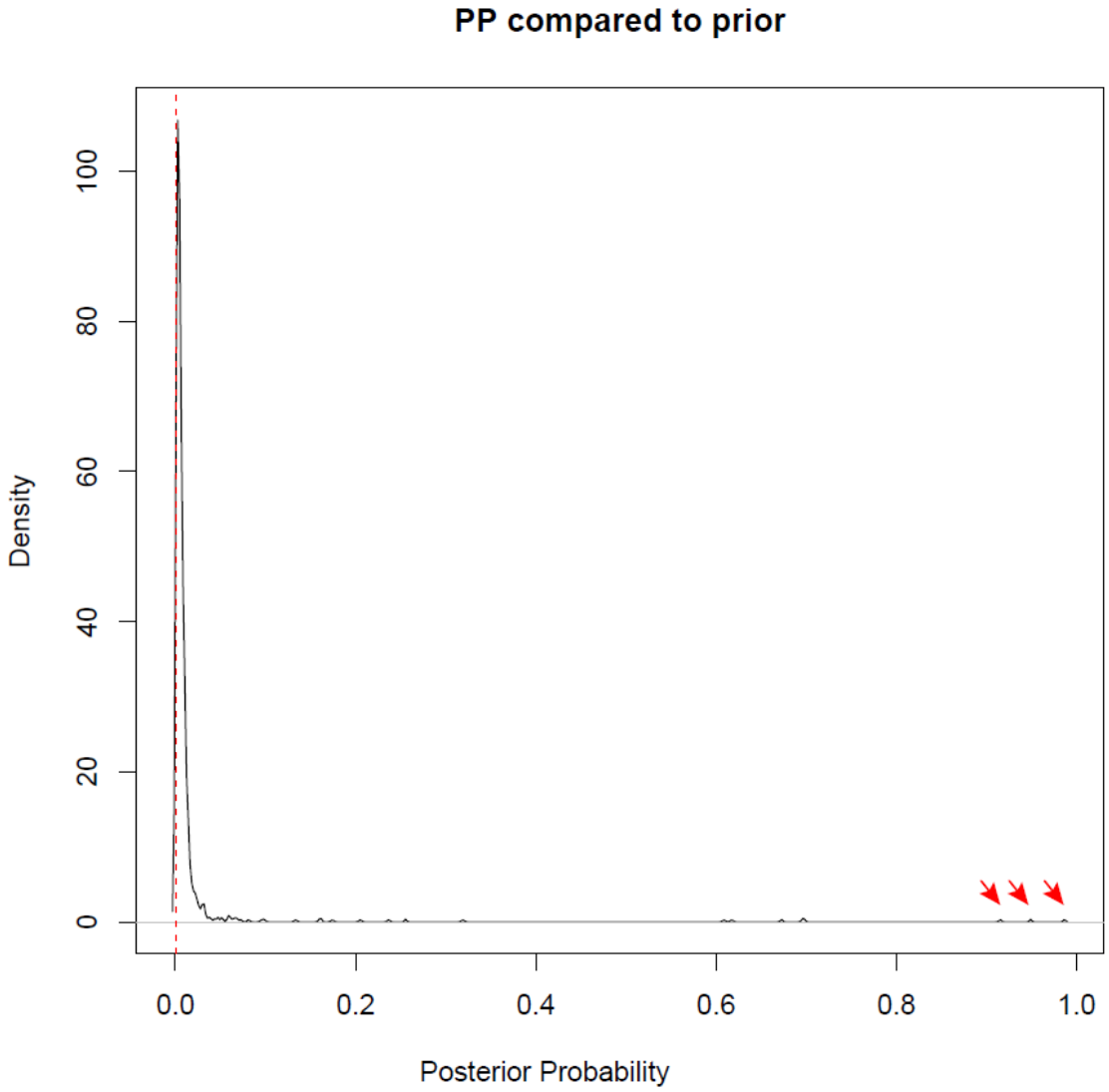

S2.10. Density distributions of the posterior probabilities of selective regime shifts of pectoral fin aspect ratio (MCMC chain 2), based on the maximum clade credibility tree. Three branches (red arrows; posterior probability > 0.9) stand out from all others, indicating very strong support for selective regime shifts along those branches. The dashed red line indicates the prior probability of a shift to occur along each individual branch in the phylogeny.

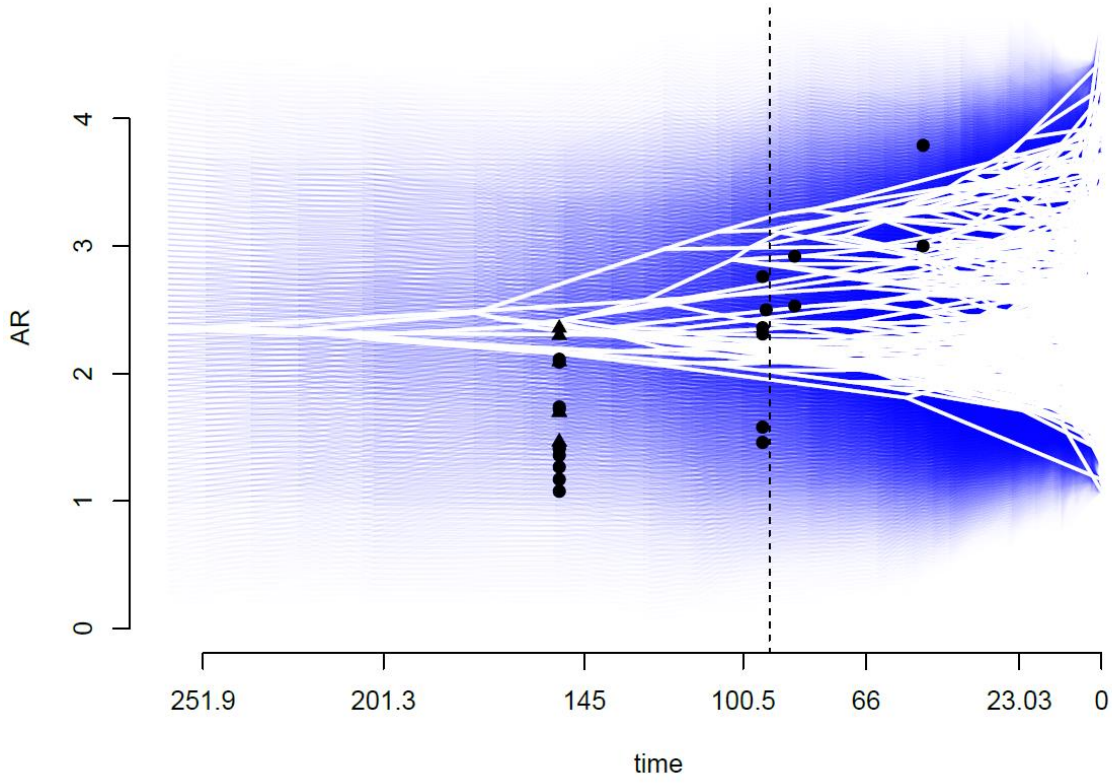

S2.11. Traitgram projections of pectoral fin aspect ratio (AR) using time calibrated phylogeny with 95% confidence intervals illustrated by a blue color transparency gradient. Increasing transparency indicates higher uncertainty, with the full range spanning the entire 95% CI. Black shapes represent measured fossil specimen pectoral fin aspect ratios.

S2.12. List of all species, habitat categorization, and pectoral fin aspect ratios from Ebert et al. (2013, 2021).

Order	Species	Habitat	Pectoral Fin Aspect Ratio
Hexanchiformes	*Chlamydoselachus anguineus*	Benthopelagic	2.207
	Chlamydoselachus africana	Benthopelagic	2.15
	Notorynchus cepedianus	Benthopelagic	2.76
	Hexanchus griseus	Benthic	2.417
	Hexanchus nakamurai	Benthic	2.178
	Heptranchias perlo	Benthopelagic	2.06
Pristiophoriformes	*Pliotrema warreni*	Benthic	2.411
	Pristiophorus japonicus	Benthic	1.641
	Pristiophorus delicatus	Benthic	2.116
	Pristiophorus nudipinnis	Benthic	2.054
	Pristiophorus schroederi	Benthic	2.83
	Pristiophorus cirratus	Benthic	1.722
	Pristiophorus nancyae	Benthic	2.012
Echinorhiniformes	*Echinorhinus brucus*	Benthopelagic	2.298
	Echinorhinus cookei	Benthopelagic	1.764
Squatiniformes	*Squatina australis*	Benthic	2.04
	Squatina albipunctata	Benthic	1.553
	Squatina tergocellata	Benthic	1.999
	Squatina pseudocellata	Benthic	1.773

	Squatina tergocellatoides	Benthic	2.42
	Squatina japonica	Benthic	2.094
	Squatina oculata	Benthic	2.157
	Squatina argentina	Benthic	1.791
	Squatina nebulosa	Benthic	1.356
	Squatina formosa	Benthic	1.393
	Squatina legnota	Benthic	2.033
	Squatina californica	Benthic	1.895
	Squatina guggenheim	Benthic	1.844
	Squatina occulta	Benthic	1.661
	Squatina dumeril	Benthic	1.719
	Squatina caillieti	Benthic	1.606
	Squatina armata	Benthic	2.055
	Squatina africana	Benthic	2.032
	Squatina aculeata	Benthic	1.966
	Squatina squatina	Benthic	1.841
Squaliformes	*Deania quadrispinosa*	Benthic	2.998
	Deania profundorum	Benthic	1.98
	Deania hystricosa	Benthic	1.797
	Deania calcea	Benthic	2.355
	Centrophorus lusitanicus	Benthic	2.561

Centrophorus seychellorum	Benthic	2.528
Centrophorus westraliensis	Benthopelagic	3.013
Centrophorus isodon	Benthic	2.116
Centrophorus harrissoni	Benthic	1.448
Centrophorus tessellatus	Benthic	2.238
Centrophorus moluccensis	Benthopelagic	1.722
Centrophorus squamosus	Benthopelagic	2.408
Centrophorus granulosus	Benthopelagic	1.754
Centrophorus zeehaani	Benthic	2.217
Centrophorus atromarginatus	Benthic	1.869
Dalatias licha	Benthopelagic	3.05
Isistius brasiliensis	Pelagic	1.865
Isistius labialis	Pelagic	1.779
Isistius plutodus	Pelagic	2.694
Euprotomicroides zantedeschia	Benthopelagic	1.782
Squaliolus laticaudus	Pelagic	2.277
Mollisquama parini	Benthopelagic	1.895
Heteroscymnoides marleyi	Pelagic	2.653
Cirrhigaleus asper	Benthopelagic	3.249
Cirrhigaleus barbifer	Benthopelagic	2.108
Cirrhigaleus australis	Benthopelagic	2.111

Squalus montalbani	Benthic	2.594
Squalus altipinnis	Benthic	3.04
Squalus notocaudatus	Benthic	3.489
Squalus chloroculus	Benthic	2.967
Squalus mitsukurii	Benthopelagic	2.331
Squalus albifrons	Benthic	2.854
Squalus formosus	Benthic	2.478
Squalus cubensis	Benthopelagic	2.224
Squalus blainville	Benthopelagic	2.472
Squalus griffini	Benthic	2.664
Squalus crassispinus	Benthic	3.377
Squalus grahami	Benthic	2.267
Squalus nasutus	Benthic	1.83
Squalus japonicus	Benthic	2.553
Squalus melanurus	Benthopelagic	2.685
Squalus edmundsi	Benthic	2.875
Squalus hemipinnis	Benthic	3.372
Squalus lalannei	Benthic	2.657
Squalus rancureli	Benthic	2.419
Squalus raoulensis	Benthic	2.728
Squalus bucephalus	Benthic	2.389

Squalus brevirostris	Benthic	2.758
Squalus megalops	Benthopelagic	3.254
Squalus acanthias	Benthopelagic	2.378
Squalus suckleyi	Benthopelagic	2.372
Somniosus longus	Benthopelagic	3.012
Somniosus microcephalus	Benthopelagic	3.447
Somniosus antarcticus	Benthic	2.806
Somniosus pacificus	Benthic	2.841
Somniosus rostratus	Benthic	3.14
Centroscymnuscoelolepis	Benthic	2.566
Oxynotus caribbaeus	Benthic	4.056
Oxynotus japonicus	Benthic	2.257
Oxynotus centrina	Benthic	3.145
Oxynotus paradoxus	Benthic	2.914
Oxynotus bruniensis	Benthic	3.374
Proscymnodon plunketi	Benthic	2.38
Proscymnodon macracanthus	Benthic	2.979
Centroscymnus owstonii	Benthic	2.337
Scymnodon ringens	Benthopelagic	2.853
Scymnodalatias oligodon	Benthopelagic	3.711
Scymnodalatias sherwoodi	Benthopelagic	2.899

Scymnodalatias albicauda	Benthopelagic	4.057
Scymnodalatias garricki	Benthopelagic	1.571
Centroselachus crepidater	Benthopelagic	2.611
Zameus squamulosus	Benthopelagic	2.282
Zameus ichiharai	Benthopelagic	2.808
Aculeola nigra	Benthopelagic	2.391
Centroscyllium nigrum	Benthopelagic	2.547
Centroscyllium kamoharai	Benthopelagic	1.995
Centroscyllium granulatum	Benthic	3.38
Centroscyllium excelsum	Benthic	1.509
Centroscyllium fabricii	Benthic	1.641
Centroscyllium ritteri	Benthic	1.563
Trigonognathus kabeyai	Benthic	1.841
Etmopterus splendidus	Benthic	2.046
Etmopterus fusus	Benthic	2.438
Etmopterus pseudosqualiolus	Benthic	1.579
Etmopterus compagnoi	Benthopelagic	3.077
Etmopterus villosus	Benthic	3.664
Etmopterus robinsi	Benthic	1.147
Etmopterus viator	Benthic	2.587
Etmopterus sentosus	Benthic	2.721

Etmopterus litvinovi	Benthopelagic	1.87
Etmopterus carteri	Benthic	1.145
Etmopterus decacuspidatus	Benthic	1.811
Etmopterus bullisi	Benthic	2.366
Etmopterus caudistigmus	Benthic	2.253
Etmopterus pusillus	Benthopelagic	2.447
Etmopterus burgessi	Benthic	2.943
Etmopterus schmidti	Benthic	2.105
Etmopterus bigelowi	Benthopelagic	1.843
Etmopterus brachyurus	Benthopelagic	2.836
Etmopterus lucifer	Benthopelagic	2.254
Etmopterus hillianus	Benthopelagic	2.092
Etmopterus sheikoi	Benthic	2.736
Etmopterus molleri	Benthic	2.577
Etmopterus evansi	Benthic	2.436
Etmopterus dislineatus	Benthic	2.261
Etmopterus schultzi	Benthopelagic	2.66
Etmopterus sculptus	Benthic	2.658
Etmopterus virens	Benthic	2.452
Etmopterus polli	Benthic	2.79
Etmopterus gracilispinis	Benthopelagic	2.65

	Etmopterus perryi	Benthic	1.406
	Etmopterus dianthus	Benthic	2.029
	Etmopterus pycnolepis	Benthopelagic	1.534
	Etmopterus spinax	Benthic	1.716
	Etmopterus princeps	Benthopelagic	1.473
	Etmopterus granulosus	Benthopelagic	2.162
	Etmopterus unicolor	Benthic	2.722
	Etmopterus joungi	Benthic	1.855
Heterodontiformes	*Heterodontus quoyi*	Benthic	2.765
	Heterodontus francisci	Benthic	2.527
	Heterodontus zebra	Benthic	2.934
	Heterodontus japonicus	Benthic	3.048
	Heterodontus galeatus	Benthic	2.257
	Heterodontus portusjacksoni	Benthic	2.199
	Heterodontus omanensis	Benthic	3.052
	Heterodontus ramalheira	Benthic	2.358
	Heterodontus mexicanus	Benthic	3.234
Orectolobiformes	*Parascyllium elongatum*	Benthic	2.602
	Parascyllium collare	Benthic	2.488
	Parascyllium variolatum	Benthic	1.516
	Parascyllium ferrugineum	Benthic	1.689

Parascyllium sparsimaculatum	Benthic	1.9
Cirrhoscyllium formosanum	Benthic	2.047
Cirrhoscyllium japonicum	Benthic	2.544
Cirrhoscyllium expolitum	Benthic	1.916
Brachaelurus colcloughi	Benthic	2.028
Brachaelurus waddi	Benthic	2.242
Eucrossorhinus dasypogon	Benthic	1.169
Orectolobus floridus	Benthic	1.997
Sutorectus tentaculatus	Benthic	1.831
Orectolobus ornatus	Benthic	1.739
Orectolobus wardi	Benthic	2.061
Orectolobus leptolineatus	Benthic	2.162
Orectolobus reticulatus	Benthic	2.272
Orectolobus halei	Benthic	2.139
Orectolobus maculatus	Benthic	2.09
Orectolobus parvimaculatus	Benthic	2.445
Orectolobus japonicus	Benthic	1.95
Orectolobus hutchinsi	Benthic	2.837
Rhincodon typus	Pelagic	2.274
Stegostoma fasciatum	Benthopelagic	2.033

	Pseudoginglymostoma brevicaudatum	Benthic	1.567
	Ginglymostoma cirratum	Benthopelagic	2.461
	Nebrius ferrugineus	Benthopelagic	2.594
	Hemiscyllium hallstromi	Benthic	1.541
	Hemiscyllium trispeculare	Benthic	1.866
	Hemiscyllium michaeli	Benthic	2.455
	Hemiscyllium galei	Benthic	1.919
	Hemiscyllium ocellatum	Benthic	2.473
	Hemiscyllium freycineti	Benthic	2.477
	Hemiscyllium strahani	Benthic	1.668
	Hemiscyllium henryi	Benthic	2.583
	Chiloscyllium hasseltii	Benthic	1.896
	Chiloscyllium griseum	Benthic	2.929
	Chiloscyllium burmensis	Benthic	2.269
	Chiloscyllium punctatum	Benthic	2.322
	Chiloscyllium plagiosum	Benthic	2.815
	Chiloscyllium arabicum	Benthic	2.019
	Chiloscyllium indicum	Benthic	2.983
Carcharhiniformes	*Cephalurus cephalus*	Benthic	1.63
	Poroderma pantherinum	Benthic	1.969

Poroderma africanum	Benthic	2.084
Scyliorhinus capensis	Benthic	2.416
Scyliorhinus canicula	Benthic	2.202
Scyliorhinus haeckelii	Benthic	1.905
Scyliorhinus tokubee	Benthic	2.988
Scyliorhinus cervigoni	Benthic	2.583
Scyliorhinus hesperius	Benthic	1.832
Scyliorhinus stellaris	Benthic	2.775
Scyliorhinus retifer	Benthic	3.544
Scyliorhinus boa	Benthic	1.717
Scyliorhinus torrei	Benthic	2.423
Scyliorhinus meadi	Benthic	1.964
Scyliorhinus comoroensis	Benthic	2.224
Scyliorhinus torazame	Benthic	1.79
Scyliorhinus besnardi	Benthic	2.042
Scyliorhinus garmani	Benthic	2.842
Cephaloscyllium signourum	Benthic	2.731
Cephaloscyllium sarawakensis	Benthic	2.292
Cephaloscyllium ventriosum	Benthic	2.549
Cephaloscyllium maculatum	Benthic	2.216
Cephaloscyllium sufflans	Benthic	2.007

Cephaloscyllium pictum	Benthic	2.174
Cephaloscyllium speccum	Benthic	2.38
Cephaloscyllium isabellum	Benthic	1.81
Cephaloscyllium albipinnum	Benthic	1.829
Cephaloscyllium hiscosellum	Benthic	2.562
Cephaloscyllium silasi	Benthic	2.02
Cephaloscyllium cooki	Benthic	2.312
Cephaloscyllium pardelotum	Benthic	2.418
Cephaloscyllium zebrum	Benthic	2.258
Cephaloscyllium laticeps	Benthic	1.514
Cephaloscyllium fasciatum	Benthic	2.602
Cephaloscyllium variegatum	Benthic	1.495
Cephaloscyllium stevensi	Benthic	2.247
Cephaloscyllium umbratile	Benthic	2.074
Schroederichthys maculatus	Benthic	2.098
Schroederichthys bivius	Benthic	2.049
Schroederichthys tenuis	Benthic	2.489
Schroederichthys chilensis	Benthic	2.327
Schroederichthys saurisqualus	Benthic	2.453
Aulohalaelurus labiosus	Benthic	1.753
Aulohalaelurus kanakorum	Benthic	2.619

Atelomycterus marnkalha	Benthic	2.163
Atelomycterus fasciatus	Benthic	1.889
Atelomycterus baliensis	Benthic	2.229
Atelomycterus macleayi	Benthic	1.505
Atelomycterus marmoratus	Benthic	1.918
Hemipristis elongata	Benthopelagic	3.63
Paragaleus tengi	Benthic	3.242
Paragaleus leucolomatus	Benthic	4.261
Paragaleus pectoralis	Benthic	3.7
Chaenogaleus macrostoma	Benthic	2.841
Hemigaleus microstoma	Benthopelagic	3.948
Hemigaleus australiensis	Benthopelagic	3.324
Galeocerdo cuvier	Pelagic	3.581
Eusphyra blochii	Pelagic	2.256
Sphyrna mokarran	Pelagic	3.896
Sphyrna zygaena	Pelagic	2.811
Sphyrna lewini	Pelagic	2.833
Sphyrna corona	Pelagic	2.862
Sphyrna tiburo	Pelagic	3.412
Sphyrna tudes	Pelagic	2.283
Sphyrna media	Pelagic	2.087

Carcharhinus wheeleri	Pelagic	3.36
Carcharhinus fitzroyensis	Pelagic	3.453
Carcharhinus melanopterus	Pelagic	3.65
Carcharhinus cautus	Pelagic	3.087
Carcharhinus limbatus	Pelagic	3.569
Carcharhinus amblyrhynchoides	Pelagic	3.63
Carcharhinus tilstoni	Pelagic	4.478
Isogomphodon oxyrhynchus	Pelagic	2.479
Carcharhinus leiodon	Pelagic	3
Carcharhinus tjutjot	Pelagic	4.047
Carcharhinus sorrah	Pelagic	3.837
Carcharhinus altimus	Pelagic	3.65
Carcharhinus plumbeus	Pelagic	3.722
Carcharhinus dussumieri	Pelagic	2.426
Carcharhinus sealei	Pelagic	4.003
Carcharhinus leucas	Pelagic	3.235
Triaenodon obesus	Benthic	3.786
Nasolamia velox	Benthic	3.404
Carcharhinus acronotus	Pelagic	2.612
Carcharhinus isodon	Pelagic	3.434
Carcharhinus porosus	Pelagic	2.922

Carcharhinus falciformis	Pelagic	4.236
Carcharhinus amboinensis	Pelagic	3.498
Carcharhinus amblyrhynchos	Pelagic	3.936
Prionace glauca	Pelagic	4.732
Carcharhinus albimarginatus	Pelagic	3.343
Carcharhinus longimanus	Pelagic	3.687
Carcharhinus obscurus	Pelagic	4.349
Carcharhinus galapagensis	Pelagic	3.963
Carcharhinus perezii	Benthic	4.447
Carcharhinus coatesi	Pelagic	3.808
Carcharhinus macloti	Pelagic	3.364
Carcharhinus hemiodon	Pelagic	2.459
Carcharhinus borneensis	Pelagic	2.783
Carcharhinus brevipinna	Pelagic	3.126
Carcharhinus brachyurus	Pelagic	4.066
Carcharhinus signatus	Pelagic	3.617
Lamiopsis temminckii	Benthic	2.065
Lamiopsis tephrodes	Benthic	3.193
Glyphis garricki	Benthic	3.025
Glyphis glyphis	Pelagic	2.78
Glyphis siamensis	Pelagic	3.238

Glyphis fowlerae	Pelagic	2.88
Glyphis gangeticus	Benthic	3.127
Negaprion acutidens	Benthic	3.185
Negaprion brevirostris	Benthic	2.85
Loxodon macrorhinus	Benthic	3.289
Scoliodon macrorhynchos	Benthic	2.453
Scoliodon laticaudus	Benthic	1.495
Rhizoprionodon terraenovae	Benthic	3.332
Rhizoprionodon porosus	Benthic	4.122
Rhizoprionodon lalandii	Benthic	2.632
Rhizoprionodon longurio	Benthic	3.138
Rhizoprionodon acutus	Benthic	2.695
Rhizoprionodon taylori	Benthic	3.401
Rhizoprionodon oligolinx	Benthic	3.185
Galeorhinus galeus	Benthopelagic	3.334
Gogolia filewoodi	Benthopelagic	2.975
Hypogaleus hyugaensis	Benthopelagic	3.094
Triakis semifasciata	Benthopelagic	2.51
Triakis maculata	Benthic	2.749
Triakis scyllium	Benthopelagic	2.444
Triakis acutipinna	Benthic	3.599

Furgaleus macki	Benthopelagic	2.79
Hemitriakis japanica	Benthic	3
Hemitriakis leucoperiptera	Benthic	3.32
Hemitriakis abdita	Benthic	3.33
Hemitriakis indroyonoi	Benthic	3.37
Hemitriakis complicofasciata	Benthic	3.384
Hemitriakis falcata	Benthic	3.099
Iago garricki	Benthic	2.398
Iago omanensis	Benthopelagic	2.754
Mustelus canis	Benthopelagic	2.52
Mustelus mangalorensis	Benthic	3.384
Mustelus fasciatus	Benthic	1.852
Mustelus henlei	Benthopelagic	3.119
Mustelus norrisi	Benthic	2.693
Mustelus albipinnis	Benthic	2.607
Mustelus californicus	Benthopelagic	2.345
Mustelus mustelus	Benthopelagic	3.249
Mustelus lunulatus	Benthic	2.941
Mustelus ravidus	Benthic	3.227
Mustelus widodoi	Benthic	2.328
Mustelus griseus	Benthic	2.696

Mustelus mosis	Benthic	2.881
Mustelus dorsalis	Benthic	2.21
Mustelus sinusmexicanus	Benthic	2.709
Mustelus punctulatus	Benthic	2.312
Mustelus asterias	Benthopelagic	2.519
Mustelus palumbes	Benthopelagic	2.519
Mustelus antarcticus	Benthopelagic	2.478
Mustelus higmani	Benthic	3.066
Mustelus lenticulatus	Benthopelagic	2.672
Mustelus stevensi	Benthic	2.687
Mustelus manazo	Benthic	2.483
Mustelus walkeri	Benthic	2.865
Mustelus schmitti	Benthopelagic	2.402
Mustelus minicanis	Benthic	2.876
Mustelus whitneyi	Benthic	2.891
Mustelus mento	Benthic	2.912
Triakis megalopterus	Benthopelagic	2.621
Scylliogaleus quecketti	Benthic	2.443
Leptocharias smithii	Benthic	2.475
Eridacnis barbouri	Benthic	2.271
Eridacnis sinuans	Benthic	2.438

Eridacnis radcliffei	Benthic	2.579
Proscyllium magnificum	Benthic	1.904
Proscyllium habereri	Benthic	2.59
Ctenacis fehlmanni	Benthic	2.535
Pseudotriakis microdon	Benthic	2.266
Planonasus parini	Benthic	1.682
Gollum attenuatus	Benthic	2.541
Gollum suluensis	Benthic	2.501
Bythaelurus clevai	Benthic	2.046
Bythaelurus canescens	Benthic	2.063
Bythaelurus lutarius	Benthic	2.247
Bythaelurus dawsoni	Benthic	2.018
Bythaelurus giddingsi	Benthic	1.484
Bythaelurus hispidus	Benthic	2.422
Bythaelurus incanus	Benthic	2.121
Bythaelurus immaculatus	Benthic	1.814
Figaro boardmani	Benthic	2.014
Figaro striatus	Benthic	1.077
Asymbolus pallidus	Benthic	2.736
Asymbolus parvus	Benthic	1.293
Asymbolus funebris	Benthic	2.057

Asymbolus galacticus	Benthic	2.835
Asymbolus rubiginosus	Benthic	2.741
Asymbolus vincenti	Benthic	2.047
Asymbolus submaculatus	Benthic	2.021
Asymbolus analis	Benthic	1.803
Asymbolus occiduus	Benthic	1.488
Galeus schultzi	Benthic	2.413
Galeus gracilis	Benthic	2.12
Galeus murinus	Benthic	2.305
Galeus piperatus	Benthic	1.518
Galeus springeri	Benthic	2.172
Galeus priapus	Benthic	1.908
Galeus antillensis	Benthopelagic	2.223
Galeus arae	Benthopelagic	2.898
Galeus atlanticus	Benthic	1.522
Galeus nipponensis	Benthic	1.613
Galeus polli	Benthic	1.643
Galeus melastomus	Benthic	2.418
Galeus cadenati	Benthic	3.051
Galeus longirostris	Benthopelagic	1.63
Apristurus riveri	Benthic	1.463

Parmaturus campechiensis	Benthic	1.901
Parmaturus xaniurus	Benthic	1.617
Parmaturus albimarginatus	Benthic	1.496
Parmaturus macmillani	Benthic	2.254
Parmaturus melanobranchus	Benthic	2.298
Parmaturus lanatus	Benthic	1.818
Parmaturus pilosus	Benthic	1.764
Parmaturus bigus	Benthic	1.396
Galeus eastmani	Benthic	1.596
Galeus sauteri	Benthic	1.795
Apristurus exsanguis	Benthic	2.083
Apristurus nasutus	Benthopelagic	2.824
Apristurus indicus	Benthic	2.643
Apristurus internatus	Benthic	2.617
Apristurus canutus	Benthic	2.597
Apristurus gibbosus	Benthic	2.861
Apristurus macrorhynchus	Benthic	1.902
Apristurus spongiceps	Benthopelagic	2.013
Apristurus sinensis	Benthic	1.393
Apristurus platyrhynchus	Benthic	2.251
Apristurus micropterygeus	Benthic	1.475

Apristurus brunneus	Benthopelagic	2.615
Apristurus laurussonii	Benthopelagic	2.554
Apristurus melanoasper	Benthic	1.834
Apristurus japonicus	Benthopelagic	2.476
Apristurus stenseni	Benthic	2.435
Apristurus macrostomus	Benthic	2
Apristurus parvipinnis	Benthopelagic	2.607
Apristurus australis	Benthic	1.952
Apristurus herklotsi	Benthic	2.929
Apristurus bucephalus	Benthic	1.514
Apristurus investigatoris	Benthic	2.311
Apristurus saldanha	Benthic	1.747
Apristurus longicephalus	Benthic	1.554
Apristurus albisoma	Benthic	1.704
Apristurus pinguis	Benthic	2.817
Apristurus profundorum	Benthic	2.783
Apristurus sibogae	Benthic	1.578
Apristurus microps	Benthopelagic	2.03
Apristurus kampae	Benthic	2.677
Apristurus fedorovi	Benthic	2.473
Apristurus aphyodes	Benthic	1.88

	Holohalaelurus punctatus	Benthic	2.501
	Holohalaelurus grennian	Benthic	1.327
	Holohalaelurus regani	Benthic	1.863
	Holohalaelurus melanostigma	Benthic	2.778
	Holohalaelurus favus	Benthic	1.624
	Pentanchus profundicolus	Benthic	1.716
	Haploblepharus kistnasamyi	Benthic	1.847
	Haploblepharus pictus	Benthic	1.966
	Haploblepharus edwardsii	Benthic	2.139
	Haploblepharus fuscus	Benthic	1.929
	Halaelurus boesemani	Benthic	1.507
	Halaelurus sellus	Benthic	2.462
	Halaelurus lineatus	Benthic	2.259
	Halaelurus maculosus	Benthic	2.086
	Halaelurus quagga	Benthic	1.676
	Halaelurus natalensis	Benthic	1.87
	Halaelurus buergeri	Benthic	1.668
Lamniformes	*Mitsukurina owstoni*	Pelagic	3.021
	Alopias superciliosus	Pelagic	3.648
	Odontaspis noronhai	Benthopelagic	3.477
	Odontaspis ferox	Benthopelagic	2.439

Pseudocarcharias kamoharai	Pelagic	2.189
Megachasma pelagios	Pelagic	3.886
Alopias pelagicus	Pelagic	3.426
Alopias vulpinus	Pelagic	3.918
Carcharias taurus	Benthopelagic	2.655
Cetorhinus maximus	Pelagic	3.389
Lamna ditropis	Pelagic	3.545
Lamna nasus	Pelagic	3.112
Carcharodon carcharias	Pelagic	2.932
Isurus oxyrinchus	Pelagic	3.169
Isurus paucus	Pelagic	3.955

S2.13. List of all fossil chondrichthyans used. Catalog number of specimens in published peer-reviewed papers and catalog number of specimens housed in the Natural History Museum in London are provided.

Species	Age	Pectoral Fin Aspect Ratio	Source
Macrourogaleus hassei	152 mya	2.357	BSP AS I 1363
Paraorthacodus sp.	152 mya	1.696	BSP 1996 I 31
Paleospinax sp.	152 mya	2.092	NHM UK PV 7788
Sphenodus macer	152 mya	1.464	SMNS 80142/44
Synechodus ungeri [juvenile]	152 mya	2.3	BSP 1878 VI 6
Paraorthacodus jurensis	152 mya	1.696	BSP 1996 I 31
Bavariscyllium tischlingeri	152 mya	1.42	SMNS 96086
Centrophoroides latidens	95 mya	2.36	NHMUK PV P4021
Centrosqualus primaevus	95 mya	1.46	NHMUK PV P3198
Cretoxyrhina mantelli	86 mya	2.92	KUVP 49490
Eogaleus bolcensis	50 mya	3	MCSN VII.B.94
Galeorhinus cuvieri	50 mya	3.79	MGGC 1976
Haimirichia	94 mya	2.5	UM AGT 1
Notidanoides muensteri	152 mya	1.359	BSP 1964 XXIII 157
Palaeocarcharias stromeri	152 mya	1.077	BSBGM 1964 XXIII
Palaeoscyllium formosum	152 mya	2.113	BSP AS I 1365
Paracestracion falcifer	152 mya	1.72	BSP AS VI 505
Paracestracion viohli	152 mya	1.41	JME SCHA728
Paratriakis curtirostris	95 mya	2.76	NHMUK PV P4022
Phorcynis catulina	152 mya	1.738	BSP 1990 XVIII 51
Protospinax annectans	152 mya	1.267	BSP 1963 I 19
Squatina acanthoderma	152 mya	1.17	SMNS 80431/20
Pseudorhina alifera	152 mya	2.09	SMNS-BSPG AS VII
Scapanorhynchus lewisii	95 mya	1.58	NHMUK PV P48099
Scyliorhinus elongatus	95 mya	2.31	NHMUK PV P49472
Squalicorax falcatus	86 mya	2.53	USNM 425665

S2.14. Equation for the mako shark was Freq = 0.16 * temp - 2.24, and the equation for the Leopard shark was Freq = 0.038 * temp + 0.0233. PPF: peak power frequency. Data are from Donley et al. (2007).

Species	Temperature (°C)	PPF (Hz)
Leopard shark (*Triakis semisfasciata*)	15	0.60
Leopard shark (*Triakis semisfasciata*)	20	0.77
Leopard shark (*Triakis semisfasciata*)	25	0.98
Mako shark (*Isurus oxyrinchus*)	15	0.19
Mako shark (*Isurus oxyrinchus*)	20	0.89
Mako shark (*Isurus oxyrinchus*)	28	2.25

S2.15. Summary statistics of the stochastic character mapping (implemented in phytools) of habitat (benthic, benthopelagic, and pelagic) for maximum clade credibility tree. ER: equal rates matrix, SYM: symmetric rate matrix, ARD: matrix with all rates different.

	ER	SYM	ARD
AIC score	631.6398	587.7936	552.8484
delta AIC score	78.79138	34.94524	0
Akaike weight	<0.0001	<0.0001	>0.9999

S2.16. Statistical support for six different PGLS models, and estimates for Pagel's lambda (for PGLS with BM correlation structure) and alpha (PGLS with Ornstein-Uhlenbeck correlation structure).

	Pagel's lambda	alpha	AIC score	delta AIC score	Akaike weight
Simple BM	0.4630204	NA	736.757	5.604531	0.0535
Simple OU	NA	5.407093	909.0977	177.945309	<0.0001
Intercept BM	0.4289251	NA	736.355	5.202543	0.0654
Intercept OU	NA	4.717104	853.1695	122.017030	<0.0001
Interaction BM	0.4426524	NA	731.1524	0	0.8812
Interaction OU	NA	4.706202	855.4522	124.299781	<0.0001

S2.17. Coefficients table of the best fitting PGLS model (interaction BM).

	Value	Std.Error	t-value	p-value
(Intercept)	2.277524	0.28357	8.031614	0
log10(pcl)	0.02006	0.1322	0.151736	0.8795
habitatbenthopelagic	-0.25116	0.400683	-0.62683	0.5311
habitatpelagic	-1.33638	0.530904	-2.51718	0.0122
log10(pcl):habitatbenthopelagic	0.167806	0.213352	0.786524	0.4319
log10(pcl):habitatpelagic	0.739447	0.243563	3.035952	0.0025